A Novel Mechanistic and Physiologically-Based Pharmacokinetic Model with Dynamic Gastrointestinal Fluid Transport

by

Alex Yu

A dissertation submitted in partial fulfillment
of the requirements for the degree of
Doctor of Philosophy
(Pharmaceutical Sciences)
in the University of Michigan
2018

Doctoral Committee:

Professor Duxin Sun, Chair
Professor Gordon L. Amidon
Professor Trachette Jackson
Dr. Robert Lionberger, Food and Drug Administration
Professor Manjunath Pai
Professor David E. Smith

Alex Yu

alexmyu@umich.edu

ORCID iD: 0000-0003-1732-2631

Dedication

This dissertation is dedicated to my wife, Dr. Siena Sun, for her constant support during my doctoral studies and for her constant reminder that she obtained her Ph.D. before me. My father, Dr. Lawrence X. Yu, for setting the bar in the pharmaceutics world and for constantly asking why it took more than one year to finish my doctoral studies. My mother, Jenny Wei, for being the voice of practicality and beacon of encouragement. My sister, Stephanie J. Yu, for being a better sister than I am a brother. My cat, Flash, for keeping me company and meowing all the time.

Acknowledgements

First and foremost, I would like to extend my sincerest gratitude to my advisor, Dr. Duxin Sun, for his advice, scientific input, financial support, and continuous encouragement. His knowledge across multiple disciplines, optimism in research, and great leadership skills has support me in my graduate studies and has set the example for me in my career.

I would also like to thank my dissertation committee, Dr. Gordon L. Amidon, Dr. David E. Smith, Dr. Trachette Jackson, Dr. Robert Lionberger and Dr. Manjunath Pai, for their time and effort providing valuable both feedback and insight on my research.

Sincere thanks to: Ann Frances for being the clinical lead on the mesalamine project; Dr. Mark Koenigsknecht for being the clinical lead on the ibuprofen project; Dr. Luca Marciani for MRI fluid quantification studies; Dr. Jason Baker for his support in intubation sampling; All the members of the hospital team that make clinical studies a reality.

I would also like to thank all fellow graduate students as well as current and former lab members. Special thanks to my roommate, Emily E. Morin, for supporting and putting up with me all these years. What. A. Journey.

Table of Contents

Lists of Tables

Lists of Figures

Abstract

A better understanding of the rate and extent for oral drug product dissolution in the gastrointestinal (GI) tract can provide an invaluable perspective in the drug development process. As it is difficult to experimentally measure the rate and extent of dissolution, the purpose of this research is to develop a validated model-based method that translates clinically observed plasma profiles into predictions of *in vivo* dissolution with validation by GI drug concentration profiles. The resulting model was based on physiologically considerations such as series-based transit, fluid volume, mucus layer, and pH to model the oral absorption process.

Local GI fluid volume was identified as a poorly characterized physiological variable that essential in modeling local GI drug concentrations, thereby influencing the simulation of drug dissolution and absorption. A dynamic fluid transport model was developed from GI fluid volumes found in literature with validation based on transport of a non-absorbable marker. The simulation found volumes in the GI tract to vary more in the upper than later GI and more at earlier timepoints than later timepoints. The simulation also found faster drug transit that reflected the earlier larger volumes followed by slower transit when volume is limited, explaining the observed extended residence time of drug in the stomach and small intestine environments.

To predict the rate and extent of *in vivo* drug dissolution, an algorithm based deconvolution of human plasma profile after 800 mg ibuprofen dose was deployed using the developed mechanistic model with the addition of a two-compartment pharmacokinetic model.

Consideration of gastric emptying lag time was essential to validating the simulated and experimental *in vivo* GI concentration profile of ibuprofen observed in a recent clinical study where lag time was determined by rapid rise of ibuprofen in plasma that reflects its significantly higher solubility in the small intestine pH environment. The simulation predicted minimal dissolution (2%) in the stomach, rapid but short dissolution in the duodenum (6.3%), core dissolution in the jejunum (63%) over 210 minute period, and completion of dissolution in the ileum (25%).

To further obtain reference data for evaluation of *in vivo* dissolution, a clinical study was conducted that found extended residence time mesalamine in the GI tract for modified release formulations. To model the extended residence time of mesalamine drug in the stomach, the deconvolution algorithm was applied to human plasma profile after 1000 mg dose of Pentasa using the developed mechanistic model with the addition of a two-compartment pharmacokinetic model. The characterization of bio-adherence from excipients used in the formulation was incorporated in the mechanistic oral absorption model by establishing additional mucus compartments where particles would "attach" and experience slower transit due to mucus. The simulation produced local GI drug concentrations similar in magnitude to the clinically observed profiles with extended residence past 7 hours.

The acquisition of local GI concentration profiles played a critical role in developing *in vivo* dissolution models with validation. The data further suggests that quantification of dynamic GI fluid and consideration of GI mucus can not only play an essential role in transit and absorption of solubilized drug, but also be a contributing factor to the transit and regional dissolution of drug particles. The resulting *in vivo* dissolution profile may be key to developing *in vivo* relevant *in vitro* dissolution studies.

Chapter 1 Introduction

Computational modeling and simulation of oral drug absorption in the gastrointestinal tract has been used to address numerous scientific questions with the potential to change the drug development and approval process (1). When successful, oral absorption models have contributed significantly to the drug development process in areas such as lead drug candidate selection, formulation development strategies, and development of regulatory policies (2).

Despite numerous models being developed to characterize oral drug product dissolution and absorption in the GI, these models often have instances of limited predictive value (3). One of the major challenges to constructing models that offer improved prediction capabilities is providing an accurate assessment of the system to ensure high quality model input (4).

The traditional focus of improving oral absorption models has focused extensively on the physiochemical aspects of drug compounds such as pKa, GI pH, solubility, particle size, crystal form, and salt diffusivity (2). However, the *in vivo* behavior of a drug product is reliant not only on these physiochemical properties but also the local available fluid volume. By association, the dynamic nature of GI fluid volume and corresponding transport can greatly affect the dissolution and absorption of oral drug products (5).

Model based evaluation have demonstrated intestinal water volumes to have a large impact on the predictive power of simulations to correctly model mean plasma concentration profiles (6). As local GI fluid content is the medium for drug dissolution and absorption, an

improvement in the physiologically characterization of GI fluid volume is a critical opportunity to improve the foundation of mechanistic oral absorption models.

This introduction reviews the current integration of GI fluid considerations in mechanistic oral absorption models, the conceptualization of fluid in *in vivo* dissolution equations, and recent imaging based studies that can experimentally determine GI fluid volume through non-invasive means. Combined, these sources form a new basis for mechanistic modeling of GI fluid in *in vivo* absorption and dissolution.

Mechanistic Oral Absorption Models

Current mechanistic oral absorption models are based on a series of Continuously Stirred Tank Reactors (CSTRs) first popularized by the Compartment Absorption and Transport (CAT) model (2, 7). The model was comprised of 7 compartments in series with an assumed first order transit and first order absorption. Because the primary dose considered was a solution dosing, the model approximated absorption to be mass driven. While this approach proved to be a sufficient approach to model oral absorption, the limited considerations resulted in a model that was difficult to integrate *in vivo* dissolution.

Numerous models have since been published that expanded the mechanistic compartments used in the CAT model approach to include considerations for solid, particle, and dissolved drug states. In combination with new basis for GI fluid volumes, the mechanistic expansion allowed for predicted absorption and/or dissolution. In addition, these models also expand beyond GI fluid volumes with numerous physiological considerations and complex mechanisms such as segmental residence times (3, 8). Three of these models are discussed in further detail: Advanced Compartment Absorption and Transport (ACAT) and Advanced Dissolution Absorption and Metabolism (ADAM), and GI-Sim (9-11).

Advanced Compartment Absorption and Transport Model

The ACAT model was the first compartmental model to expand the single serial compartment of the CAT approach into three unique compartments as a method to characterize the solid, particle, and dissolved states drug phases (Figure 1). The ACAT model defined oral drug absorption by Equation 1 (9).

$$\text{absorption}_{(i)} = k_{(i)a} V_{(i)} \left(C_{(i)L} - C_{(i)E} \right) \quad (1)$$

Where $\text{absorption}_{(i)}$ is the absorption rate, $k_{(i)a}$ is the absorption rate constant for compartment i , $V_{(i)}$ is the volume of compartment i, $C_{(i)L}$ is the lumen concentration and $C_{(i)E}$ is the concentration in enterocyte. Through this approach, the ACAT could make considerations for the available fluid volume and local drug concentration when calculated absorption.

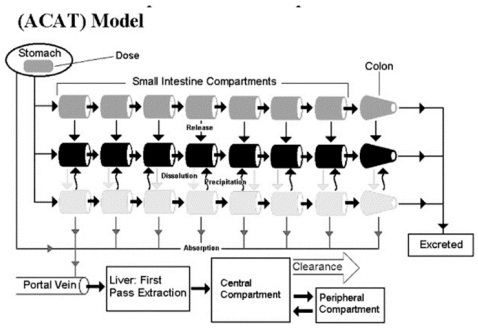

Figure 1. ACAT model schematic. (reproduced) (9)

The volume term used in the ACAT model is a static volume and does not represent the changing environment of the GI tract and as such, ensures that the driving gradient for absorption is generally dependent on the amount of drug available in the GI tract. Based using this approach, the ACAT model could replicated with absolutely certainty the results obtained by the CAT model. In addition, the addition of volume terms allowed the ACAT model to be customized with regional variations that allowed for better model fitting when evaluating the absorption process.

In addition, the physiology of the GI tract was approximated in the ACAT model with the length, transit time, and radii of the intestine environment was based on published values (12). However, when the actual fluid volumes used in the ACAT model are compared with experimental results, the default volume settings for the small intestine needed to be reduced by 60% and the colon by 90% (13). If these volumes are directly used to simulate dissolution and absorption, the availability of more than double the local GI fluid volume limits the realistic predictive value of the model.

While it is unclear how the fluid volumes used in the model were determined, predictive methodology of the ACAT model is confounded using an artificial scale factor (ASF). The ASF term is a coefficient that encapsulates inter-compartment variation such as surface-to-volume ratio, pH effects, influx, or efflux transporter differences, and other absorption-rate-determining effects (14). This term mathematically minimizes the importance of well characterized GI fluid volumes [as input which not well defined] and functions as an additional modeling layer. The resulting model can be fit to any plasma profile based on adjustments to coefficient values (15).

Advanced Dissolution Absorption and Metabolism

The ADAM model continues the use of three states to define drug in the small intestine as a solid, particle and dissolved drug (Figure 2).

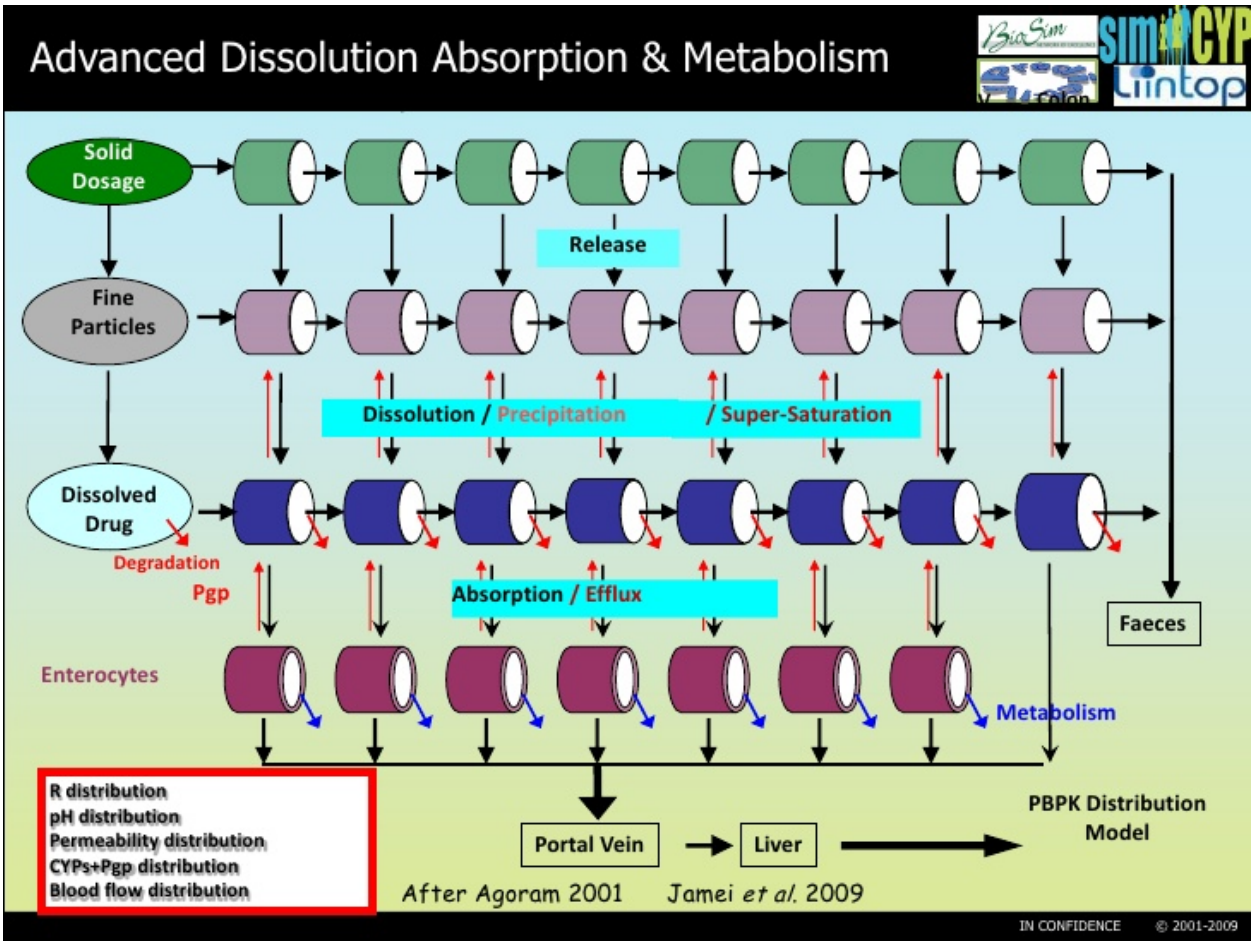

Figure 2. ADAM Model Schematic Slide (reproduced) (16)

The criticality of the changing volume due to fluid intake, secretion, and absorption was recognized in the development of the ADAM model as an important consideration that is ignored in many models of oral drug absorption (10). To calibrate the model's use of physiologically relevant GI fluid volumes, the GI fluid volumes were based on a water-sensitive magnetic resonance imaging (MRI) to define the volume of each compartment (10). Despite this however, the ADAM model's ordinary differential equation does not appear to consider fluid volume in defining absorption (Equation 2).

$$\frac{\mathrm{d}A_{\mathrm{D,n}}}{\mathrm{d}t} = \frac{\mathrm{d}A_{\mathrm{diss,n}}}{\mathrm{d}t} - \left(k_{\mathrm{deg},n} + \mathrm{ka}_n + k_{\mathrm{t},n}\right)A_{\mathrm{D},n} + k_{\mathrm{t},n\text{-}1}A_{\mathrm{D},n\text{-}1} + \gamma_n \mathrm{CLu}_{\mathrm{int\text{-}T},n}\,\mathrm{fu}_{\mathrm{gut}}C_{\mathrm{ent},n} \qquad (2)$$

Where $A_{D,n}$ is the amount of dissolved drug in compartment n, A_{diss} refers to the dissolution rate term, $k_{\text{deg},n}$ and ka_n are the drug degradation (luminal) and absorption rate constants, k_{t} is the transit rate, γ_n is a unit adjustment factor for the amount of drug transported out of the enterocyte, fu_{gut} is the fraction of drug unbound in the enterocyte, and $\text{CLu}_{\text{int-T},n}$ and $\text{CLu}_{\text{int-G},n}$ are the net efflux clearance from the enterocyte and net metabolic clearance within the enterocyte.

In this approach, the absorption of the drug from the GI tract is limited to a first order rate constant ka_n and dependent on the amount of dissolved drug in the compartment A_{D}. This conceptualization is consistent with the mass-driven CAT model as well as the ACAT model after excluding the pseudo concentration consideration. While availability of fluid data presents a valuable opportunity to consider fluid in model concentration driven absorption, the lack of inclusion ensures model parity and similarity with existing approaches.

In addition to characterization fluid volumes, the ADAM model incorporates extensive physiological data such as gastric emptying of solids and GI pH. Where the original CAT model focused on characterization of solution residence in the stomach, the ADAM's simulation of gastric emptying for solid oral dosage forms was based on experimental data and can be assigned based on a Weibull distribution to allow randomization (10, 17, 18). Experimental pH data was also integrated based on regional data and considerations made based on food effects (19, 20). These considerations can be used to improve the quality of model input for dissolution equations.

For drugs that are heavily metabolized, the ADAM model's limited consideration of fluid in absorption may not be the largest factor. The ADAM model utilizes an enterocyte compartment that is complimentary to each intestinal compartment. The use of this compartment adds an additional model layer of complexity that introduces capabilities such as modeling

transporter effects. Analogous to how the ASF for ACAT functions, the consideration of enterocytes and metabolism allow for improved prediction of pharmacokinetics (21).

GI-SIM

The GI-Sim absorption model is one of the latest mechanistic oral absorption models to adopt the compartmental approach. This approach mimics the compartmentalizing of drug phases into solid, particles, and dissolved drug (compartment names altered) of earlier models. Unlike earlier models however, the GI-Sim introduces additional complexity using an aqueous boundary layer that can further separate absorption and the conceptualization of micelles that can partition dissolved drugs (Figure 3). The use of enterocyte compartments is mimicked in the GI-Sim using a gut wall compartment. The inclusion of an aqueous boundary layer in addition to the gut wall creates additional parameterization that can be further used to fit predictions similar to the ASF of the ACAT model.

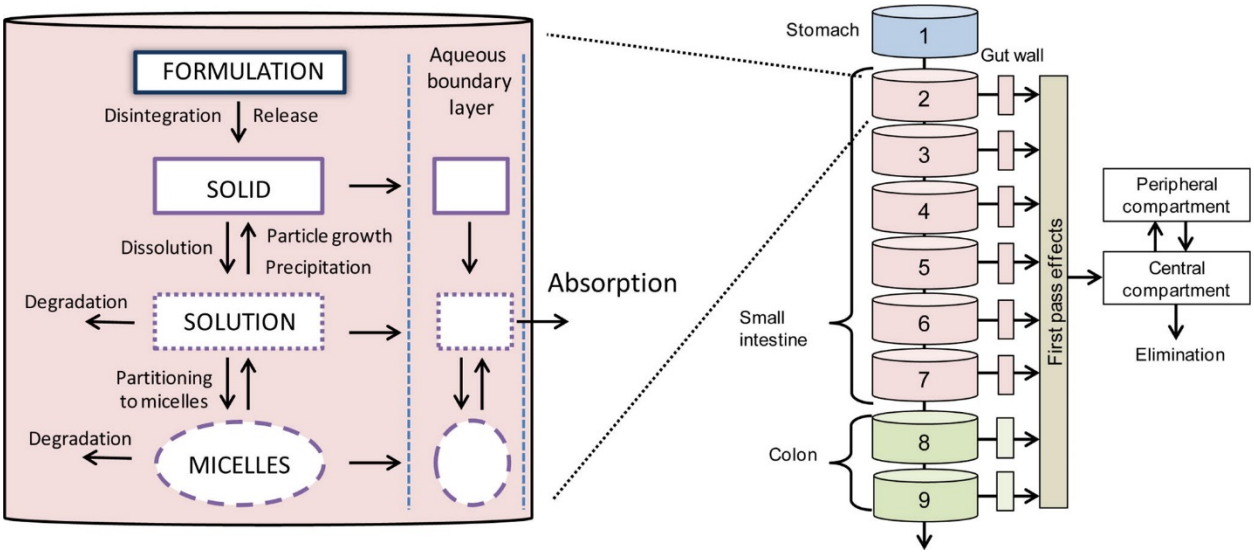

Figure 3. A schematic view of the absorption model GI-Sim. To the left a representation of the processes occurring in each compartment is shown. To the right, the nine ideal GI-compartments of the gastrointestinal tract linked with first pass effects and a pharmacokinetic two-compartmental model is shown (reproduced) (11)

The physiological parameters for volume, transit times, and pH in the intestine were adopted from Heikkinen et al (22). The source of the physiological parameters used was stated to originate from the ACAT model. The GI-Sim model incorporates a slightly different approach by characterizing the fraction of absorption.

$$F_{absorption} = P \cdot C_b \cdot SA \quad (3)$$

Where $F_{absorption}$ is the mass transport of free dissolved API molecules, P is the permeability, C_b is the bulk concentration, and SA is the available surface area for absorption. In this approach, the degree of absorption is a function of drug characteristics and local drug concentration. As the surface area does not change, this conceptualization of absorption assumes it to be entirely dependent on the local concentration which is a reasonable approximation of a first order mechanism. While the concentration term includes a bulk concentration term, the presentation as a static term makes the default assumption that the concentration is unchanging.

Dissolution Equations

For solid oral dosage forms, dissolution is one of the components that determine the bioavailability resulting from the oral absorption process. As dissolution is a highly complex process, mathematical characterization of dissolution equations simplifies the complexity into key variables. These considerations can include the concentration in the local environment, the solubility of the compound, and the diffusion coefficient of the molecule. When combined with physiologically based oral absorption models, dissolution equations can support the prediction of drug dissolution in the GI tract (23). The application of these models can also be used to guide *in vitro* assay development (15). Given the implications of being able to predict oral absorption, physiologically meaningful dissolution equations represent a highly valuable source of insight to

guide drug development. In this review, the Noyes-Whitney, Nernst-Brunner, and Wang-Flanagan equations are explained in further detail.

Noyes-Whitney Dissolution Equation

The Noyes-Whitney equation is a mass based differential equation to characterize the dissolution process (Equation 4) (24).

$$\frac{dx}{dt} = C(S - x) \tag{4}$$

The dissolution rate is dependent on a pre-determined solubility value S, the remaining mass in formulation x, and the local concentration (C). Based on the terms used in the equation, the equation is a reasonable reflection of an instantaneous rate of dissolution as the local concentration term is static. Alternatively, the equation also suffices if the proportional rate of change of drug mass is significantly larger than the rate of change for concentration. Regardless of approach, both assumptions reflect the consideration of a concentration term which inherently incorporates a volume. Therefore, a volume term is key to determining the released concentration of drug as well as the resulting dissolution rate.

Nernst-Brunner Dissolution Equation

The Nernst-Brunner equation expands on the Noyes-Whitney concept by incorporating consideration of diffusivity and a boundary layer (Equation 5) (25).

$$\frac{dC}{dt} = \frac{DS}{Vh}(C_S - C) \tag{5}$$

Despite being written as a differential of concentration, the equation incorporates a static volume term which suggests that the equation is like the Noyes-Whitney equation as primarily a mass based-differential equation. The presence of a volume term however, suggests recognition that volume is a key part in determining the released concentration of drug as well as resulting

dissolution rate. Other key considerations in the equation include the diffusivity of the drug as well as the boundary layer dimensions. This represents additional insight that physical transport rate limitations of the drug molecule itself is also key in calculating dissolution.

Wang and Flanagan Dissolution Equation

The Wang and Flanagan dissolution equation is a mass based differential focused on the dissolution based on particle physics (Equation 6) (10, 26)..

$$\frac{dA_{diss,n}}{dt} = -4\pi r^2(t) D \left(\frac{1}{r(t)} + \frac{1}{h}\right)\left(C_{S,n} - \frac{A_{D,n}}{V_{\text{lumen},n(t)}}\right) \quad (6)$$

One of the key assumptions in this equation is that the rate of dissolution is solely dependent on the gradient between peak solubility and the exist concentration. Like the Nernst-Brunner, the equation has separated the volume term and has recognized volume to be a major contributing term to the dissolution rate. Additional considerations primarily focus on expanding the characterization of diffusion and boundary layer to be a function of the available surface area of the drug. In this equation, the radius of the particle is assumed to be dynamic and shrinking over time with a constant boundary layer thickness.

Volume Considerations

The approach by these dissolution equations incorporate inherent recognition that the available local volume plays a role in determining the rate. The Noyes-Whitney equation accomplished this by embedding volume in the concentration term. Both the Nernst-Brunner and Wang-Flanagan equation clarified the local GI volume with an independent term. A key difference between these equation is temporal consideration of local volume. Only the Wang-Flanagan equation considered the local GI volume to be dynamic which subsequently can

modify the dissolution rate. This represents a closer attempt at capturing the contributing factors to in vivo dissolution.

Imaging Based Quantification of Gastrointestinal Volume

The basis of current mechanistic oral absorption models have focused on a primarily mass based approach to predict oral absorption. This was reasonably established on the basis of the results obtained by the CAT model. However, there is a recognized need for better model input to improve predicative capabilities. For mechanistic gastrointestinal models, this lies in determining accurate local GI fluid volume to calculate local GI drug concentrations for absorption. As such, GI fluid volume is a major focal point for the ACAT, ADAM, and GI-Sim models with the reference values used in each model listed in Table I (8).

Each commercialized software package has utilized different numerical values for GI fluid volumes. The degree of variation between the models, however, is significant. The total of all the compartments used (at the time referenced) is 205mL in the ADAM model which is comparable with just one compartment in the ACAT model at 175mL.

Table 1. Comparison of fluid volumes used in oral absorption models (reproduced) (8).

GI COMPARTMENT	SIMCYP (ADAM)	GASTROPLUS (ACAT)	GI-SIM
1	53	50	47
2	35	48	42
3	24	175	150
4	24	140	120
5	14	109	94
6	14	79	71
7	14	56	50
8	14	53	
9	13	57	

The quantification of GI fluid volumes to improve physiological relevance have been primarily based on two imaging technologies: Magnetic Resonance Imaging (MRI) which incorporates a magnetic field and pulses of radio waves to create pictures of organs and structures inside the body and Position Emission Topography (PET) which uses the emission of photos from radiolabeled markers to determine volume (27-29).

The quantification of GI fluid used in the ADAM and GI-Sim model are based on the MRI study that investigated the quantity of water in the GI tract during fastest and one hour after a meal (27). The study observed that the fluid is not homogenously distributed along the gut which can contributed to the individual variability of drug absorption. Another MRI study involved the dosing of a standard water dosing (240mL/8oz) in fasted healthy human volunteers (28). Both studies obtained valuable quantification of GI fluid content that can be translated

directly for use in oral absorption models. It should be noted that the MRI was only able to capture freely mobile fluid with long transverse relaxation times resulting in fluid components with restricted mobility and shorter transverse relaxation times (ie. mucus) not accounted for (28, 30).

PET imaging technology was recently used to capture the GI absorption and bio-distribution process (31). The study dosed humans with soft gelatin capsules containing 2-[(18)F]fluoro-2-deoxy-D-glucose ([(18)F]FDG) and was able to estimate GI tract volume from PET image analysis. Unlike the MRI imaging studies however, PET imaging was dependent on a molecule based marker that could diffuse and cover the outer regions of the intestine. This resulted in quantification values that may have captured the maximum volume of the GI tract rather than the local GI fluid volume available for dissolution and absorption.

Specific Aims

The predictive capabilities of current mechanistic oral absorption models are limited by physiologically relative local GI fluid volumes. Through characterization of local GI fluid volume and application to demonstrate the value of a fluid centric approach, the specific aims for this project are as follows:

1. Develop a mechanistic GI fluid transport model determines the quantity and transport of GI fluid volume in the GI tract
2. Develop a mechanistic deconvolution approach that incorporates the mechanistic GI fluid transport model to predict in vivo dissolution
3. Determine *in vivo* concentration of modified release mesalamine in human GI tract to improve connection with local GI fluid volume
4. Develop a mechanistic deconvolution model that can predict drug dissolution of delayed release mesalamine in the human GI tract based on established GI fluid transport model

Chapter 2 Mechanistic Gastrointestinal Fluid Model to Determine Volume and Transport Over Time[1]

Gastrointestinal (GI) fluid volume is a key factor in the dissolution and absorption process of oral drug products. For solid oral dosage forms, the local quantity of fluid can affect disintegration, dissolution, and absorption. Because local GI fluid volume varies significantly due to transit, secretion, and absorption, characterizing the *in vivo* environment is essential to accurately model the oral drug dissolution and absorption process. An accurate model of the oral drug product dissolution and absorption process can facilitate lead drug candidate selection, establish formulation development strategies, and support development of regulatory policies (2).

To predict oral drug absorption, models have incorporated physiological parameters of the GI tract (3, 8). The Compartment Absorption and Transit (CAT) model utilized a small intestine mean residence time to define transit rate (7). The Advanced Compartment Absorption and Transit (ACAT) model utilized mass balance approximations to define each compartment's volume and transit (9). The Advanced Dissolution Absorption and Metabolism (ADAM) utilized volumes reported by water-sensitive magnetic resonance imaging (MRI) to define the volume of each compartment (10).

The Dynamic Fluid Compartment Absorption and Transport (DFCAT) model was developed to characterize the fluid volume and its dynamic changes in the human GI tract from

[1] Adapted by permission from Springer Customer Service Centre GmbH: Springer Nature The AAPS Journal Mechanistic Fluid Transport Model to Estimate Gastrointestinal Fluid Volume and Its Dynamic Change Over Time, Alex Yu, Trachette Jackson, Yasuhiro Tsume, Mark Koenigsknecht, Jeffrey Wysocki, Luca Marciani, Gordon L. Amidon, Ann Frances, Jason R. Baker, William Hasler, Bo Wen, Amit Pai, and Duxin Sun, 2017

MRI imaging of fluid volume and to evaluate its accuracy of *in vivo* fluid transport based on human GI local concentration of the non-absorbable maker phenol red from a human intubation study. The MRI study quantified the content of water in the stomach and small intestine after dosing healthy human volunteers with 240mL of water (8). The human intubation study measured local GI concentration (stomach, duodenum, proximal jejunum, middle jejunum) of phenol red in healthy human volunteers after dosing 240 mL water with phenol red. These two studies in addition to literature data served to verify and validate the DFCAT model. In future applications, the DFCAT model can be expanded to estimate the *in vivo* drug dissolution process and therefore predict oral drug absorption of oral drug products.

Materials and Methods

A mathematical model, described in detail in the following sections, was derived to capture the essential features of GI fluid transport. The model consists of 62 nonlinear ordinary differential equations (ODE). The stomach is represented by two ODEs (dissolved drug and fluid) with the small intestine represented by 60 ODEs representing a 30-compartment model (each compartment connected in series with a dissolved drug and fluid component). 30 compartments were selected to represent the localized fluid volume as well as capture most cases of small bowel fluid pocket counts observed in the MRI fluid study (28). The conceptualization of a large number of compartments also reflects the long length vs diameter ratio of the small intestine representing the local physiological situation of the small fluid volumes available for dissolution. An illustration of the proposed compartment model and avenues of transport is drawn in Figure 4.

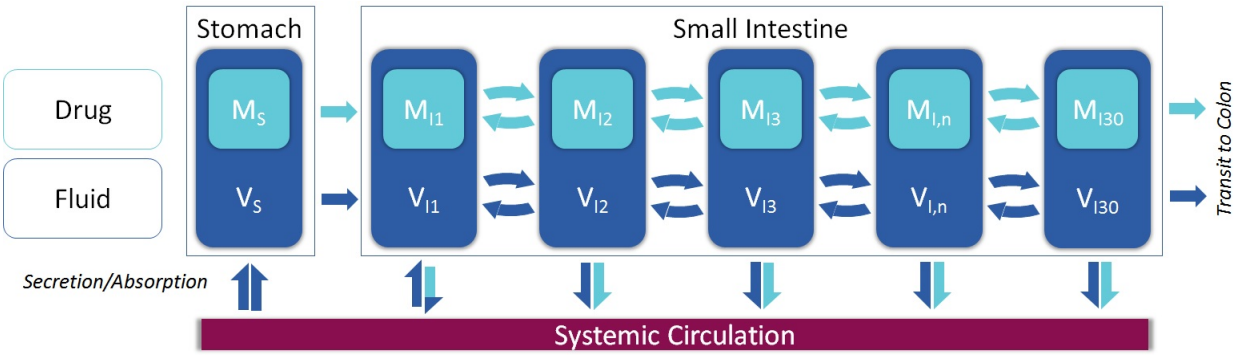

Figure 4. Dynamic Fluid Compartmental Absorption and Transit (DFCAT) approach to mimic physiologically-relevant fluid volumes and to predict corresponding transit of the gastrointestinal tract (compartment number denoted by subscript).

Matlab 2017a was used for both the simulation of model ODEs and the prediction of rate coefficient parameters. A fixed step ODE solver from the Simulink Package (ODE4) was used in 1s intervals. Calculations were run in parallel model using the parfor method. Visualized data graphics were rendered using Matlab's plot and surf packages. Table 2 summarizes the parameters obtained and used in the model.

Table 2. Variable values used in the DFCAT model

Symbol	Parameter	Literature Value	Model Value	Units	Model Value Source
k_{qS}	Gastric emptying rate constant		0.699	min^{-1}	Experimental fit
k_{sS}	Gastric secretion rate	1.39-2.08 $mLmin^{-1}$[32]	1.425	$mLmin^{-1}$	Experimental fit
k_{sI}	Duodenal secretion rate	2.78 $mLmin^{-1}$ daily [33]	0-4.5	$mLmin^{-1}$	Experimental fit
V_b	Volume of mucus in the small intestine compartment	200-400 µm [34-36]	5	mL	Estimate
V_{bS}	Volume of mucus in the stomach	1mm thick[37]	40	mL	Estimate
k_{tF}	Small intestine transit rate (forward)	199 min small intestine mean residence time [38]	0.92	min^{-1}	Literature fit
k_{tR}	Small intestine transit rate (reverse)		0.269	min^{-1}	Literature fit
k_{aw}	Small intestine water absorption rate constant	0.0715[39]	0.0715	min^{-1}	Literature value

Stomach Compartment Fluid Compartment

The stomach compartment is represented by one ODE for transport of fluid and one ODE for transport of solubilized drug. Fluid transport in the stomach was assumed to be a component of gastric emptying and net gastric secretion (secretion > absorption). A first order process was used to approximate the typical gastric emptying process (40, 41). Based on the observed trend, secretion on average was assumed to be constant. The result is a fluid transport ODE (Equation 7) that is defined by a first order gastric emptying and a zero-order gastric secretion process.

$$\frac{dV_S}{dt} = -\underbrace{k_{qS}V_S}_{\text{Emptying into Intestines}} + \underbrace{k_{sS}}_{\text{Stomach Secretion}} \quad (7)$$

V_S is the volume of fluid in the stomach compartment, k_{qS} is the first order gastric emptying rate constant, and k_{sS} is zero order gastric secretion rate (Table 2).

Stomach Compartment Dissolved Drug Compartment

The MRI study quantified fluid as the available free water. However, it is well known that the stomach environment is lined with mucus which can contribute to dissolved drug transport. The model assumed dissolved drug equilibrated instantaneously between the mucosal layer and the fluid. A mucus volume (V_{bS}) was estimated to be a static entity that lines the wall of the stomach but has not yet been fully quantified by clinical measurements. Mucus volume was estimated to be 40 mL based on a cylindrical abstraction of the stomach with an average capacity of 0.94L, 10cm diameter, and 1mm thick mucosal layer (37).

Transport of solubilized drug was assumed to follow the gastric emptying process of fluid based on the fraction available in free water. Drug absorption in the stomach is typically assumed to be negligible relative to the small intestine and as such, there is no drug absorption term for the stomach. Drug degradation was also assumed to be minimal. Equation 8 defines the transport of drug in the stomach compartment where M_S is the mass of drug in the stomach compartment.

.

$$\frac{dM_S}{dt} = -\underbrace{k_{qS} M_S \left(\frac{V_S}{V_S + V_{bS}}\right)}_{\text{Emptying into Intestines}} \tag{8}$$

Small Intestine Fluid Compartments

The small intestine was represented by thirty compartments each with one ODE for transport of fluid and one ODE for transport of solubilized drug. Fluid transport in the small intestine was assumed to consist of transit, absorption, and secretion. Small intestine transit behavior was modeled using first order to characterize the forward (anterograde) and reverse

(retrograde) transit observed in human physiology (42). Water absorption was characterized by a deuterium-labeled water to approximate a first order absorption process with an absorption rate of 0.0715 min^{-1} (39) (Table 1). Net secretion was assumed to occur primarily in the duodenal region from bile and pancreatic secretions. Equation 9 defines the behavior for a small intestine compartment (the temporal zero order secretion term for the first compartment is not shown).

$$\underbrace{\frac{dV_n}{dt}}_{\text{Net Volume}} = + \underbrace{k_{tF}V_{n-1}}_{\text{Foward In}} - \underbrace{k_{tF}V_n}_{\text{Forward Out}} + \underbrace{k_{tR}V_{n+1}}_{\text{Reverse In}} - \underbrace{k_{tR}V_n}_{\text{Reverse Out}} - \underbrace{k_{aw}V_n}_{\text{Absorption}} \quad (9)$$

The forward and reverse transit rate constants are defined by k_{tF} and k_{tR} respectively. The first order water absorption rate constant is defined as k_{aw}(Table 1).

Small Intestine Dissolved Drug Compartments

Transport of dissolved drug in the small intestine was assumed to mimic the mucosal behavior in the stomach compartment as various clinical studies have observed a range of thicknesses of the mucosal layer in the GI tract ranging from 200 to 400 µm (34-36). Based on an average small intestine length of 6.35m, a small intestine diameter assumption of 2.48 cm and an average thickness of 300 µm, the volume of the mucosal layer in the small intestine was estimated to be 5 mL (43, 44). The resulting Equation 10 describes the behavior of drug with M_n as the mass of the drug presently in n compartments. Absorption is assumed to be first order processes with rate coefficients of k_a.

$$\underbrace{\frac{dM_n}{dt}}_{\text{Net Drug}} = + \underbrace{k_{tF}M_{n-1}\left(\frac{V_{n-1}}{V_{n-1}+V_b}\right)}_{\text{Forward In}} - \underbrace{k_{tF}M_n\left(\frac{V_n}{V_n+V_b}\right)}_{\text{Forward Out}} + \underbrace{k_{tR}M_{n+1}\left(\frac{V_{n+1}}{V_{n+1}+V_b}\right)}_{\text{Reverse In}} - \underbrace{k_{tR}M_n\left(\frac{V_n}{V_n+V_b}\right)}_{\text{Reverse Out}} - \underbrace{k_a\left(\left(\frac{M_n}{V_n+V_b}\right) - \left(\frac{M_{central}}{V_d}\right)\right)}_{\text{Absorption}} \quad (10)$$

Model Verification

The DFCAT model was fitted to the small intestine mean residence time (MRT) distribution and observed GI fluid content from an MRI clinical study conducted at the

University of Nottingham (28). The study consisted of twelve healthy and fasted individuals. Each individual was administered 240 mL and the subsequent GI fluid volumes were measured via MRI at designated intervals over 120 minutes. The variables in the model such as duodenal secretion was adjusted to best fit the average observed fluid over time in the study. Small intestine MRT distribution was obtained from existing models that aggregated clinical data (28, 45). The inclusion of small intestine MRT in the DFCAT model mirrors a major design verification criteria of the original CAT model.

Human Intubation Clinical Study for Model Validation

The DFCAT Model was validated based on the local GI concentration acquired through a human clinical intubation study at the University of Michigan using the non-absorbable marker phenol red.

Ethics Statement

The study was approved by University of Michigan IRBMED HUM00085066 and the Food and Drug Administration (RIHSC protocol 14-029D. Study volunteers provided written informed consent. The study was in accordance with study protocol, the International Conference on Harmonization of Good Clinical Practice guidelines, and applicable local regulatory requirements. The ClinicalTrials.gov identifier is NCT02806869.

Materials

USP grade phenol red (phenolsulfonphthalein) was purchased from USP (Rockville, MD, USA) and Avantor Performance Materials (Center Valley, PA, USA). The 0.1 mg/ml phenol red solution was prepared in 250 ml of water. Phenol red was dispensed by the Investigational Drug Service (IDS) at the University of Michigan.

Study Inclusion and Exclusion Criteria

Healthy human volunteers between the ages of 18 and 55 were eligible for the study. Volunteers completed a physical exam and medical history screening by physician to confirm study eligibility. Volunteers all had normal values for vital signs, electrocardiogram, urine drug screen, serum pregnancy test (women only), comprehensive metabolic panel, complete blood count with platelet and differential, and lactate dehydrogenase.

Volunteers were excluded if any of the following applied: inability to consent; mentally incapacitate; prisoners; significant clinical illness within 3 weeks prior to screening; use of concomitant medications including but not limited to prescription drugs, herbal and dietary supplements, over the counter medications and vitamins within 2 weeks prior to study; received an investigational drug within 60 days prior to study; history of allergy to ibuprofen or other non-steroidal anti-inflammatory drugs (NSAIDS); pregnant or lactating females; history of severe allergic diseases including drug allergies; history of drug addiction or alcohol abuse within 12 months; clinically significant abnormal lab values during screening; any other factor, condition, or disease including but not limited to, cardiovascular, renal, hepatic or gastrointestinal disorders that may, in the opinion of the investigator, jeopardize the safety of the patient or impact the validity of the results.

Study Procedure

Clinical procedures were conducted at either the Michigan Clinical Research Unit or the Medical Procedures Unit of the University of Michigan hospital. Volunteers were instructed to fast 14 hours prior and to avoid consuming water 11 hours prior to dosing. A physical exam was performed to ensure the health of subject prior to GI catheter intubation procedure. Volunteers received a topical anesthetic (1mL of 4% lidocaine before catheter insertion. Lubricating jelly

was applied to the GI catheter which was then orally inserted into the GI tract of the volunteer. Catheter placement was confirmed under abdominal fluoroscopy to ensure proper positioning in the GI tract. Upon placement completion, the GI catheter was taped and kept open with saline solution throughout the study duration.

Volunteers were administered a single oral dose of ibuprofen (800 mg tablet) administered with 250 mL of phenol red. This was swallowed by the volunteer and not administered through catheter. GI fluid samples were collected through aspiration of available ports from the catheter. Prior to sample collection, contents from previous aspirations were collected and discarded. This discard volume ranged from 1.7mL to 3.2mL. If air bubbles were observed, at least 30 cc of air/fluid mixture was collected and discarded. GI sample collection times include 0, 0.25, 0.5, 0.75, 1, 1.5, 2, 2.5, 3, 4, 5, 6, and 7 hours post dose. Supernatant was collected after sample centrifugation at 21,000 x g for 5 minutes and stored at -80^{0} C. The GI catheter was removed from the volunteer at 7 hours.

HPLC analysis of Phenol Red in GI Fluid

All samples of phenol red were analyzed with an Agilent 1200 series HPLC system HPLC system (Agilent Technologies, Santa Clara, CA). The HPLC system consisted of Agilent pumps (1100 series), an Agilent autosampler (1200 series), and an Agilent UV-Vis detector (1100 series) controlled by Chemstation® 32 software (version B.01.03). Samples were resolved in Agilent Eclipse XDB-C18 reverse-phase column (3.5 µm, 4.6 × 150 mm) equipped with a guard column for phenol red. The mobile phase consisted of 0.1% TFA/water (Solvent A) and 0.1% TFA/acetonitrile (Solvent B) with the solvent B gradient changing from 0–56% at a rate of 2%/min during a 14-minute run. Standard curves generated for phenol red were utilized for quantitation of integrated area under peaks. The detection wavelength was 430 nm.

Results

Gastric Secretion and Emptying

Average gastric emptying behavior was observed to be first order and net fluxes were attributed to either be emptying or secretion. Temporal stomach fluid content data from the MRI study was fitted using Matlab's fitting toolbox. The equation for fitting is defined in Equation 11. The fitted equation is illustrated in Figure 5.

$$V(t) = (242) * e^{-k_{qS}*t} + \frac{k_{sS}}{k_{qS}} \tag{11}$$

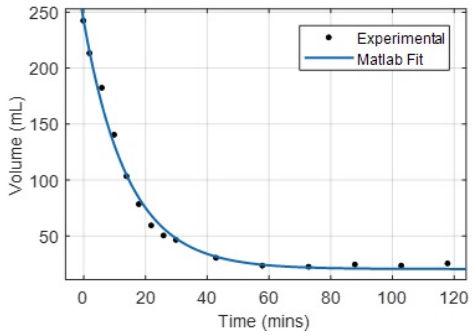

Figure 5. Best fit of the gastric emptying behavior (Equation 5) to clinical data.

The initial stomach volume was based on the first observed time point (242 mL). The resulting fit found the coefficients for k_{sS} and k_{qS} to be 1.425 mL/min and 0.0699min^{-1} respectively (table 1). The R square for the goodness of fit was 0.993. This is within the range of the typical daily adult gastric secretion of 2-3L or 1.39 to 2.08 mL/min. (32)

Small Intestine Transit Rates

To determine the optimal transit rate coefficients, a compartment model was used to simulate the transit of drug through the small intestine based on a 199 min mean residence time (50% exit from small intestine to colon) determined by a previous study (38). Due to having

more than one transit variable to solve, a range of forward and reverse rate coefficients were evaluated. A 3D visualization of residual fit as a function of forward and reverse rate coefficients is shown in Figure 6a. Figure 6a visualizes the natural relationship between the forward and reverse coefficients which minimizes the predicted transit vs. experimental measurement. The combination of forward and reverse rate transit coefficients with the lowest residual was chosen as the optimized values (0.92 min^{-1} forward and 0.269 min^{-1} reverse) (Table 1). The optimized transit rates were then used in the model. The resulting cumulative drug exit in Figure 6b closely resembles the small intestine MRT of the original CAT approach.

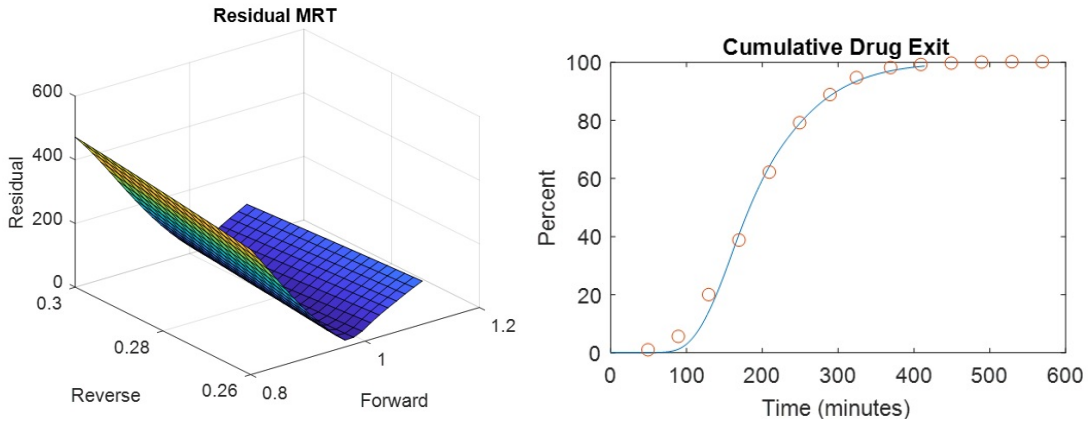

Figure 6a. Residual evaluation of overall transit behavior for various forward and reverse rate coefficients relative to small intestine MRT. 6b. DFCAT MRT compared with the MRT used in the CAT model.

Small Intestine Secretion Rate

Assuming net absorption throughout the small intestine, the resulting term that allows for the variation necessary to govern total small intestine volume is duodenal secretion. Duodenal secretion was assumed to change over time and the values for duodenal secretion were determined via an optimization algorithm to determine an estimate for duodenal secretion based on the total volumes observed in the simulation. Values for duodenal secretion rate range from 0 to 4.5 mL/min (table 1). The final secretion value represents the duodenal secretion necessary to

return the system to the basal volume observed in the beginning of the fluid MRI study. Secretion below the pylorus is roughly 4 liters daily (1 liter bile and 3 liter pancreatic) (33) This translates to roughly 2.78 mL/min which is reasonable with the values used in the model.

Average Gastrointestinal Fluid Volume Over Time

Model verification was conducted based on fluid MRI study data that ranged from 0 to 120 minutes. The upper and lower small intestine were categorized by the MRI study as the proximal duodenum to proximal jejunum and distal jejunum to distal ileum respectively. This was recognized in model form as small intestine compartments 1-4 and 5-30 respectively based on the approximate distance for each compartment (roughly 20 cm). The observed and simulated stomach and small intestine physiological fluid volumes over time (excluding mucosal volume) are shown in Figure 7.

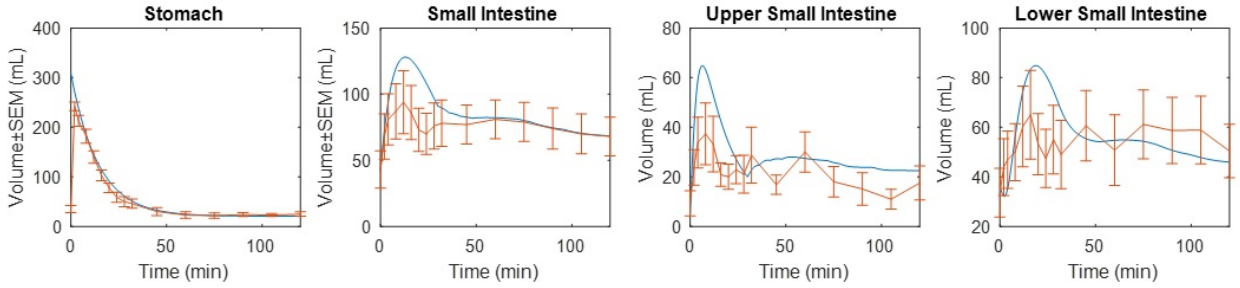

Figure 7. Simulated volume over time in different regions of the GI tract. Upper intestine is designed by compartments 1-4 based on physiology with the lower by compartments 5-30. (Blue line represents simulated average. Red line represents experimental mean ± SEM).

The simulation of stomach volume generally fit within the standard error of the mean (SEM) as the volume decreased after the initial water dose. The use of first order gastric emptying and zero order gastric secretion appear to capture the average transport behavior in the stomach. In comparison, the simulated small intestine results do not follow the experimental profile as well as the stomach volumes. This could be due to the use of an absorption rate

constant from another clinical study with a different population, mixing of water with the fluid layer lowering observed fluid volume, and/or large variation in regional absorption. In addition to these possibilities, the observation differences between simulated and experimental fluid volumes in the upper and lower small intestine can also be explained by the natural formation and transport process of fluid pockets in the GI tract. A comparison of fluid volumes used in the DFCAT and currently used mechanistic oral absorption models is provided as a reference in Table 3.

Table 3. Comparison of fluid volumes used in mechanistic oral absorption models

	Volume (mL)				
GI Compartment	SimCyp**	GastroPlus**	GI-Sim**	DFCAT*	GI Resize
1	53	50	47	5.6-63.9	1-4
2	35	48	42	5.1-38.6	5-8
3	24	175	150	4.3-24.6	9-12
4	24	140	120	3.5-16	13-16
5	14	109	94	2.7-10.5	17-20
6	14	79	71	2.1-6.9	21-24
7	14	56	50	1.6-5.6	25-28
8	14	53		0.6-2.8	29-30
9	13	57			

*Compartments have been resized for comparison. Compartment numbers are listed in the GI resize column. Values do not include mucus volume.
**Values from Sjögren et. al (8).

Model validation with Non-absorbable Phenol Red in the GI

Since phenol red is a non-absorbable maker in the GI tract, the GI local concentration change of phenol red after oral dosing of 100 μg/ml solution is only affected by the GI fluid volume change and transit. Therefore, phenol red GI local concentration is used to validate the DFCAT model. A simulation was conducted for fluid volume and phenol red transit replicating the dosing scenario observed in the phenol red intubation clinical study. The average phenol red

concentration was used. The initial dose volume was 274 mL with an average phenol red dose of 23.4mg (85 µg/ml). The simulated volume (excluding mucosal layer), mass, and concentration are shown in Figure 8. The blue line corresponds with the first compartment or duodenum.

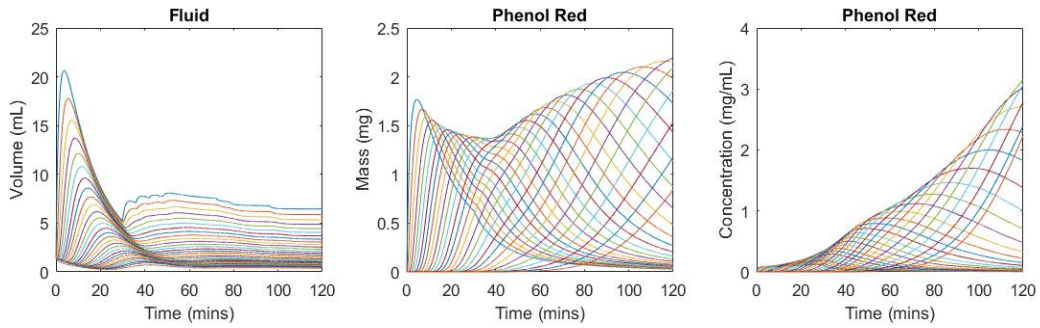

Figure 8. Simulated volume/phenol red mass/phenol red concentration over time in different compartments of the small intestine (each line represents a different compartment)

The design validation results of comparing simulation with experimental results are shown in Figure 9.

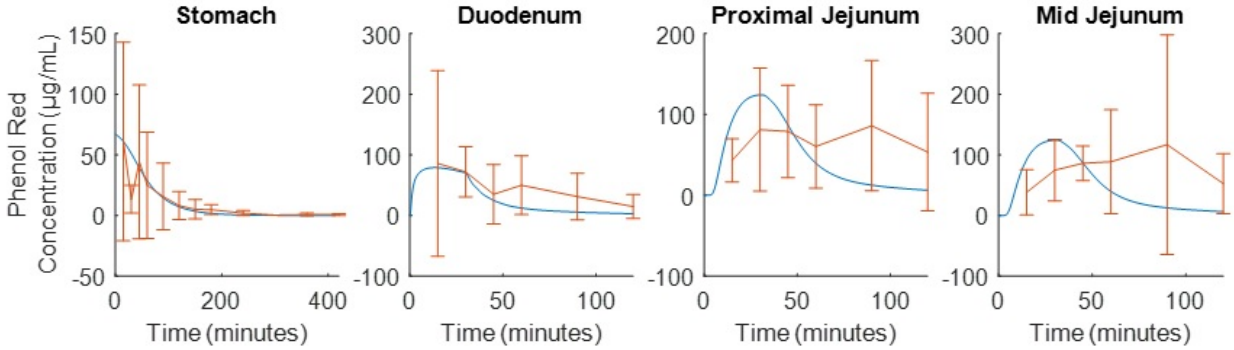

Figure 9. Comparison of local GI concentration samples of phenol red (red) vs Simulation (blue)

The predicted concentration generally falls within the average and standard error of the mean observed phenol red concentrations. While the behavior cannot be considered ideal in the proximal and mid jejunum as the simulation results in a higher concentration at the early time points, the study volunteers and physiology as well as stochastic variation differ between the two clinical studies. The closeness of the trend was considered well replicated by the simulation.

While the duodenum is the first compartment to peak in terms of total phenol red content, other compartments follow rapidly as it transports down the small intestine, and there is an extensive distribution of phenol red through the small intestine. Within two hours, there is significant phenol red distribution throughout the small intestine. On the other hand, the large initial quantity of fluid ingested means that initial compartments do not experience the highest concentration possible. This occurs in the later compartments where water absorption has contributed significantly to alter the fluid volume in the GI tract.

An illustration of the DFCAT GI fluid volume, phenol red mass, and phenol red concentration at 30 minutes post dose is shown in Figure 10.

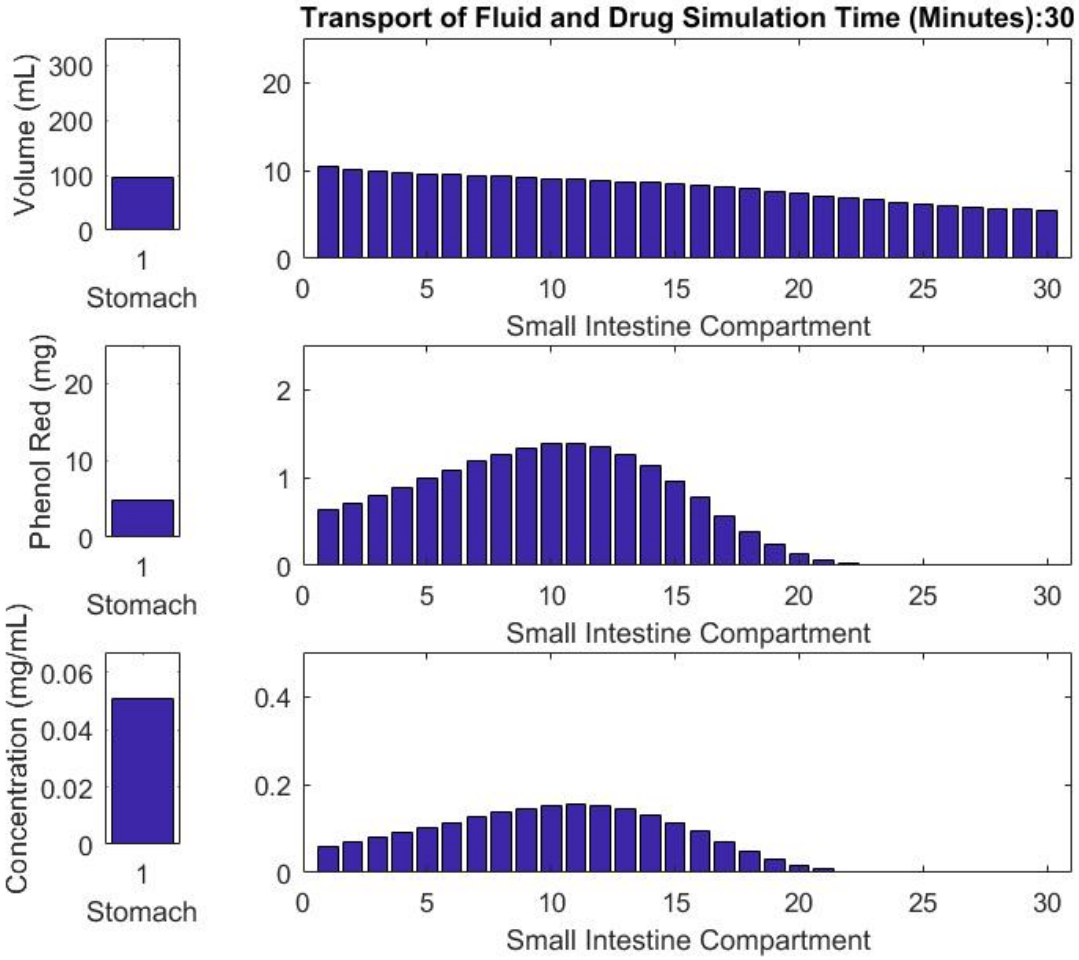

Figure 10. DFCAT GI fluid volume, phenol red mass, and phenol red concentration at 30 minutes post dose.

The transit of phenol red is rapid, reaching past the middle small intestine by 30 minutes. On an average basis, there is fluid distribution throughout the small intestine with 10 mL in the duodenal compartment and just over 5mL in the last ileum compartment. After the initial dosing of water, the average basis fluid volumes do not change rapidly in the small intestine and as such, lead to an overall shape of the mass profile that is like the concentration profile over all the small intestine compartments.

Discussion

Recent research efforts have been focused on clarifying the numerous complexities in the oral drug absorption process. The OrBiTo project is such an initiative dedicated to establishing new frameworks and tools for predictive biopharmaceutics regarding oral drug delivery (46). One topic of interest is the local GI fluid volumes within the gut lumen resulting from fluid intake, secretion, and reabsorption. This is a critical factor in the oral absorption process as the change of fluid volume within the gut lumen can have a significant effect on the dissolution of the drug and hence the concentration presented to enzymes and transporters within the enterocyte (3). While MRI studies have provided quantification of GI fluid volumes, the dynamic change of the fluid volume as well as the intermediate process of fluid absorption, secretion, and transit that occurs GI tract remains difficult to characterize.

Understanding the dynamics of GI fluid transport is essential to improvements in predicting *in vivo* dissolution from mechanistic models. Measurement of GI fluid volume through imaging has provided valuable knowledge of GI fluid quantification. However, the data obtained remains as snapshots in time and does not detail the degree of absorption, secretion, and transit that occurs. The DFCAT model was established to mechanistically interpret the dynamic changes and intermediate knowledge using a methodical approach based on design verification and validation using phenol red concentration in the GI tract.

Design verification was based on the GI fluid quantification via MRI. The MRI method (30) used to obtain the *in-vivo* fluid volume (28) measured only freely mobile water with long transverse relaxation time, hence fluid components with restricted mobility and shorter transverse relaxation times (e.g. water in mucous) were not accounted for. If the mixing of fluid and mucus prevents the fluid from being quantified, it would explain why the total volume of

fluid measured was underestimated and that the simulated volume may be closer to reality. This could explain the significant drop when assessing the mass balance of fluid from the stomach into the small intestine. The quantity of mucus in the GI tract has not been well characterized and is not usually considered a major contributor to drug dissolution and oral drug absorption. However, the weight of evidence from this model suggests the mucus layer is present and its volume can affect local GI concentrations given the surface area of the small intestine.

In addition, in the MRI measured fluid volume, a minimum threshold of 0.5 mL per fluid pocket was applied to the quantitation in (28). This was done since the contribution of very small pockets of fluid in the small bowel comprised only 0.5% of the total volume detected in the small bowel whilst their inclusion confused the display and interpretation of data. The 0.5mL is not a lower detection limit, but rather a single MRI image pixel of adequate brightness against the validated calibration (30). Therefore, the total volume of fluid measured by MRI was likely be underestimated.

Other imaging techniques such as Positron Emission Tomography (PET) have obtained an average volume of 313mL which is significantly larger than the MRI derived volume of 105 mL (27, 31). However, this tends to overestimate the total volume as the marker can spread along the small intestine walls. This difference can be explained by the presence of a mucus layer and would suggest that an estimated volume of 150 mL is reasonable to describe the small intestine mucus layer. Design validation of DFCAT was based on the experimentally determined local GI concentrations of phenol red. Despite the variation that was observed between the simulated and experimental fluid profiles, the simulation and experimentally observed phenol red concentrations in the GI tract were similar suggesting the model is representative. It is critical to note that there is a significant variation in the GI local phenol red concentration due to the

stochastic nature of the GI tract. The use of a continuous model was to simplify the approach to characterize average tendencies and trends. In this regard, the DFCAT model can explain the change in local GI fluid volumes.

A primary assumption in the DFCAT model is that transport is defined by first order kinetics. First order kinetics was used in the model to define gastric emptying, transit rate in the small intestine, and water absorption. Of these processes, only gastric emptying and water absorption have been experimentally determined to be well approximated by first order kinetics (39-41). The transit rate in the small intestine has only noted to be faster in the proximal regions and slower in the more distal regions (5). The use of first order kinetics can mathematically approximate this behavior to a certain extent but certainly does not mimic the complete peristaltic effect observed in the small intestine.

The use of verification and validation in establishing the DFCAT model also presents limitations. The model presently is only designed to simulate the fluid volume after intake of water in the fasted state. There are numerous physiochemical aspects in the GI tract such as conductivity, pH, and osmolality that can impact oral drug delivery (5). Changing the drink or simulating a fed state may result in a significantly different profile with different GI secretions. Each change in study conditions would require a new MRI fluid study to quantify the fluid model as well as a new intubation study to obtain the local GI concentrations under fed condition.

The DFCAT as presented is a methodology to model GI fluid transport based on experimentally obtained fluid volume, which is also validated by local phenol red concentration in the GI tract. While the verification and validation do not include drug absorption, the framework can be expanded to predict drug dissolution and oral drug absorption as referenced in

the compartmental equations. Since local GI fluid content is critical to drug dissolution and oral absorption, the approach used to construct the DFCAT model can be integrated with existing physiologically based pharmacokinetic (PBPK) models. Along with the fundamental knowledge of the GI tract developed by the OrBiTo project, the integration of local GI fluid and other physiological considerations can integrate in vitro and in silico approaches to improve the oral drug development process.

Chapter 3 A Novel GI Fluid Transport-Based PBPK Model to Enable Prediction of Regional GI Drug Dissolution and Establishment of In Vitro-In Vivo Relationship

Accurate prediction of *in vivo* dissolution can assure therapeutic efficacy and safety of oral drug products. As such, extensive effort has gone into characterizing and reproducing the physiochemical properties of the gastrointestinal environment as a basis for *in vitro* dissolution testing. This is well intended to support dissolution testing as a convenient surrogate test for *in vivo* biopharmaceutical performance. However, both the absolute rate and extent of dissolution *in vivo* difficult to define and the *in vitro-in vivo* relationships between dissolution and plasma profiles can be difficult to define. Therefore, it is difficult to conclude whether an *in vitro* dissolution is reflective of an oral drug product's *in vivo* performance.

Quantification of both the rate and extent of dissolution in different regions of the gastrointestinal (GI) tract would provide a valuable reference for designing and calibrating *in vitro* dissolution tests to better reflect *in vivo* biopharmaceutical performance. However, direct quantification of *in vivo* dissolution rate and extent in the human body is currently unfeasible due to technological limitations and as such, an indirect method such as a computational method must be used to estimate *in vivo* dissolution.

Deconvolution methodologies such as the Wagner-Nelson and Loo-Riegelman have been used to estimate rate of absorption and used in support level A *in vitro-in vivo* correlations (IVIVC) (48-50). Application of deconvolution can further be applied to mechanistic models. For example physiologically based pharmacokinetic (PBPK) models have demonstrated potential

to bridge the dissolution and absorption gap and establish improved IVIVC (51). However, the complexity of the system requires the use of factors such as time scaling/time shifting and absorption time cut-offs to successfully deconvolute plasma profile (52). While the use of these models can predict an extent of release and a local drug concentration in various regions of the GI tract, the limited validation of the gastrointestinal compartments is unable to provide confidence in prediction.

There have been many efforts to further clarify the GI environment and the resulting *in vivo* dissolution. GI fluid has been quantified by MRI and a dynamic model that integrates these results has been developed. Intubation based clinical studies have experimentally observed human *in vivo* GI concentration samples. These clinical studies provide a new reference perspective for the consideration and application of computational models regarding the human gastrointestinal environment.

The Expanded Dynamic Fluid Compartment Absorption and Transport (EDFCAT) integrates the original model's characterization of human *in vivo* GI fluid transport and expands the conceptualized compartments to include the three different drug phases of solids, particles, and dissolved drug (53). The *in vivo* dissolution profile of an 800mg ibuprofen tablet was determined by deconvolution of the observed plasma profile using EDFCAT and a computational algorithm based on a least residual approach. Extent of regional dissolution was determined through a deconvolution of individual plasma profiles tailored to unique gastric emptying times specific to ibuprofen appearance in plasma. The distribution of simulated *in vivo* GI concentrations was used to validate against the observed *in vivo* GI drug concentrations from a clinical study. In future applications, the use of deconvolution combined with the EDFCAT

can be used to estimate in vivo dissolution rate, dissolution location, dissolution profile and extent of dissolution.

Material and Methods

An expansion of the Dynamic Fluid Compartment Absorption and Transport model is detailed in this section to capture the essential components of drug disintegration, dissolution, and absorption (53). The model consists of 126 nonlinear ordinary differential equations (ODE). The stomach is represented by four ODEs (solid dose, drug particles, dissolved drug and fluid) with the small intestine represented by 120 ODEs representing a 30-compartment model. Systemic circulation is represented with a central body and peripheral compartment. An illustration of the proposed compartment model and avenues of transport is drawn in Figure 11.

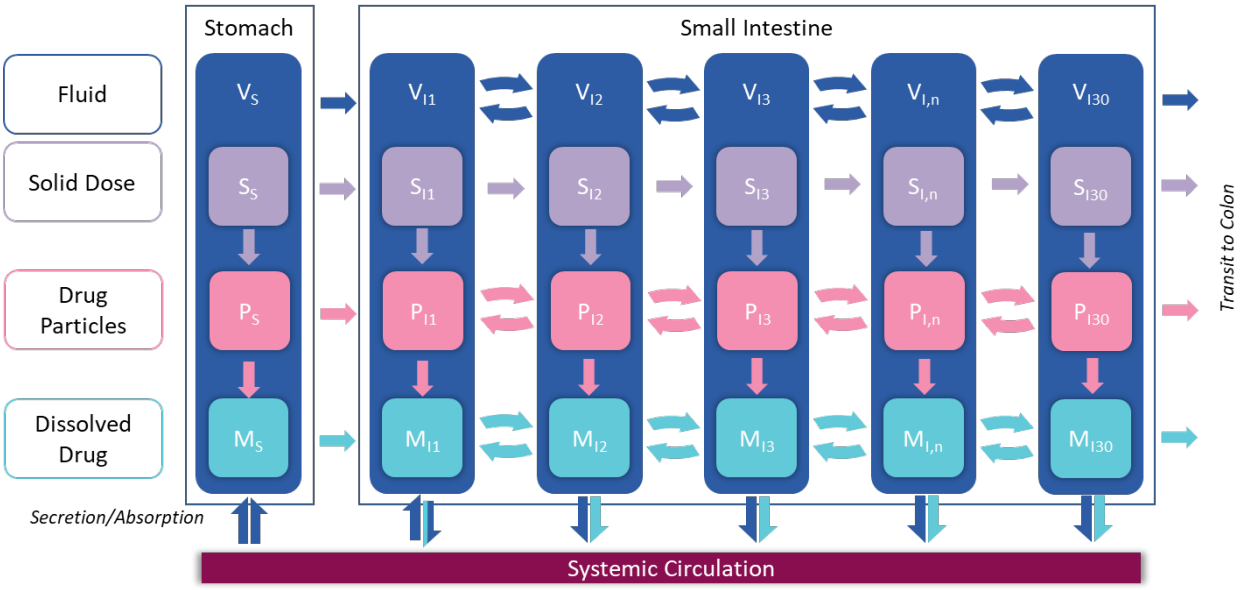

Figure 11. Dynamic Fluid Compartmental Absorption and Transit (DFCAT) approach with drug disintegration and dissolution

Matlab 2017a was used for both the simulation of model ODEs and the prediction of rate coefficient parameters. A fixed step ODE solver from the Simulink Package (ODE4) was used in 1s intervals. Visualized data graphics were rendered using Matlab's plot packages.

Pharmacokinetic fitting was conducted using Phoenix 64 Build 6.3.0.395 WinNonlin version 6.3 by Pharsight.

Experimental Data

The experimental data modeled is from an intubation based clinical study conducted at the University of Michigan (54). Study volunteers were fasted prior to dosing and rested for three hours after intubation. Each study volunteer was then administered an 800 mg immediate-release (IR) ibuprofen tablet (Dr. Reddy's Laboratories Limited (Shreveport, LA; IBU™ – Ibuprofen Tablets, USP, 800 mg, Lot number L400603) and phenol red in water (100 μg/mL). GI samples were obtained from the intubation tubes at specified time points and ibuprofen was quantified by LC-MS/MS. Plasma samples were drawn from blood and quantified by LC-MS/MS. The protocol of the clinical study and detailed information about the LC-MS/MS method are shared by Hens et al (55).

Determining Thermodynamic Equilibrium Solubility of Ibuprofen in Fasted State Human Gastric and Intestinal Fluids

The thermodynamic solubility of ibuprofen was determined by the shake-flask method (25 RPM). Gastrointestinal fluids were incubated for 24 h with an excess amount of ibuprofen (Acros Organics, New Jersey, NY) at 37°C. The fluids that were used for measuring the thermodynamic solubility of ibuprofen were aspirated gastric, duodenal and jejunal fluids of three different time points of subject B005-F2 (56). Following the 24 h incubation, samples were centrifuged for 15 min at 17,000 g (AccuSpin Micro 17, Fisher Scientific, Pittsburgh, PA). The supernatant was diluted 10-fold with methanol (Fisher Scientific, Pittsburgh, PA) and again centrifuged for 5 min in order to discard any proteins that could interfere with the HPLC analysis

Solubility samples were analyzed by HPLC-UV (Hewlett Packard series 1100 HPLC Pump combined with Agilent Technologies 1200 Series Autosampler). A volume of 5 µL was injected into the HPLC system connected to a UV-lamp that was able to detect ibuprofen at a wavelength of 220 nm (Agilent 1100 Series UV lamp). An isocratic run containing 70% acetonitrile (VWR International, West Chester, PA) and 30% purified water (both containing 0.1% trifluoroacetic acid (TFA; Fisher Scientific, Pittsburgh, PA)) was used to detect ibuprofen at a retention time of 2.9 min using a reversed-phase C-18 column (Eclipse Plus C18, 4.6 x 150 mm, 5.5 µm, Agilent Technologies) and a 1 mL/min flow rate. The calibration curve was made in methanol based on a stock solution of ibuprofen in methanol (1 mM). Linearity was observed between 10.32 µg/mL and 0.32 µg/mL. The observed peaks were integrated using ChemStation software (Agilent Technologies). The developed analytical method met the FDA requirements for bioanalytical method validation.

Determining Pharmacokinetic Parameters for Deconvolution

Deconvolution of plasma profile requires a mathematical conceptualization for the system of interest. A two-compartment model is used to characterize the bio-distribution of ibuprofen in the body with one compartment representing a central and the other as the peripheral compartment. By fitting the plasma profile of intravenous infusion of 800mg dose of ibuprofen to a two-compartment based pharmacokinetic model, pharmacokinetic parameters (k_{12}, k_{21}, k_e) can be obtained (57). The drug absorption rate constant (k_a) was obtained by utilizing the pharmacokinetic parameters obtained and fitting the solution dosing based on the clinically observed plasma profile after a 420mg solution dose of ibuprofen using the DFCAT model (58, 59).

Model verification criteria was based on the experimentally observed ibuprofen plasma concentration profile. If the algorithm could determine the appropriate dissolution rate, the simulated plasma profile would align closely with experimental observations. Model validation criteria was based on the experimentally observed ibuprofen GI drug concentration profile. The mechanistic deconvolution of ibuprofen dissolution from plasma profile results in a simulated continuous model of fluid, dissolved drug, drug particles, and solid drug in the GI tract. If the resulting local GI concentration profiles are reasonable, the simulated GI concentration profile would align closely with experimental observations.

Determining *in vivo* Dissolution Rate Using Deconvolution Based Algorithm

Dissolution was assumed to be the limitation factor in the absorption of ibuprofen from the GI tract. The dissolution profile was obtained with an algorithm (Figure 12) that determine the necessary dissolution rate coefficient based on the least residual difference between simulated and experimentally observed plasma concentrations. Linear interpolation was used to determine a continuous plasma profile between experimental time points as Area-Under-the-Curve (AUC) is traditionally determined by trapezoidal rule.

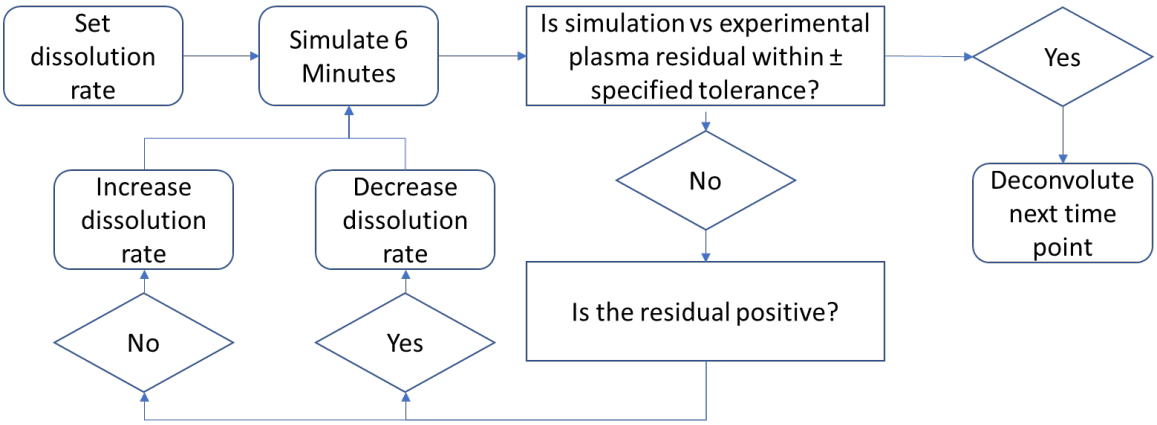

Figure 12. Residual based mechanistic deconvolution algorithm based on the DFCAT model.

Determining Individual Variability Based on Inflect in Plasma Profile

Individually observed plasma profiles in the clinical study were typically observed to be low until a certain time had been reached (t_{lag}). This time varied between individuals with an average of 82 minutes. Upon reaching this time, the observed plasma profile increased at a significant rate. Based on ibuprofen's classification as a BCS Class IIa drug, it is reasonable to associate this behavior with gastric emptying. This is supported by the physiological understanding where motility is linked with extra pancreatic secretions to neutralize incoming stomach acid (60). To best determine the rate and extent of dissolution *in vivo* that is representative of actual rather than averaged behavior, each observed plasma profile was assigned a t_{lag} based on the observed inflection time. Estimation of regional dissolution was dependent on a point of inflection (second derivative) or a notable visual increase plasma profile which was assumed to reflect the event of a stochastic gastric emptying event. Individual gastric emptying rates were adjusted to match the limited absorption and a corresponding differential equation term was developed to approximate complete gastric emptying. Individual dissolution profiles were then deconvoluted from each fasted volunteer's plasma profile. All pharmacokinetic parameters were assumed to remain identical with volume of distribution being the primary variable that differentiates individuals.

Model Verification and Validation

To evaluate model cogency, a series of model verification and validation checks conducted with figure xx describing the overall approach. The dissolution profile over time is determined by deconvoluting the plasma profile using the EDFCAT model. A model verification check is conducted by comparing the resulting simulated plasma profile with the experimentally observed plasma profile. As the observed plasma profile is not a continuous measurement but rather distinct temporal observations, an interpolation method can be used to draw continuous

linear lines from one time point to the next. As the mechanistic model also simulates the distinct local GI concentrations, a validation check can be conducted based on comparing the simulated GI concentration with the experimentally observed GI concentrations. This was based on the duodenum being compartment 1, jejunum being compartments 2-13 and the ileum being the remaining 14-30 compartments. The compartment assignments were analogous to the physiology of the GI tract based on 21cm per compartment assignments.

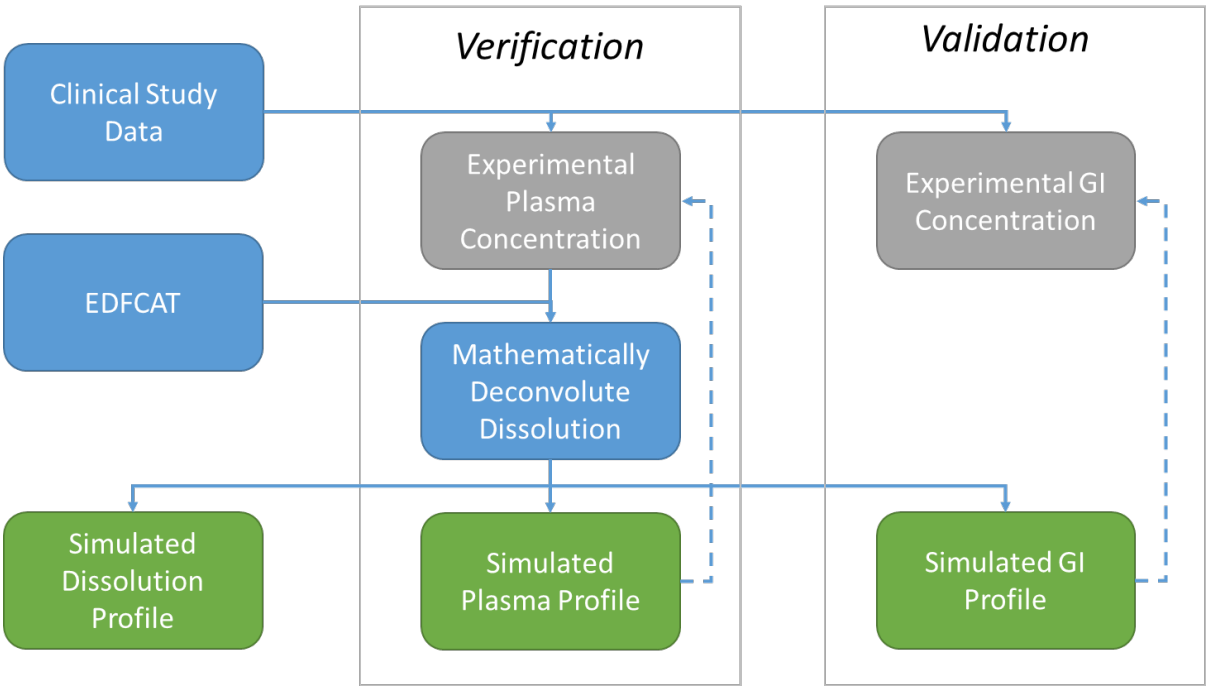

Figure 13. Overview of Conducted Verification and Validation in Developing a Prediction of in vivo Dissolution.

Equations

Disintegration of Solid Dose into Particles

The disintegration of solid dose into drug particles was assumed to have a minimal effect on oral absorption of ibuprofen based on the immediate release formulation used. The solid dose was assumed to disintegrate and rapidly and completely by reference time T_{ref}. Based on this assumption, disintegration can be represented by a hyperbolic tangent function (Equation 12).

$$\frac{1}{2} * \tanh\left(\frac{T-T_{ref}}{5} + \frac{1}{2}\right) * 0.1 * S_n) \quad (12)$$

Where T_{ref} is the referenced time of complete disintegration and S_n is the amount of dose in the solid dosage form.

Forward Transit of Solid Dose

Like existing models, the transit of solid dose was modeled to occur based on set points in time. To provide a continuous function for the solving of ordinary differential equations, a hyperbolic tangent was used to define the timing of the transfer of solid dose from one compartment to the next (Equation 13).

$$\frac{1}{2} * \tanh\left(\frac{T-T_{transit}}{5} + \frac{1}{2}\right) * 0.1 * S_n) \quad (13)$$

Where $T_{transit}$ is the reference time for the transit of solid from the and S_n is the amount of drug as in solid form.

Transit of Particles in the Gastrointestinal Tract

Transport of drug particles was characterized by disintegration from solid, dissolution into solution, and transit through the GI tract. Transit of particles is assumed to be completely analogous to transit of dissolved drug and is represented by equation 14.

$$dP_{\text{transit}} = k_{T,F|R} * P_n * \frac{V_n}{V_b+V_n} \quad (14)$$

Where $k_{T,F|R}$ is the rate coefficient for forward and reverse transit as determined in the DFCAT model, P_n is the amount of drug in particle form in compartment n, V_n is the volume of the compartment n, and V_b is the mucus volume. Mucus volume was assumed to not affect the general transport dynamics of drug particles and as such, this equation conceptualizes the drug particles instantaneously equilibrium distribution between fluid and mucus volume.

Dissolution of Particles into Solution

As disintegration was assumed to be completed rapidly, dissolution from particle into solution becomes the limitation factor to drug absorption. The dissolution of drug particles into solution was represented by a modified Nernst-Brunner equation (Equation 15) (25) .

$$\frac{dm_n}{dt} = k_{diss}(t)(C_S - C_n) \quad (15)$$

Where k_{diss} is the first order dissolution rate coefficient, C_S is the maximum *in vivo* solubility determined experimentally, and C_n is the concentration of the compartment. The use of a temporal first order coefficient $k_{diss}(t)$ was used to represent temporal changes in dissolution and as a modifier of dissolution rate for deconvolution. This approach has been previously explored in Margolskee *et al* (61). In comparison with the Nernst-Brunner dissolution equation, this temporal coefficient serves as an approximation of the diffusion coefficient, surface area, and thickness of the boundary layer.

Continuous Gastric Emptying Term Based on t_{lag}

To simulate gastric emptying based on a t_{lag}, a double hyperbolic tangent equation was applied to provide an approximation of a binary situation (Equation 16). In the provided equation, if:

$t < t_{lag}$: $\frac{dm_n}{dt} = 0$

$t_{lag} < t < t_{lag}+10$: $\frac{dm_n}{dt} = 1$

$t > t_{lag}+10$: $\frac{dm_n}{dt} = 0$

A total possible gastric emptying time of 10 minutes was assumed based on phase III migrating motility complex.

$$\frac{dm_n}{dt} = \left(\frac{1}{2} * \tanh\left(\frac{T-10-T_{ge}}{0.01}\right) - \frac{1}{2} * \tanh\left(\frac{T-T_{ge}}{0.01}\right)\right) * m_n \quad (16)$$

Results

Determining 2-Compartment Pharmacokinetic Parameters

Pharmacokinetic parameters were determined based on a 2-compartment infusion using Winnonlin. The determined pharmacokinetic parameters are as follows: k_{10} is 0.013min^{-1}, k_{12} is 0.047min^{-1}, k_{21} 0.069min^{-1}, and Vd=5.32L. A graph of the fitted compartment model is shown in Figure 14a. The adoption of the 2 compartment pharmacokinetic parameters used in the DFCAT approach to model the resulting plasma profile. A range of absorption terms were simulated with the lowest residual difference between simulation and experimental plasma profile determining the absorption rate. The absorption rate coefficient of ibuprofen was determined to be 3 min^{-1}. A graph of the comparison between simulation and experimental solution dosing is shown in Figure 14b.

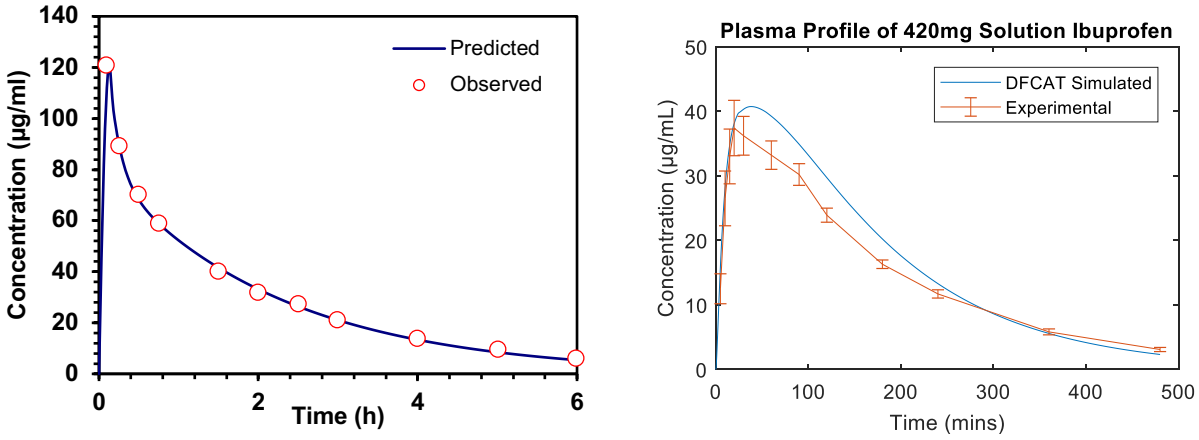

Figure 14. (a,left) Fitted two compartment pharmacokinetic model based on 800mg IV infusion. (b,right) Fitting the absorption rate value based on 420mg solution dosing IV determined pharmacokinetic parameters in the DFCAT model.

Quantifying Solubility in Human Gastrointestinal Fluids

The *in vivo* solubility of ibuprofen was determined to be low at pH <3.5 at roughly 55 µg/mL. The solubility increases at higher pH's reaching a solubility of 1990 µg/mL at pH 6.2. An illustration of thermodynamic solubility of ibuprofen over a range of pH values based on human intestinal fluid samples is shown in Figure 15. A study conducted by Heikkila et al. also observed an ibuprofen thermodynamic solubility to be 1990 µg/mL in fasted human intestinal fluid (62).

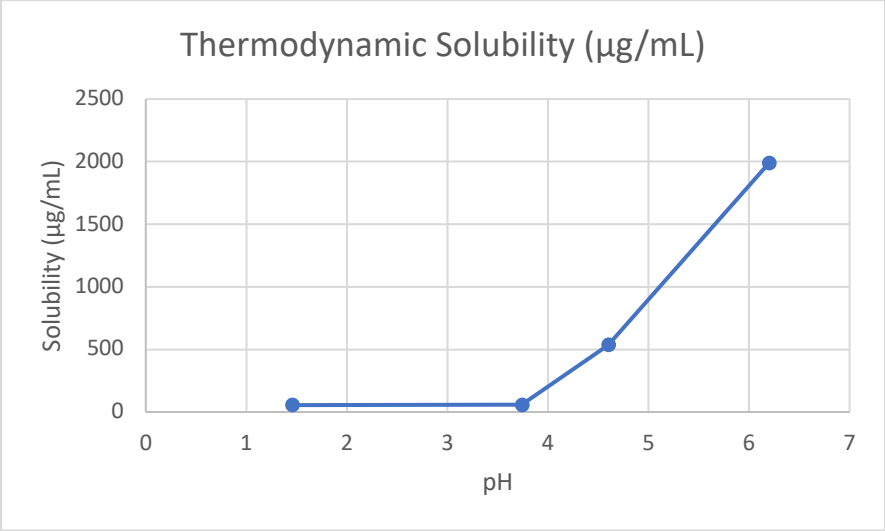

Figure 15. Experimentally determined thermodynamic solubility profile of ibuprofen based on human gastrointestinal fluids

Predicted Dissolution and Model Verification with Average Plasma Concentration Profile

The deconvolution algorithm was set to ±0.5µg/mL tolerance check at every six minutes. Based on this criterion, the algorithm could successfully determine a dissolution rate coefficient to simulate a plasma concentration profile similar to the experimental profile (Figure 16). Slight variation as evident around the 200-minute time point is minor and could be reduced by tightening the min-max of the allowed residual bounds.

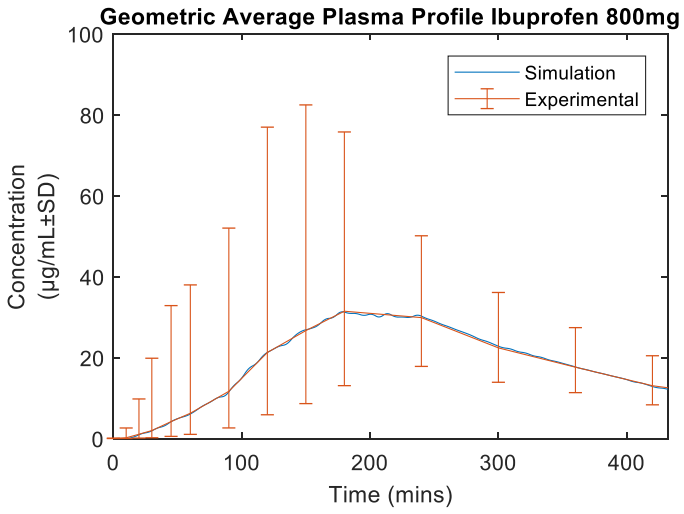

Figure 16. Comparison of simulated vs experimental ibuprofen plasma concentration profile based on mechanistic deconvolution using the DFCAT model.

Predicted Dissolution and Model Verification of Individual Plasma Concentration Profile

The deconvolution algorithm was applied to each individual plasma profile identical to the approach used for the average plasma profile. Based on this criterion, the algorithm could successfully determine a dissolution rate coefficient that was necessary to simulate the plasma concentration profiles (Figure 17). Table 4 references each individually estimated t_{lag} and the amount that was determined to have dissolved by the estimated t_{lag}.

Table 4. Estimated Dissolution Between Upper and Lower Regions of the Small Intestine

ID	TLAG	PRE-TLAG DISSOLUTION (MG)
1	60	16.6
2	150	42.4
3	150	193
4	60	147
5	60	45.9
6	90	83.2
7	90	26.4
8	12	0
9	90	42.6
10	150	104.6
11	180	90.8
12	60	65.5
13	12	0
14	60	21

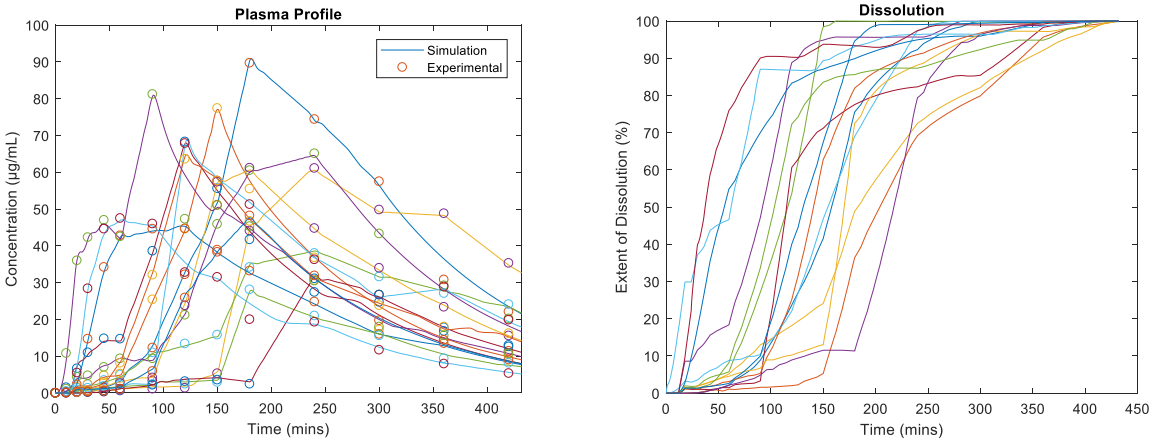

Figure 17. (left) Deconvolution algorithm fitting based on individual plasma profiles. (right) Deconvolution profiles based on individual plasma profiles

Predicted Rate and Extent of *in vivo* GI Dissolution

The mechanistic nature of the EDFCAT model resulted in the following dissolution profiles when the temporal dissolution rate coefficient was obtained (Figure 18). The stomach had a small amount of total dissolution (<4%).

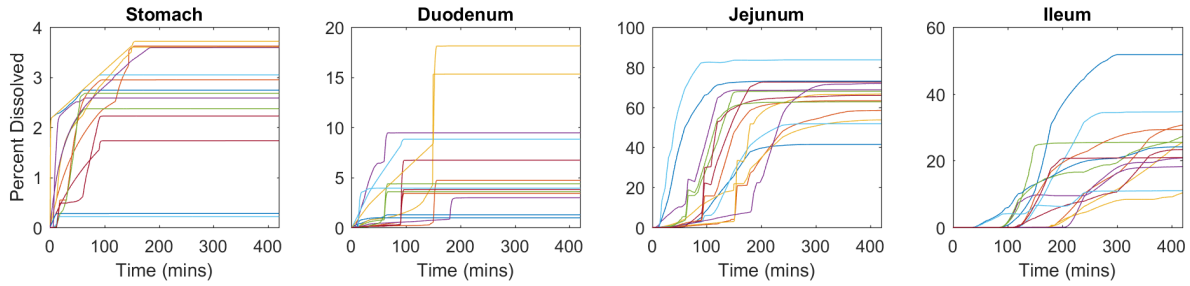

Figure 18. (left) Deconvolution algorithm fitting based on individual plasma profiles. (right) Deconvolution profiles based on individual plasma profiles

Based on the assumption that complete emptying of the gastric contents occurs at the tlag timepoint, the amount of dissolution in the stomach region clearly ceases as there is no remaining undissolved content in the stomach. Dissolution behavior in the duodenum is similarly defined by the tlag time where a significant increase in the amount dissolved occurs. In most individuals, it was predicted to be a sharp increase in dissolution which ceased due to transit away from the duodenal region. This varied significantly between individuals ranging from around 1 to 18 percent of the total 800mg ibuprofen dissolving. The jejunum was predicted to be the largest site of dissolution where roughly 40 to 82% of the drug dissolved was predicted to dissolve. Analogous to the stomach and duodenal regions, dissolution in the jejunum is reflected by the tlag time. Individual comparisons between the different individuals found a similarity amongst the different dissolution profiles regarding the slope. It is likely that the rate of dissolution *in vivo* is similar amongst many individuals and is reflected by the gastric emptying event. Based on the assumption that ibuprofen has nearly complete bioavailability, the ileum was found to contribute

varying degrees to the extent of ibuprofen dissolution. In absolute terms, this ranged from 10 to 52% of the ibuprofen's overall 800mg active pharmaceutical ingredient. The two highest percent dissolution in the ileum (35 and 52%) corresponded with the two individuals who had the shortest t_{max} in the observed plasma profile.

Model Validation Based on Observed GI Concentration Profile

The deconvoluted model simulation results in an *in vivo* GI profile similar in magnitude to the experimental profiles (Figure 19). Geometric mean and 90% geometric confidence intervals were used to observe the overall tendency of the GI concentrations due to the large observed variations in the GI. Previous studies hypothesize that this large variation can be explained by the lack of homogeneity in the local GI region (63). Large experimental concentrations variations could also be related to local GI solubility differences from GI secretions such as bile. Additional differences in GI concentration between simulation and experimental were expected as the fluid, pharmacokinetic, and GI sampling were all separate clinical studies. The model was evaluated on whether the general trend of observed GI concentration could be reproduced using deconvolution to determine *in vivo* dissolution and as such, appear as a realistic model.

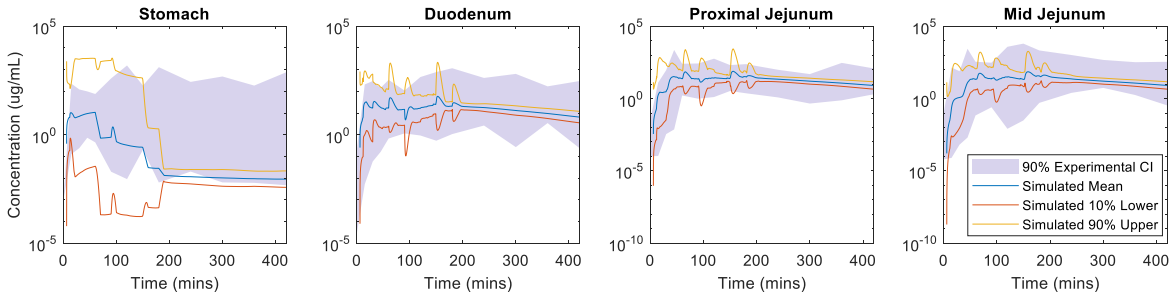

Figure 19. Comparison of simulated vs experimental ibuprofen GI concentration profile based on mechanistic deconvolution using the DFCAT model.

Average Predicted *in vivo* Dissolution Profile

The resulting simulation based on the predicted *in vivo* dissolution rate and the use a compartmental approach provides a quantifiable amount of drug released in different regions of the GI tract. The average and 90% confidence interval of the individual predictions were calculated and are presented in Figure 20.

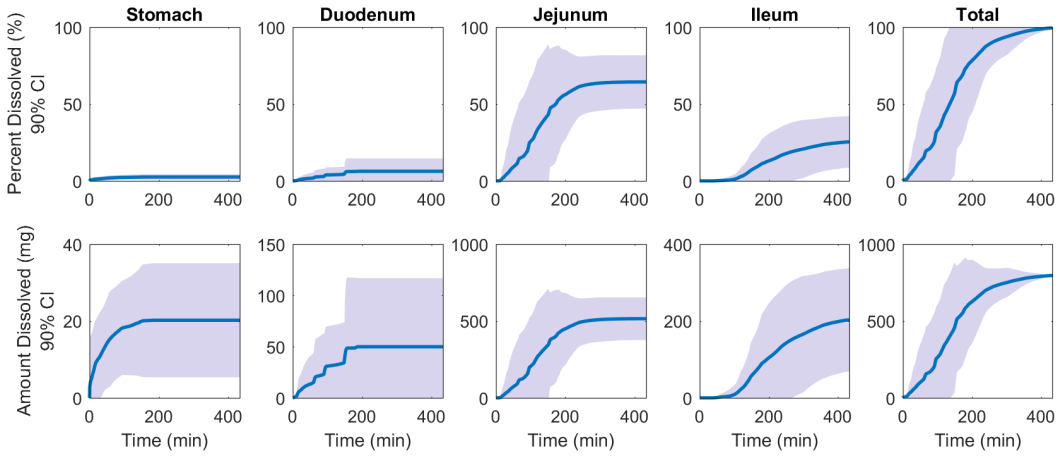

Figure 20. Predicted in vivo percent dissolved and mass dissolved of ibuprofen over time.

On average, stomach was calculated to contribute minimally to the overall dissolution of ibuprofen (2%). This is consistent with expectations that there would be limited dissolution in the stomach due to pH . The duodenal environment was calculated to contribute more than double the stomachs with a total of 6.3% dissolving. This is also consistent with expectations that dissolution is increased due to the higher pH but overall dissolution is limited as due to the small residence time of GI content in the duodenum. The jejunum was calculated to be the primary site of dissolution with a total of 63% of ibuprofen dissolving in this region over a 210-minute period on average. This long dissolution time frame likely reflects the significant variability regarding the lag time for gastric emptying. The dissolution in the ileum (25%) was

calculated to begin after a lag time that likely reflects a combination of both gastric emptying and transit times.

Discussion

Physiologically based *in silico* models have often combined *in vitro* dissolution and absorption experiments with *in vivo* physiological parameters to create a dynamic representation of the *in vivo* oral absorption process (61). Because the *in vivo* GI environment differs significantly from current *in vitro* models, there is a high possibility for a poor estimation of physiological performance such as *in vivo* drug solubility. A phosphate buffer (pH 1.2, 4.5, 6.8, 7.2) prepared accordingly to USP 30 determine ibuprofen solubility to be 2.1, 5.1, 5.57, and 5.86 μg/mL respectively (64). This contrasts significantly with the thermodynamic solubility experiment conducted based on fluids obtained from the human gastrointestinal tract. In this study, the solubility was observed to be 55, 58, 535, and 1990 μg/mL with a corresponding pH of 1.5, 3.7, 4.6, and 6.2 respectively. This is an order of magnitude difference in solubility with 26 times the solubility at low pH levels and 357 times at higher pH. As many implementations of the dissolution equation utilize a solubility term, it is critical to ensure that the solubility used is representative of the true *in vivo* solubility of a drug compound.

By applying a deconvolution method to a mechanistic system, the model is also simultaneously able to solve for the total dissolution profile. Because many aspects of the model design such as fluid transport and plasma for deconvolution are from mean values or central tendencies, the solved total dissolution profile is representative of an average basis. This suggests that dissolution profile averaged across many individuals in the clinical study is likely not representative of exact *in vivo* performance but rather an approximation of overall expectations with roughly 70% dissolved around 200 minutes and 90% around 350 minutes.

The simulation predicted an average basis of dissolution for each region with a total of 16, 37, 508, 188 mg dissolving in the stomach, duodenum, jejunum, and ileum respectively. The predictions regarding stomach and duodenum align with expectations regarding regional drug dissolution. While the gastric environment was not anticipated to be a major site of dissolution due to the limited solubility at low pH, the model calculated a total dissolution of 16 mg on average. The duodenum was also not expected to be a significant contributing site due to its proximity to the stomach, the lower pH, and the limited residence time for transit. As such, the observed 37mg total dissolution on average is reasonable when compared with the stomach. In comparison, over half of the ibuprofen oral drug product was calculated to dissolve in the jejunum with the remainder dissolving in the ileum. This is consistent with the observation that bioavailability of all ibuprofen formulations (100-800mg) are high.

When examining individual dissolution profiles, mechanisms such as the secretomotor complex where gastric emptying is accompanied by extra pancreatic secretions is evident (60). In the individually based simulations conducted, a significant increase in plasma profile was conceptualized using a gastric emptying lag time. The resulting simulation determined high rate of dissolution for ibuprofen upon conclusion of the gastric emptying lag time. In a few individuals where sufficient time had elapse, a second gastric emptying event was observed followed by a period of increased dissolution/increase in plasma profile. Given the small increase and the complexity in modeling a second gastric emptying event based on the method used, the modeled application was restricted to a singular gastric emptying event. In general, fluid transport was found to becomes less variable after 30 minutes. As such, the use of individually based deconvolution can be a reasonable estimate of *in vivo* dissolution performance. This is

further supported by approximately parallel slopes of the *in vivo* dissolution profile across multiple individuals.

In conclusion, the applicability of the approach developed to predict *in vivo* dissolution should be considered based on a weight-of-evidence approach and based on physiochemical interactions with drug properties. With the use of validation to evaluate the simulated *in vivo* concentration profiles, the model is a potentially strong approximation of *in vivo* behavior. With future studies and methods providing additional data such as the GI concentrations used in this model, additional improvements in both *in vitro* study considerations and the *in silico* oral absorption models can be used to guide further research and experimental design.

Chapter 4 Direct Measurement of Three Mesalamine Formulations in the Human Gastrointestinal Tract to Evaluate In Vivo Solubility, Absorption, and Transit[2]

Inflammatory Bowel Disease (IBD) such as Ulcerative Colitis (UC) and Crohn's disease affects approximately 1.6 million Americans with as many as 70,000 new cases diagnosed each year (65). Mesalamine (mesalazine) is commonly used to treat mild to moderate UC by presenting drug locally in the gastrointestinal (GI) tract at the site of inflamed mucosa (66, 67). To achieve high local concentration and minimize absorption in the GI tract, mesalamine oral drug products are designed with modified-release (MR) technology to delay drug release and delivery in GI tract to maximize local therapeutic effect and limit systemic exposure (68, 69).

Currently approved mesalamine formulations in the U.S. for the treatment of UC fall into three major design strategies: delayed release (Pentasa), pH-dependent release granules (Apriso), and multi-matrix release (Lialda). Pentasa consists of microspheres encapsulated with an ethylcellulose semi-permeable membrane which allows for time and moisture dependent release (70). This allows for the formulation to distribute gradually throughout the GI tract (71). The Apriso capsule contains Eudragit L resin on each granule which is a pH sensitive polymer that disintegrates at pH greater than 6 (72). The polymer matrix for each granule swells to release

[2] Reprinted (adapted) with permission from Alex Yu, Jason R. Baker, Ann F. Fioritto, Ying Wang, Ruijuan Luo, Siwei Li, Bo Wen, Michael Bly, Yasuhiro Tsume, Mark J. Koenigsknecht, Xinyuan Zhang, Robert Lionberger, Gordon L. Amidon, William L. Hasler, and Duxin Sun. Mol. Pharmaceutics, 2017, 14 (2), pp 345–358. DOI: 10.1021/acs.molpharmaceut.6b00641. Copyright (2017) American Chemical Society

mesalamine. Lialda contains a more stringent Eudragit S resin which disintegrates at pH >7 and is made in a Multi-Matrix System (MMX) which contains additional lipophilic and hydrophilic matrices (73). These formulations are expected to have different GI regional-dependent release, leading to different clinical pharmacokinetics and efficacy.

Clinical studies have shown that different mesalamine formulations have a large degree of inter-individual pharmacokinetic variability [C_{max}, T_{max}, Area Under the Curve (AUC), and fecal excretion] for both healthy subjects as well as patients with active and inactive UC (74, 75). When Pentasa (1g), Apriso (1.5g), and Lialda (1.2g) were dosed in colitis patients in three separate clinical studies, plasma exposure varied with AUC_{0-n} of 4.4±1.8, 11±5, and 9±5 µgh/mL and a C_{max} of 0.99±0.53, 2.1±1.1, and 0.86±0.64 µg/mL respectively (76-78). The large variation in AUC is accompanied by an equally large variation in T_{max}; Pentasa (3.5±1.8h), Apriso (2-16h), and Lialda (4-32h). A further complication of the variable pharmacokinetic properties between different formulations is that the various studies use a different dose regimen (ie. 4x 250mg vs. 2x 500mg Pentasa) which further confounds comparability of pharmacokinetic results.

While efficacy has been proven in induction and maintenance of remission in patients with UC (79, 80), comparisons between different clinical studies have been difficult due to each study utilizing its own criteria in evaluating mesalamine efficacy. For example, one study concluded Asacol (2.4g/day) had 49% of patients improving after 5 weeks of treatment based on physician global assessment versus 23% placebo (81). Another study concluded Asacol (2.4g/day) achieved a 33.7% clinical remission rate versus 22.1% placebo in colitis patients after 8 weeks (82). Comparing these two studies, the treatment endpoint varied and the assessment of colitis severity likely varied between physicians. The global assessments are based on the

severity of the condition by a physician with the disease activity accessed as quiescent, mild, moderate or severe. There has been a lack of formulation comparison studies. A clinical study involving a 2g daily dosing of Pentasa concluded 29% of patients achieved remission by physician global assessment compared with 12% from placebo after 8 weeks (83). Lialda (2.4g/day) and Asacol (2.4g/day) achieved a 41.7% and 33.7% clinical remission rate, respectively, versus 22.1% placebo in colitis patients after 8 weeks in a comparison study (82). This difference in baseline placebo remission may be a result of a variety of study differences such as, but not limited, to baseline level of the disease and endpoints assessed.

Meta-analysis of literature data have generally found oral 5-ASA products to be more effective than placebo in induction and maintenance of remission of UC with similar remission rates (84). A comparison study between pH-dependent release and time-release mesalamine formulations reported no difference in induction of remission (85). While cross study analysis can be conducted, head-to-head comparison is not conclusive to determine whether one formulation is superior in clinical efficacy to another as study methods differ(66, 82, 86-90). Further, it is unclear whether different mesalamine formulations will have different efficacies in IBD patient subgroups. Furthermore, it is not known if mesalamine in systemic circulation can be used as an indicator of efficacy or even formulation GI release behavior. While a direct comparison of mesalamine concentration in the GI between different formulations would be ideal, there are no reported results regarding the GI concentration of mesalamine from each formulation in the GI tract.

The lack of critical results simultaneously measuring local drug release and drug dissolution in the GI tract and plasma levels, creates uncertainty in determining whether these locally-acting mesalamine formulations have clinically relevant differences and whether these

drug products are clinically interchangeable. It is thus difficult to assess the bioequivalence of generic drug products for locally acting mesalamine products. Current bioequivalence (BE) standards oral drug products for a majority of systemic delivery are well-established and well-validated using plasma C_{max} and AUC. However, whether the use of plasma pharmacokinetics can be used to ensure BE for locally-acting gastrointestinal drugs has been debated over the past many years (91-93). BE for locally acting GI drug products would ideally correlate with the drug's local GI availability.

The aim of this study was to conduct a human GI intubation clinical study to directly measure mesalamine levels (release and dissolution) for three different formulations (Pentasa, Apriso, and Lialda) in different regions of the human GI tract (stomach, duodenum, jejunum, ileum); and to estimate mesalamine content in colon by measuring mesalamine and metabolite excretion in feces; and finally to investigate the relationship between plasma concentration-time profiles and drug concentration-time profiles in the GI tract. These results will provide a direct scientific basis for using pharmacokinetic plasma endpoints to evaluate the bioequivalence of locally acting drug products in the GI tract where local in vivo dissolution directly impacts the efficacy of the drug product.

The aim of this study was to conduct a human GI intubation clinical study to directly measure mesalamine levels for three different formulations (Pentasa, Apriso, and Lialda) in different regions of the human GI tract (stomach, duodenum, jejunum, and ileum) to evaluate *in vivo* solubility, the dissolution of these mesalamine products based on traditional deconvolution, and the contribution of GI transit. These results will provide a direct scientific basis to improve mechanistic oral absorption models by integrating *in vivo* drug solubility, prediction of absorption rate, and the contribution of GI transit variability.

Materials and Methods

Materials

Pentasa (500 mg capsule, Shire US Inc., Wayne, PA), Apriso (375 mg capsule, Salix Pharmaceuticals, Inc., Raleigh, NC) Lialda (1200 mg tablet, Shire US Inc., Wayne, PA) were purchased through the Investigational Drug Service (IDS) of the Department of Pharmacy at the University of Michigan Health System. The solution of mesalamine (100 mg/125 mL) was prepared by dissolving the crushed mesalamine tablet from Delzicol (400 mg capsule, Warner Chilcott (US), LLC, Rockaway, NJ) in water. The intubation tube was custom designed by the study team and manufactured by Arndorfer Inc., Greendale, WI.

Clinical Study

Male and female subjects between the ages of 18 and 55 years were eligible for inclusion into the study. The body mass index (BMI) requirement for healthy subjects was BMI 18.5 to 35. Exclusion criteria included adults unable to consent for themselves, prisoners, clinical illness within 3 weeks, concomitant medication use, history of gastrointestinal surgery, allergy to non-steroidal anti-inflammatory drugs (NSAIDS) or the mesalamine formulations (Pentasa, Apriso, Lialda, Delzicol), drug allergies, history of drug addiction or alcohol abuse within 12 months, pregnant or lactating females, surgery within the past 3 months, investigational drug use within 60 days, or any clinically significant abnormal lab values during screening. All subjects were in good health as determined by medical history, physical examination, vital signs, electrocardiography, and clinical laboratory tests. The study protocol was approved by the institutional review boards (IRB) at the University of Michigan (IRBMED, HUM00053912) and the Food and Drug Administration IRB (also known as the Research Involving Human Subjects Committee or RIHSC, #11-072D). All subjects provided written informed consent to participate.

The study was carried out accordance with the protocol, International Conference on Harmonization Good Clinical Practice guidelines, and applicable local regulatory requirements.

Study Design

The study consisted of a Crossover Arm (modified release formulations) followed by a Single-Arm Treatment (oral mesalamine solution). Each participating subject completed at least one MR dosing with one of the three formulations assigned at random using block randomization. Upon completion of the first MR dosing, subjects could elect to participate with the remaining formulations chosen at random until all three formulations were administered. After successful completion of any MR dosing, study subjects could elect to complete the oral solution dosing arm. In the MR dosing, subjects received a dose of mesalamine (IIA: Pentasa (2x 500mg), IIB: Apriso (3x 375mg), IIC: Lialda (1x 1200mg)). Blood, intestinal fluid, and feces were collected for the MR treatment. In the oral solution dosing, study subjects received a single 100mg oral dose of mesalamine (i.e. crushed and dissolved mesalamine tablet given in water). After study drug administration, only blood, and feces were collected for the oral dosing group. Both mesalamine and its metabolite were quantified for each sample. pH values were also measured for intestinal fluid samples. A minimum of 10 days was used as the washout period between the studies.

Crossover Arm (MR dosing) Study Procedure

All clinical procedures were performed at the University of Michigan Hospital in the Michigan Clinical Research Unit (MCRU). The study subject was required fast for 4 hours prior to arrival at MCRU, the evening before study drug administration. A physical exam was performed by the study physician prior to GI tube insertion. To prevent gag reflex, study subjects

were administered a topical anesthetic (1mL of 4% lidocaine) before the tube insertion. The tube was lubricated with 2% lidocaine jelly or MediChoice® medical grade lubricating jelly. Then the tube was inserted orally into the GI tract.

Prior to inserting the GI tube, 5 mL of tap water was introduced in the subject's mouth. Next, the GI tube was placed on the subject's tongue and slowly advanced toward the subject's epiglottis. The subject was asked to swallow the water as the GI tube advanced beyond the upper esophageal sphincter. The subject performed dry swallows as the GI tube progressed toward the lower esophageal sphincter and intubated into the stomach. Subjects were instructed to execute reverberation sounds and coughs in combination with varying radiological positioning as the GI tube moved forward through the pylorus bypassing the Ligament of Treitz. Using gravity and Trendelenburg positioning, augmented by abdominal pressure, the GI tube was traversed through the small bowel anatomical regions. Finally, the balloon located at the distal end of the GI tube was inserted with 7-10mL of sterile water. The GI tube was taped loosely to the subject's chin using medical tape. The subject was encouraged to walk periodically around the medical procedures unit to allow antrum and small bowel peristalsis to migrate the GI tube further into the small bowel. Following a one-hour time mark, the subject underwent fluoroscopic imaging to verify final placement of the GI tube. The 7-10mL of sterile water was removed from the balloon and the GI tube was securely taped to the subject's chin using medical tape.

Abdominal fluoroscopy was conducted to ensure the GI tube was correctly placed. Fluoroscopy was performed by a radiology technologist. The radiation exposure time was limited to a maximum of 1.5 minutes for each Crossover Arm (the MR dosing arm) procedure by the use of the fluoroscopy machine in a pulse mode. The x-ray radiation was only delivered when a picture was taken. Since the fluoroscopy was not constant, this

limited the participant's radiation exposure. The study team monitored the total fluoroscopy time during each GI tube insertion procedure to ensure the maximum exposure time was not exceeded.

Study subjects were given a light liquid snack and then requested to fast overnight and until 7 hours post drug administration. Prior to dosing, an intravenous catheter was placed in the forearm vein of the subject and the GI tube placement was confirmed with fluoroscopy. Subjects were asked to empty their bladder, if possible, prior to study drug administration. At approximately 8:00 AM, the study subject ingested one of the three MR formulations of mesalamine accompanied by 240 mL of water.

Blood samples (5 mL each) were obtained at 0, 0.5, 1, 2, 3, 4, 6, 7, 8, 10, 12, 24, 48, and 72 hours following dosing. For Lialda dosing, an additional 96 hour blood sample was collected. Plasma was separated from blood samples and stored at -80^{o}C until processing. The subject was also provided a container for collecting feces. Collection occurred between 0-12, 12-24, 24-48, and 48-72 hours following dosing. For Lialda dosing, an additional 72-96 hour feces sample was collected. Feces samples were refrigerated until processing. Intestinal fluid samples were aspirated from the multi-luminal GI tube to obtain samples from the stomach, duodenum, and jejunum at 0, 1, 2, 3, 4, 5, 6, 7 hours following dosing. Approximately 0.5 mL of GI fluid was collected from each location of the GI tract at each time point. The pH of the GI fluid was measured *ex vivo* using a pH meter with a micro pH electrode (Thermo Scientific). The GI fluid samples were processed and stored at -80^{o}C until analysis. The supernatant was used for analysis.

At 7 hours post-dose, the GI tube was removed and the subject was served a standardized snack. At 10 hours post-dose, the subject was served a standardized meal. The subject remained

in the medical unit to facilitate blood and fecal collection until 12 hours post-dose. The subject was then discharged and asked to return for blood sample collection at 24, 48, and 72 hours post dose (as well as at 96 hours post-dose if Lialda is dosed). All samples were then transferred, prepared, and analyzed by the Pharmacokinetics Core at the University of Michigan College of Pharmacy.

Single-Arm (oral solution dosing) Study Procedure

A mesalamine solution was prepared by the pharmacist. A 400 mg Delzicol capsule was opened and the tablet inside the capsule was removed. The mesalamine tablet was crushed using a mortar and pestle. Then 500mL of water was added to the crushed tablet and stirred in a beaker for 30 minutes. Next 125mL was removed from the agitated solution for administration to the study subject. The study subject was instructed to fast from 10:00 PM to 8:00 AM. Upon arrival at MCRU, an intravenous catheter was placed in the forearm vein of the subject. The subject was administered the 100 mg dose of mesalamine in 125mL water followed by 120mL of water chase. Blood samples (5mL each) were obtained at 0, 0.25, 0.5, 1, 2, 3, 4, 6, 8, 10, 12, and 24 hours post-dose. Plasma was separated from blood samples and stored at -80^{o}C until processing. The subject received a standardized snack at 4 hours post-dose and a standardized meal at 10 hours post-dose. The subject was discharged at 12 hours and asked to return to the medical unit at 24 hours to collect the last time point. All samples were then transferred, prepared, and analyzed by the Pharmacokinetics Core at the University of Michigan College of Pharmacy.

LC-MS/MS Analysis of Mesalamine and its Major Metabolite in GI Fluid, Plasma, and Feces

Human plasma, GI fluid, and feces samples of mesalamine (5-ASA) and its metabolite (Ac-5-ASA) were analyzed by a validated LC-MS/MS assay under FDA validation guidelines. For feces samples, feces were assumed to have a density of 1g/mL. The total content of 5-ASA and Ac-5-ASA collected was estimated with the following equation:

$$M_{\text{5-ASA}} = C_{sample} * (V_{methanol} + M_{feces}/\text{Density})$$

For plasma samples, 5-ASA and Ac-5-ASA were directly extracted by protein precipitation method. Briefly, 100µL of plasma samples were precipitated by addition of 400µL of acetonitrile containing the internal standard (4-ASA). After thorough mixing, the samples were centrifuged for 7 min at 15000g under freezing condition. Then a 400µL aliquot of the supernatant was diluted with 600µL of 0.1% formic acid water in a new polypropylene tube and transferred into the autosampler. For GI fluid and feces samples, 10-fold dilution was obtained by mixing 10µL of the raw samples with 90µL of drug-free plasma, respectively. Once the GI fluid and feces samples were well-dispersed in plasma, the same sample preparation steps used in plasma preparation were carried out.

The quantitative LC-MS/MS analysis was conducted using a Shimadzu HPLC system coupled to an API 5500 mass spectrometer (Applied Biosystems, MDS Sciex, Toronto, Canada) equipped with an API electrospray ionization (ESI) source. Chromatography of 5-ASA, Ac-5-ASA and internal standard (4-ASA) was performed on a reversed-phase column (15 cm x 4.6 mm I.D., 3.5 µm, XBridge C18, Waters), eluted with a gradient solvent system consisting of 0.1% formic acid and acetonitrile, and monitored by mass spectrometer with a MRM method as

follows: the transition of m/z 152.0 to the production ion m/z 108.0 for both 5-ASA and 4-ASA, m/z 194.0 to the m/z 150.0 for Ac-5-ASA; all analyses were in ESI negative mode with the ion spray voltage set up at -4500V. Under these conditions 5-ASA, Ac-5-ASA and 4-ASA were separated within 6 min. The analyst software version 1.6.1 was used for evaluation of chromatograms.

Weighted linear regression (1/X) was applied for calibration in human plasma, GI fluid, and feces samples. Linearity of the calibration for both 5-ASA and Ac-5-ASA has been proven in human plasma over the range of 5 ng/mL to 2 μg/mL ($r > 0.99$), and in GI fluids and feces samples over the range of 50 ng/mL to 20 μg/mL ($r > 0.99$). Lower limits of quantification were identical with the lowest calibration levels. Inter-assay coefficient of variation (%CV) was between 2.5% and 11.7% for 5-ASA and between 2.6% and 5.6% for Ac-5-ASA, and the analytical recoveries of 5-ASA and Ac-5-ASA were respectively greater than 80.2% and 86.9% in plasma matrix. For human GI fluid and feces, the variation of the measured concentration from the nominal concentration was used as an indicator of the matrix effect. The results suggested that the matrix effect was insignificant for the %CV value was less than 15% at the given dilution factor.

Data Presentation and Deconvolution

Data analysis and visualization was conducted with the R 3.2.3 software package. Average plasma and GI concentrations were represented as mean ± standard error of the mean (SEM) based on all available samples. Pharmacokinetic parameters (C_{max}, T_{max}, and Area Under the Curve (AUC)) were reported as mean ± standard deviation (SD). Individual plasma concentrations, GI concentrations, and pH values were represented using different colors. Feces were represented as an accumulation of collected endpoint. Individual feces portrayal was

depicted per individual case and sorted per endpoint. Parent vs. metabolite based on transit was depicted using the final value of accumulated collection. Statistics was not calculated due to limited sample size.

Deconvolution was conducted using the Pheonix 64 Build 6.3.0.395 WinNonlin version 6.3 by Pharsight. The two compartment PK model with a lag time and first order absorption was used to calculate the baseline pharmacokinetic characteristics for each individual. The model's parameters were used to deconvolute the crossover study's plasma data to best estimate total absorption.

Results

Demographics of Human Subjects

As part of this study, 65 screening visits were performed. There were 30 eligible subjects who participated in a total of 38 MR dosing: 24 subjects participated in one MR dosing, 4 subjects participated in 2 MR dosing, and 2 subjects participated in 3 MR dosing.

Study subjects were randomized to receive one of three mesalamine formulations during the MR dosing (IIA: Pentasa, IIB: Apriso, IIC: Lialda). Out of 38 MR dosing conducted, there were 26 MR dosing successfully completed and 12 MR dosing that were discontinued. After successful completion of at least one MR dosing, subjects were eligible to participate in an oral solution dosing and a total of 20 oral solution dosing were conducted (and all completed). A summary of demographics of study subjects is presented in Table 5.

Table 5. Demographics of Study Subjects

Study Arm	**Number of Subjects Completed**	**Age (years)**	**Body Mass Index (BMI)**	**Sex**		**Race**			**Ethnicity**	
	N	Mean ± SD (Min-Max)	Mean ± SD (Min-Max)	Male	Female	Caucasian	African-American	Asian	Not Hispanic or Latino	Hispanic or Latino
I Oral mesalamine solution	20	33 ± 9 (18-51)	26.1 ± 4.2 (17.8-35.2)	13	7	18	1	1	19	1
IIA Pentasa	10	38 ± 11 (22-51)	27.0 ± 7.9 (17.6-45.2)	7	3	8	2	0	9	1
IIB Apriso	7	37 ± 29 (20-51)	29 ± 8.2 (21.3-44.7)	4	3	6	1	0	7	0
IIC Lialda	9	33 ± 8 (25-51)	28 ± 7 (21.7-43.9)	7	2	7	1	1	8	1

Crossover Phase (MR dosing) Study Discontinuations

There were 12 MR dosing that were discontinued. For 5 subjects, the GI tube could not be advanced past the pylorus into the small intestine. There were 3 subjects who requested removal of the GI tube, 1 subject who vomited during the tube insertion procedure, and 2 subjects who vomited after study drug administration. There was 1 subject who experienced an adverse event. This subject experienced a vasovagal syncope event due to nerves and dehydration prior to the GI tube insertion procedure. In addition, all subjects who had the tube successfully placed into the GI tract experienced mild sore throat. This was an expected risk of the study and was resolved through the use of home remedies, including gargling with warm salt water and/or use of Ricola™ throat drops.

Plasma Concentration After Administration for Three Mesalamine Drug Products

Healthy human subjects were dosed with mesalamine solution (100 mg), Pentasa (500 x 2 capsules), Apriso (375 mg x 3 capsules) and Lialda (1200 x 1 mg tablet).

Mesalamine and its metabolite concentration in human plasma were measured using LC-MS/MS (Figure 21).

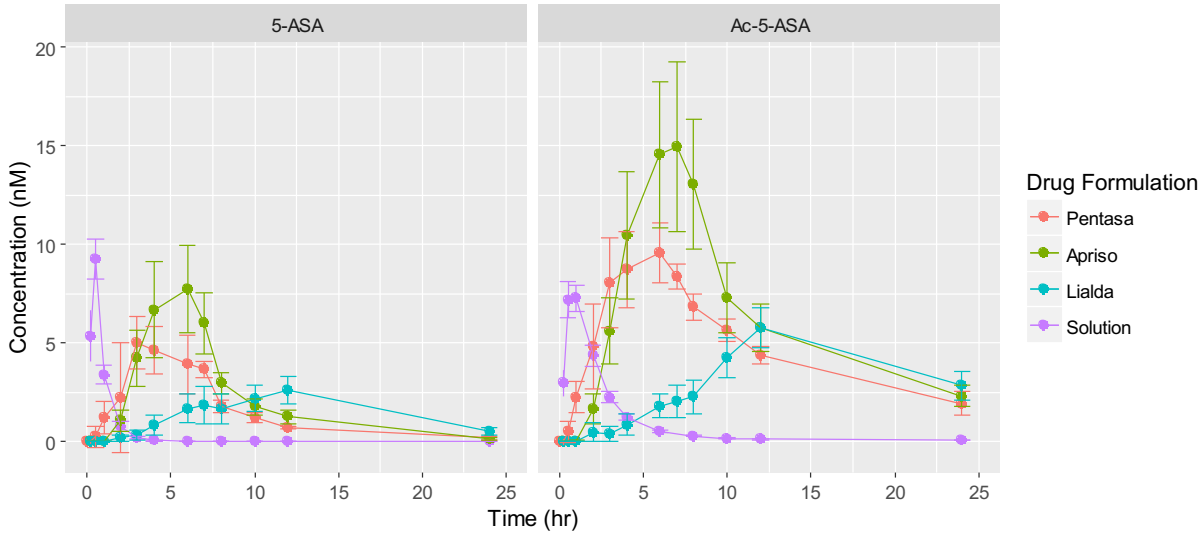

Figure 21. Average plasma concentrations observed for 5-ASA and Ac-5-ASA when administered a dose of 100mg mesalamine solution, 1000mg Pentasa, 1125mg Apriso, or 1200mg Lialda.

After ingestion of the mesalamine solution (100 mg), there is an immediate appearance of mesalamine (5-ASA) in the plasma by the first 15-minute time point. The C_{max} (10.1 nM) was reached at T_{max} (0.5 hr). The metabolite 5-acetyl-mesalamine (Ac-5ASA) reached C_{max} (8.6 nM) at 0.9 hr (T_{max}). The AUC of Ac-5ASA was significantly higher than that of its parent (5-ASA) (20.4 vs 7.9 nM•h respectively). The terminal slope of the metabolite concentration vs. time curve was parallel to that of parent drug suggesting clearance of metabolite is formation rate limiting.

Comparing the three mesalamine MR drug products, the plasma concentration of mesalamine and its metabolite are shown in Figure 21. Pentasa and Apriso had similar plasma AUC (normalized by dose given to 1g) of 0.040 and 0.049 nM•h/mg respectively, while Lialda had a lower AUC (0.035 nM•h/mg). Similarly, Pentasa and Apriso have a

similar C_{max} of 8 and 9.8 nM respectively, which is significantly higher than that of Lialda (3.5 nM). However, Lialda had the longest T_{max} (14.1 h) compared to T_{max} (5.1 h) of both Pentasa and Apriso. The relative bioavailability of Pentasa, Apriso, and Lialda compared to the mesalamine solution is 0.52, 0.62, and 0.45 respectively (Table 6).

Table 6. Mean parameters of systemic mesalamine (mean ± SD).

	5-ASA				Ac-5-ASA			
	Solution	Pentasa	Apriso	Lialda	Solution	Pentasa	Apriso	Lialda
Plasma (n)	20	10	7	9	20	10	7	9
AUC_{0-n} (nMh)	7.9±3.7	40.8±29.5	57.6±24.1	42.4±22.4	20.4±7.7	162±59.7	189±92.2	124.9±75.4
C_{max}(nM)	10.1±4.8	8.0±8.4	9.8±4.8	3.5±2.3	8.6±3.9	11.6±6.3	16.8±9.6	5.8±2.6
T_{max}(hr)	0.5±0.1	5.1±2.8	5.1±1.5	14.1±12.3	0.9±0.4	6.1±2.4	5.9±1.6	16.2±12.3
Relative Bioavailability		0.52	0.62	0.45				

The plasma concentration of mesalamine in each individual subject is shown in Figure 22. The data shows less variability in plasma concentration of mesalamine and its metabolite when the oral solution was administered. The three locally-acting mesalamine formulations exhibited large variability (mean C_{max} of 3.5nM to 9.8nM).

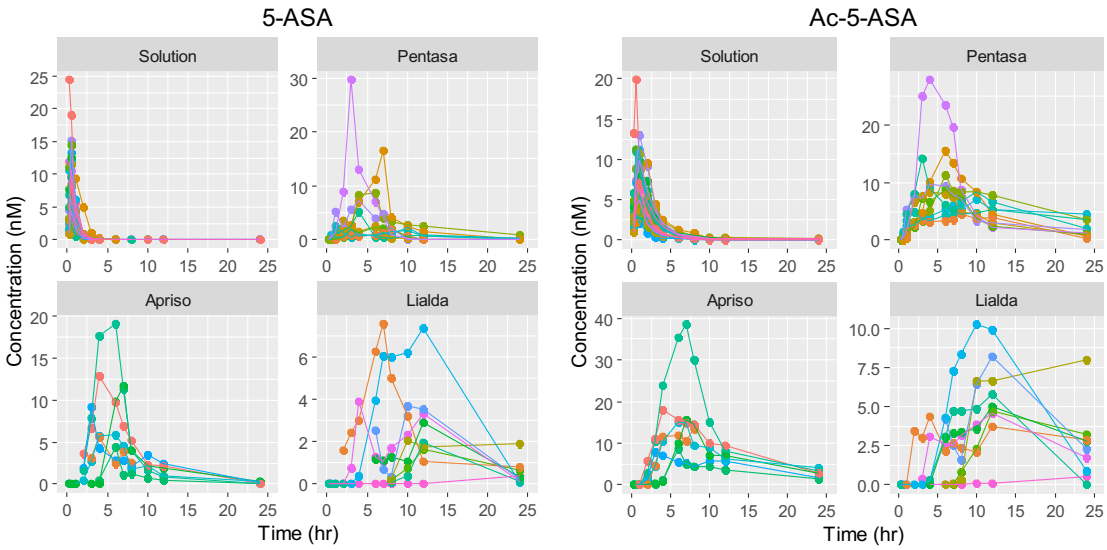

Figure 22. Individual plasma concentrations observed for 5-ASA (left) and Ac-5-ASA (right) when administered a dose of 100mg mesalamine solution, 1000mg Pentasa, 1125mg Apriso, or 1200mg Lialda. Each color line represents one individual subject (note scale differences).

In Vivo Gastrointestinal Concentration during Drug Dissolution after Administration for Three Mesalamine Drug Products

In order to directly measure and compare *in vivo* drug dissolution in the human GI tract, healthy human subjects were intubated to obtain GI samples from four different locations in the GI tract: (stomach, duodenum, jejunum, and ileum). Subjects were dosed with Pentasa (500 mg x 2 capsules), Apriso (375 mg x 3 capsules) and Lialda (1200 x 1 mg tablet). The intestinal concentration of mesalamine (5-ASA) and its metabolite acetyl-5-mesalamine (Ac-5-ASA) were measured using LC-MS/MS (Figure 23).

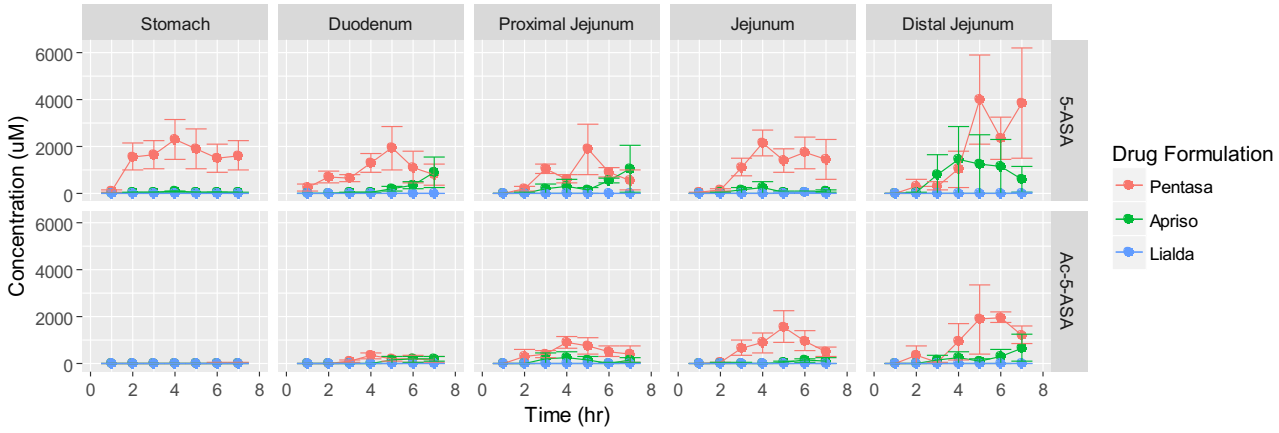

Figure 23. Average concentrations of 5-ASA and Ac-5-ASA in different regions of small intestine when administered a dose of 1000mg Pentasa, 1125mg Apriso, or 1200mg Lialda.

The three mesalamine MR drug products exhibited very different release profiles. A pharmacokinetic summary is provided in **Table 5**. Pentasa was the only formulation to have significant drug release in stomach where a high 5-ASA concentration (1500-2000 µM) was observed. This high 5-ASA concentration range (1000-4000 µM) continued throughout the sampled GI tract from duodenum to distal jejunum. This suggests that Pentasa begans to release early in the stomach and that this release continues as the dosage form transits through the GI tract.

Subjects with orally administered Apriso exhibited a very low 5-ASA concentration in stomach (<100 µM) indicating minimal drug release. In the duodenum, minimal Apriso appears after 4 hours. In the distal jejunum, Apriso appeared in large quantities (800 µM) by 3 hours. Overall, the intestinal AUC and C_{max} of 5-ASA in subjects that received Apriso was significantly higher in the distal jejunum region than any other sampled region. These data suggest that Apriso had limited release of 5-ASA in earlier regions such as in the duodenum with increasing drug release in the later regions of the small intestine.

In contrast, subjects that were orally administered Lialda had very low 5-ASA concentration from stomach (C_{max} <0.7 μM) to distal jejunum (C_{max} <8 μM) which suggests very minimal 5-ASA release from Lialda in the sampled regions of the small intestine.

Although Pentasa had much higher concentrations of 5-ASA in the upper GI tract in comparison to Apriso, subjects that received Pentasa exhibited a slightly lower plasma C_{max} and AUC for both 5-ASA and Ac-5-ASA than Apriso. Interestingly, more metabolite (Ac-5-ASA) was detected in the GI tract of subjects with Pentasa than Apriso. This suggests that the early release of Pentasa may expose more of the drug to intestinal metabolism which would reduce the overall plasma exposure of 5-ASA in subjects. Alternatively, Apriso may have released more drug in the ileum region which in turn may have better systemic absorption than the regions of the GI tract sampled in this study.

Table 7. Mean parameters of gastrointestinal mesalamine concentrations (mean ± SD).

	5-ASA			Ac-5-ASA		
	Pentasa	Apriso	Lialda	Pentasa	Apriso	Lialda
Stomach (n)	7	4	9	7	4	9
$AUC_{0\text{-}8hr}$ (μM•h)	6451±5706	157±134	2.0±2.9	93.5±188	10.9±10.1	1.2±1.9
C_{max}(μM)	2029±1430	72.2±30.4	0.6±0.5	32.2±56.1	4.6±2.1	1.1±2.0
T_{max}(hr)	3.2±2.0	4.8±1.3	3.7±1.6	6.4±1.1	5.0±1.5	4.1±3.1
Duodenum (n)	7	6	4	7	6	4
$AUC_{0\text{-}8hr}$(μM•h)	6238±4654	828±916	3.5±2.9	1036±1087	435±583	3.6±3.5
C_{max}(μM)	2549±2097	829±1225	1.8±0.4	422±322	297±297	4.0±4.2
T_{max}(hr)	3.8±1.5	4.8±2.6	4.7±1.5	4.7±1.3	5.5±2.6	5.1±3.2
Proximal Jejunum (n)	3	2	6	3	2	6
$AUC_{0\text{-}8hr}$(μM•h)	4867±2017	1698±323	7.4±13.0	3212±2010	825±953	1.8±1.9
C_{max}(μM)	2176±1403	1395±733	3.8±6.6	951±388	408±121	1.5±2.2
T_{max}(hr)	5±1.6	6.5±0.5	5.2±1.2	3.7±1.2	5.6±1.5	4.9±2.0
Mid Jejunum (n)	5	3	4	5	3	4
$AUC_{0\text{-}8hr}$(μM•h)	7237±4598	378±608	27.9±53.2	4509±3508	357±368	16.7±24.1
C_{max}(μM)	2609±1441	169±211	15.6±27.8	1677±1404	169±139	9.1±9.6
T_{max}(hr)	4.7±1.5	5.4±1.3	5.4±2.5	4.8±0.7	6.4±1.0	5.2±2.6
Distal Jejunum (n)	3	3	3	3	3	3
$AUC_{0\text{-}8hr}$(μM•h)	8456±7444	4923±8506	2.9±3.9	5048±5553	1225±2024	3.4±3.4
C_{max}(μM)	4495±2156	1434±8506	5.3±7.0	2422±2001	681±824	5.3±6.6
T_{max}(hr)	5.6±0.95	6±1.4	4.6±2.7	5.3±0.5	7±0	6.4±0.5

We also note that the 5-ASA concentration in GI tract exhibited high variability. The drug concentration in each regions of small intestine of each individual subject is shown in Figure 24. In each region of the small intestine, the concentrations varied at different time points due to variation in drug relese, dissolution, GI transit, metabolism, and absorption permeability. These factors contributed to the data variability. In addition, the different pH

values in different regions of the small intestine likely contributed to the differences in drug release.

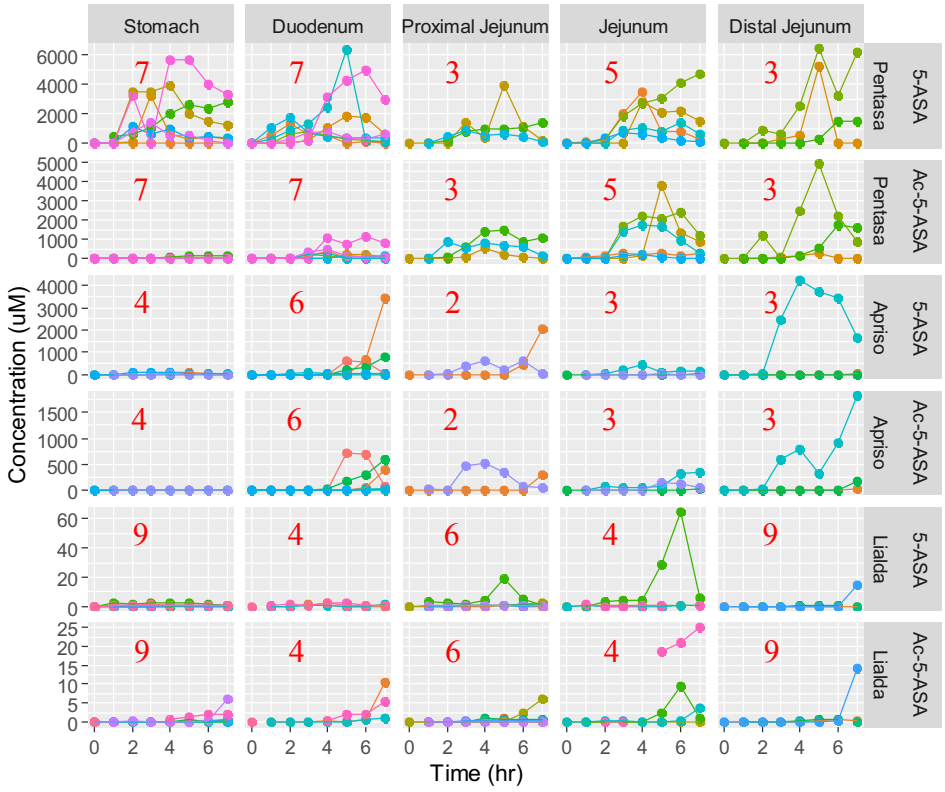

Figure 24. Concentrations of 5-ASA and Ac-5-ASA in different GI regions for each individual subject when administered a dose of 1000mg Pentasa, 1125mg Apriso, or 1200mg Lialda. Each colored line represents one individual subject. Red number indicates number of subjects sampled at specified location.

There is a significant distinction between the three formulations in the early GI from stomach to jejunum. While the plasma exhibited a fairly similar overall drug exposure between Pentasa and Apriso, the concentrations in GI differ significantly. The pH triggered release of Apriso and Lialda is noted by the minimal exposure (157 and 2 nM•h, respectively) in the stomach. Pentasa's pH-independent exposure was an order of magnitude higher than Apriso (6451 nM•h) in the stomach. Notably, there was detectable exposure of

metabolite in the stomach for Pentasa, Apriso, and Lialda (93.5, 10.9, and 1.2 nM•h respectively).

In general, the C_{max}, AUC, and T_{max} are as expected for these three delivery systems. Pentasa maintains a significant exposure (>4000 nM•h in all regions) throughout the measured regions in the GI tract suggesting extensive GI distribution. Apriso's delayed-release mechanismis effective in delaying release in low pH but begins to release significantly by the distal jejunum. The low AUC value for Apriso in the mid jejunum (378 nM•h) is likely due to the variation between subjects. Although Apriso has distinct delayed drug release from small intestine (until later Jejunum or early Illeum) in comparison with Pentasa, Apriso has similar exposure to that of Pentasa. This may suggest that Apriso has more drug release and absorption in ileum regions. Lastly, Lialda has a highly -pH-dependent release mechanism with with very little mesalamine in small intestine regions (max 15.6 nM).

In Vivo Dissolution of Mesalamine Drug Products in Stomach

Subjects dosed with Pentasa had minimal 5-ASA concentration (84 µM) in the stomach at 1h after dosing which then increased to 1554 µM by the next time point (2h) and stayed consistently high until 7h. There was greater 5-ASA concentration in the duodenum (260 µM) at the 1h time point suggesting that transit and pH both affect mesalamine release and availability. From the 2h mark and onward, there is typically a high 5-ASA concentration (1800-2200 µM) throughout the sampled GI tract, suggesting that Pentasa distributes quickly throughout the small intestine (within 2h). It is surprising that the 5-ASA concentration was observed at high concentration until 7 hrs. Minimal amounts of metabolite (Ac-5-ASA) were found in the stomach (Cmax <360 µM) suggesting a low level

of metabolism in the stomach. In contrast, subjects with Apriso and Lialda had minimal 5-ASA concentration (<75 μM) and Ac-5-ASA concentrations (<3 μM) from 1h to 7h.

In Vivo Dissolution of Mesalamine Drug Products in Duodenum

Subjects dosed with Pentasa had low 5-ASA concentration and had a continuously increasing 5-ASA concentration in the duodenum from 1h to 6h (259 to 1103 μM, respectively). The concentration then decreased to 787 μM by the 7h time point. The concentration of Ac-5-ASA in the duodenum after Pentasa administration was also low with a C_{min} of 12 μM (1h) and a C_{max} of 1590 μM (5h), suggesting an extensive metabolism in the duodenum.

Apriso's duodenal concentrations also increased gradually but were lower than Pentasa throughout the duration of the study, with a concentration of 0.2 to 876 μM for 1 to 7 hours respectively. The duodenal Ac-5-ASA concentration after administration was below the limit of quantification by the first time point (1h). There was a presence by 5h with a concentration of 185 μM.

Lialda's duodenal concentration was extremely low for each time point, with a high of 1.1μM and a low of 0.3 μM. There was a very low concentration of Ac-5-ASA after dosing with Lialda with hours 1 to 3 being below the limit of quantification. The C_{max} was at the final time point with a concentration of 5.6 μM.

While individuals may vary for each administration of mesalamine, each formulation had a detectable amount of 5-ASA in the duodenum by 7h which was accompanied by some metabolite. Apriso had significantly lower release than Pentasa in the duodenum, and Lialda had very low mesalamine concentrations in the duodenum suggesting very minimal drug release.

In Vivo Dissolution of Mesalamine Drug Products in Proximal Jejunum

Pentasa's average 5-ASA concentration in the proximal jejunum was extremely low in the first hour (0.04 μM) followed by extremely high concentration (188 to 1868 μM) for subsequent time points (2 to 7h). The concentration of Ac-5-ASA mirrored the profile of 5-ASA with an extremely low concentration (0.01 μM) in the first hour followed by a high concentration (324 to 921 μM) in the later time points. The concentration of metabolite was nearly equivalent to the parent suggesting there is extensive metabolism in this region.

Apriso's average 5-ASA concentration behavior in the proximal jejunum was similar to Pentasa's. The first hour had an extremely low concentration followed by a high concentration at 2 hours (199 μM) where the highest value was at 7 hours (1046 μM). The Ac-5-ASA profile also reflected a similar concentration profile behavior. The C_{min} value was at 2 hours (7 μM). From 3 hours onward, the concentration in the proximal jejunum ranged from 42 to 266 μM. The metabolite formation was more limited relative to Pentasa.

Lialda's average 5-ASA concentration behavior in the proximal jejunum was similar in profile to that observed in the duodenum. There was extremely limited release from Lialda tablets with a C_{max} of 3.6 μM. This extremely limited release also explains the limited quantities of Ac-5-ASA with a C_{max} of 1.2 μM at the 7 hour time point.

In Vivo Dissolution of Mesalamine Drug Products in Middle Jejunum

Subjects dosed with Pentasa had a low jejunal 5-ASA concentration (2 μM) at one hour indicating that transit was fast (within 1h). The concentration gradually increased to 2141 μM at 4 hours and maintained a high concentration (1402 to 1713 μM) from 5-7 hours. The concentration of metabolite mirrored that of parent with low Ac-5-ASA concentration (12 μM) at one hour, increasing steadily to 1590 μM by 5 hours.

Apriso had a similar profile between the mid jejunum and the proximal jejunum. The concentration was low at 1 hour (0.8 μM) but increased to 14 μM by the second hour and maintained that range of concentration (12 to 73 μM) from 2 to 7 hours. Similar to Pentasa, the concentration of metabolite for Apriso also mirrored the parent. The concentration was low at 1 hour (0.2 μM) but increased to 35 μM by the second hour and maintained that range of concentration (22 to 155 μM) from 2 to 7 hours, suggesting high metabolism in mid jejunum.

Lialda maintained its limited release in the mid jejunum reaching a C_{max} of 7.4 at the 5 hour time point. Similar to earlier regions, the concentration of Lialda was limited and only begins to be quantifiable by the five hour time point (5.2 μM).

In Vivo Dissolution of Mesalamine Drug Products in Distal Jejunum

Subjects dosed with Pentasa had very low concentrations in the first hour (0.2 μM) followed by a consistently high concentration (298 μM) in the second hour and gradually increasing to 3850 μM at hour 7. This suggested rapid drug transit to distal jejunum (early ileum) from 1 to 2 hours. This concentration profile was also reflected in the metabolite with a low concentration in the first hour (0.08 μM) followed by a concentration of 59 μM at the second hour and increased to 1899 μM by hour five.

Apriso had a similar concentration profile to Pentasa where the first hour had limited concentration (0.3 μM) which quickly increased to 18 μM in the second hour and increased continually to 1419 μM at hour 4 where it maintained that concentration level for the next three hours. This concentration was somewhat higher than the concentration in the mid jejunum which likely reflected the higher pH levels seen in the distal jejunum. The parent profile was reflected in the metabolite profile, where the first hour showed limited

concentration followed by a concentration of 10 μM at the second hour and increased to 680 μM by hour 7.

Lialda again had limited release even in the distal jejunum with a Cmax of 7.3 μM at hour 7. The metabolite profile showed similar behavior with a Cmax of 7.5 μM at hour 7. All other time point concentration values were below 0.5 μM for both 5-ASA and Ac-5-ASA.

The 5-ASA concentration in GI tract exhibited very high variability. The drug concentration in each regions of small intestine of each individual subject is described in Fig 4. In each region of the small intestine, the concentration varies at various time points due to drug transit, intestinal segment fluid mixing due to contractal activity, pH variation in drug release, metabolism, and absorption/permeability variation. These factors need further investigation.

Composite Appearance Rate (CAR) of 5-ASA in Systemic Circulation for Three Mesalamine Drug Products.

For modified release drug formulations, disintegration, dissolution, transit, and absorption will be complex. CAR is intended to capture these processes. Plasma concentration is the primary observed value of systemic presence that is a result of three components: absorption, clearance, and volume of distribution. These three components are the confounding variables that determine the final plasma profile that arises from a single dosing. Deconvolution is a predictive process that separates these confounding variables to isolate a certain aspect. In this case, deconvolution was used to isolate the absorption component to predict the necessary appearance of drug in the body to produce the resulting profile.

The plasma from each individual dosed with mesalamine solution was used to obtain a baseline pharmacokinetic parameters of 5-ASA. These parameters were then used as an individual basis to calculate the CAR of mesalamine appearance in the plasma vs time of the three mesalamine MR formulations (Figure 23). The motivation for performing individual deconvolution based on individual solution dosing plasma profiles was to minimize bias due to inter-individual confounding factors such as variation in distribution volume and clearance rates. The result is that CAR predicts the expected absorption rate of the drug from GI as a composite parameter of drug release, dissolution, transit, metabolism, and absorption from the entire GI tract.

The three mesalamine MR formulations showed distinct CAR profiles, which indicate different release, dissolution, transit and absorption in different regions of GI tract. On average, individuals dosed with Pentasa had high levels of CAR immediately following dosing from 1 hour until about 10 hours, then decreased to minimal CAR after 12 hours. This is consistent with the high levels of 5-ASA found in the GI fluids. On average, those dosed with Apriso had low levels of CAR from 1 to 4 hours and high levels of CAR from 5 to 10 hours, which decreased to minimal levels after 12 hours. This is consistent with the GI results where significant release occurs after either a sufficient time or pH was reached. Lialda showed minimal levels of CAR from 0-5 hours, then increased to medium levels from 5 to 12 hours, then decreased to further lower levels after 12 hrs. One of the individuals had a high gastric pH which explains the rapid CAR. Overall, the CAR of the three different mesalamine formulations mirrored the release and dissolution in the GI tract, therefore, the CAR may distinguish the differences among three different mesalamine MR drug products and be a useful BE determinate.

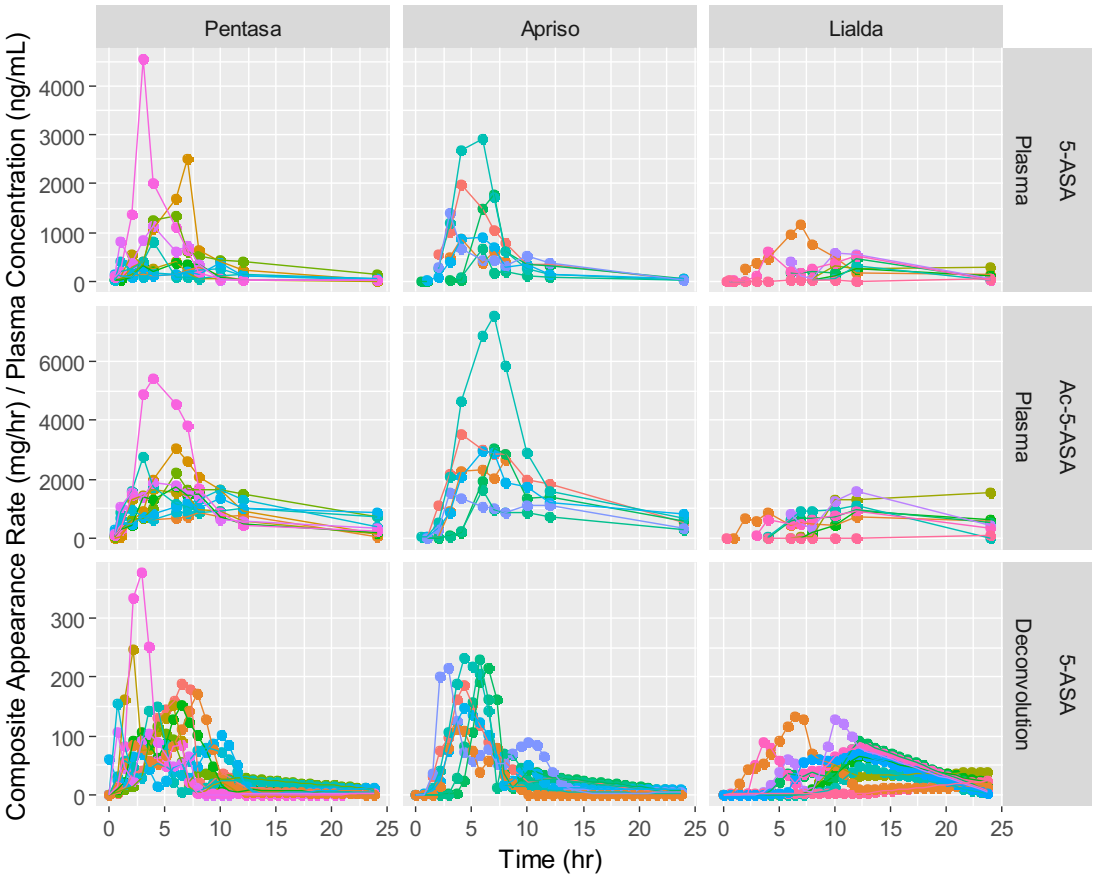

Figure 25. Composite Appearance Rate (CAR) vs. time plot of three mesalamine MR formulations in human subjects after administration of Pentasa (500 mg x2 capsules), Apriso (375 mg x3 capsules) and Lialda (1200 mg x1 tablet). Each colored line represents one individual subject.

Gastrointestinal pH in Different Regions of Human Small Intestine

The pH values were measured for each GI fluid sample and the results are depicted in Figure 26. In general, the pH is as expected for each region of the GI tract. Individuals that had a high gastric pH, high drug concentration in plasma and high drug release in stomach were observed, indicating that the high gastric pH had caused the dissolution process to start prematurely.

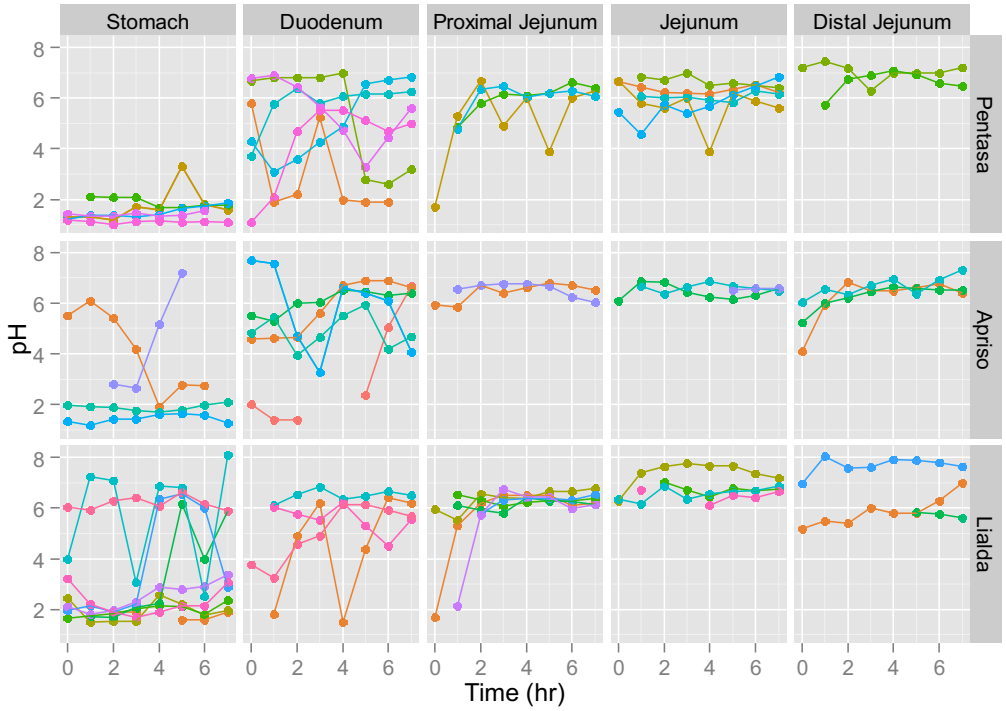

Figure 26. Individual pH values of human subjects obtained during GI fluid sampling. Each colored line represents one individual subject.

Colon Content of Mesalamine Drug Products

Pentasa (500 mg x 2 capsules) and Apriso (375 mg x 3 capsules) had a similar amount (0-200 mg range) of 5-ASA accumulation in feces despites differences in starting dose. Most individuals that were administered Lialda had a similar but slightly higher 5-ASA accumulation (25-250 mg range). There were two individuals that were administered Lialda that had high amounts of 5-ASA in feces (430 and 820 mg). It is possible that the drug product did not experience either complete dissolution during transit and instead exited the body combined with feces. In addition, it is worth noting that most of the 5-ASA in the feces typically appears within 48 hours for most individuals. However, the high 5-ASA accumulation in feces for the two individuals appeared by the 24-hour collection point.

The accumulation of metabolite Ac-5-ASA in feces from 0 to 96 hours is similar in all individuals between the different formulations. Since the metabolism of 5-ASA in the GI from duodenum to distal jejunum is significant, the similarity of metabolite content present between the three formulation was unexpected.

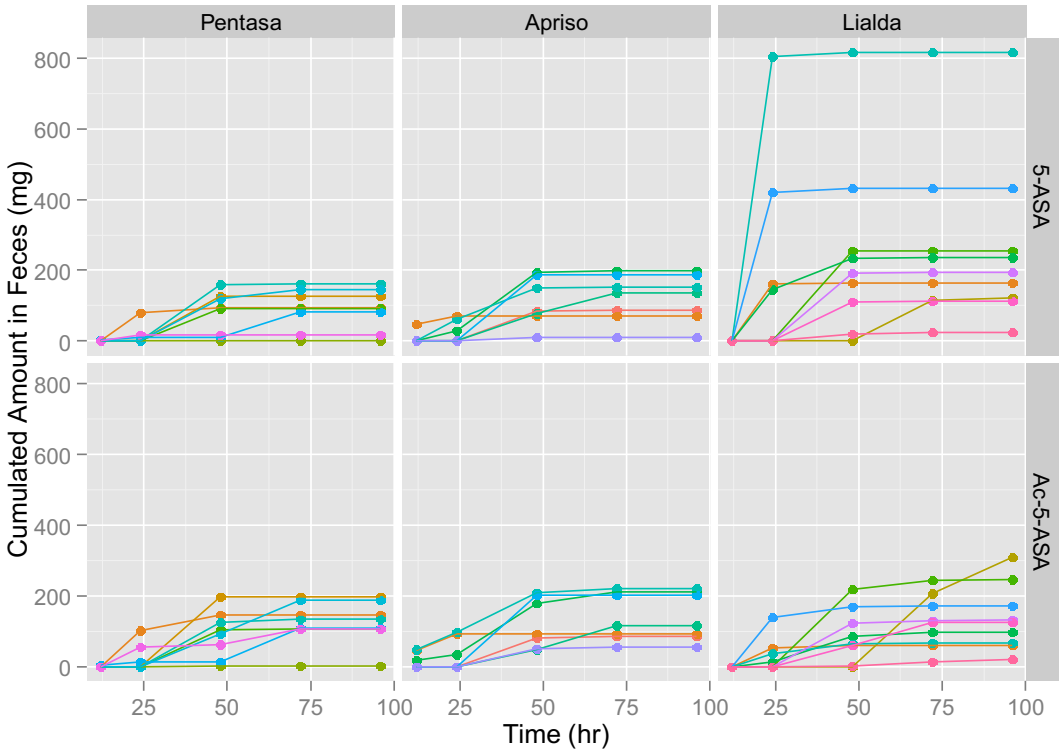

Figure 27. Accumulated 5-ASA and Ac-5-ASA in feces in individual subjects administered 1000mg Pentasa, 1125mg Apriso, or 1200mg Lialda. Each color line represents one individual subject.

Approximating Colonic Transit of 5-ASA from Fecal Appearance of Mesalamine Drug Products

Colonic transit rate will significantly affect the accumulated drug and drug dissolution in colon. In this study, fecal samples data was limited as samples were only collected as designated time points. Since we were only able to collect feces samples every 24 hours, the sample at 24 hour represents the total amount collected preceding the 24 hour mark.

Classification of colonic transit rate was estimated by two criteria. If largest drug amount was appeared in 24 hour feces samples (compared to 48 hours and 72 hours), these subjects were classified in fast transit group. If drug amount in feces at 24 hours is more than 20 mg, these individuals were classified to fast transit rate group even if more drugs appeared in feces at 48 hrs. Similar method was used to classified average and slow transit. Based on this classification, the amount of 5-ASA collected at each time point was plotted in Figure 28. Three groups of subjects with fast, average, and slow colonic transit were observed. The fast transit group was considered when large amount of 5-ASA appeared in feces within 24 hours. The average transit group was considered when large amount of 5-ASA appeared in feces from 24 to 48 hours. The slow transit group was considered when large amount of 5-ASA appeared in feces from 48 to 96 hours.

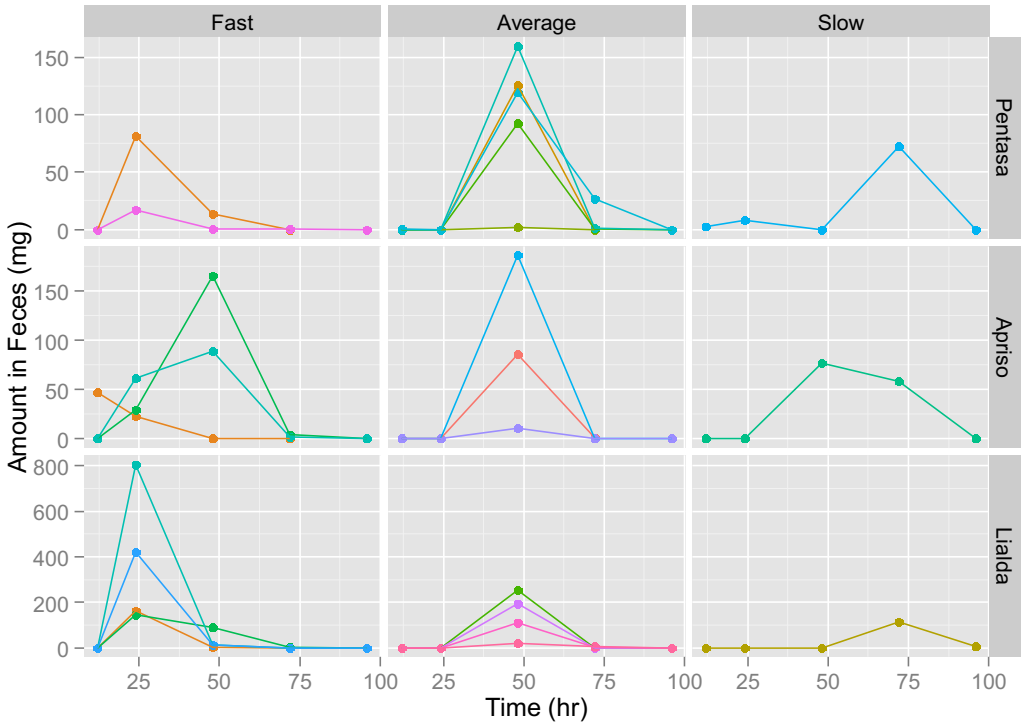

Figure 28. Amount of 5-ASA in feces at different time points in subjects administered 1000mg Pentasa, 1175mg Apriso, or 1200mg Lialda. Each colored line represents one individual subject.

Correlation of Colonic 5-ASA and Ac-5-ASA content considering Colonic Transit

The correlation of 5-ASA and Ac-5-ASA from colonic transit were plotted to show the 5-ASA metabolism difference in colon between fast and average colonic transit (Figure 29) and difference between the three formulations (Figure 30). In Figure 29, individuals with average colonic transit exhibited a proportionate amount of parent 5-ASA and metabolite Ac-5-ASA. In contrast, individuals with fast colonic transit had a large amount of parent 5-ASA in feces, but lower amount of metabolite Ac-5-ASA in feces.

In Figure 30, subjects with Pentasa and Apriso had a seemingly linear relationship between parent 5-ASA and metabolite Ac-5-ASA in the feces. In contrast, subjects with Lialda had more variable relationship between parent 5-ASA and metabolite Ac-5-ASA,

even if excluding the two cases with significantly high 5-ASA. However, overall presence of metabolite appeared to be within 100mg of the average regardless of parent drug presence. These data suggest that the three formulations can have a similar amount for both 5-ASA (active) and Ac-5-ASA (metabolite) and that rapid transit may prevent Lialda's MMX formulation from complete release.

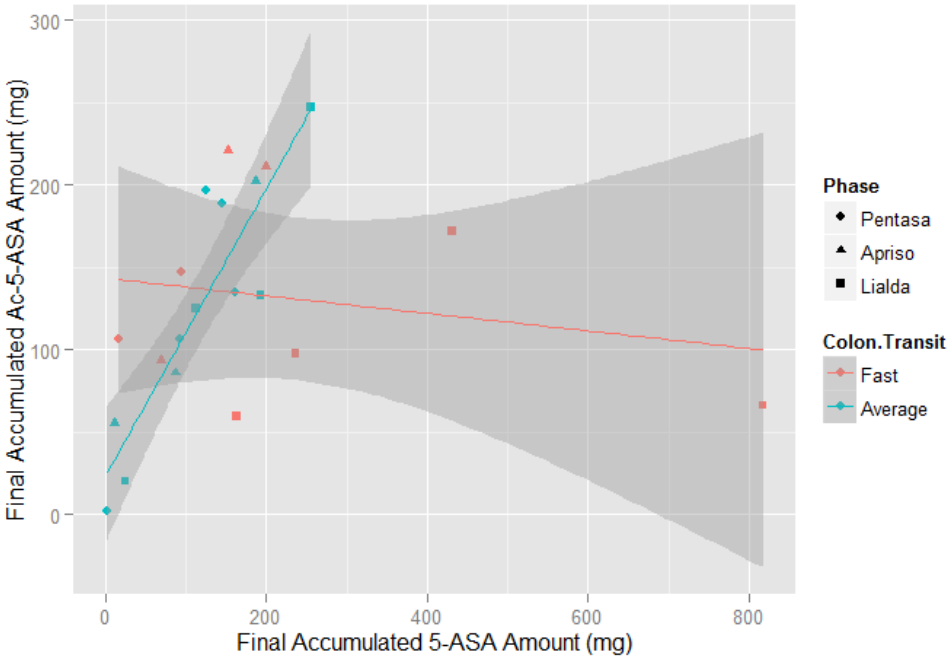

Figure 29. Correlation of accumulated 5-ASA vs Ac-5-ASA in feces in subjects with fast vs. average colonic transit after oral administration of 1000mg Pentasa, 1125mg Apriso, or 1200mg Lialda.

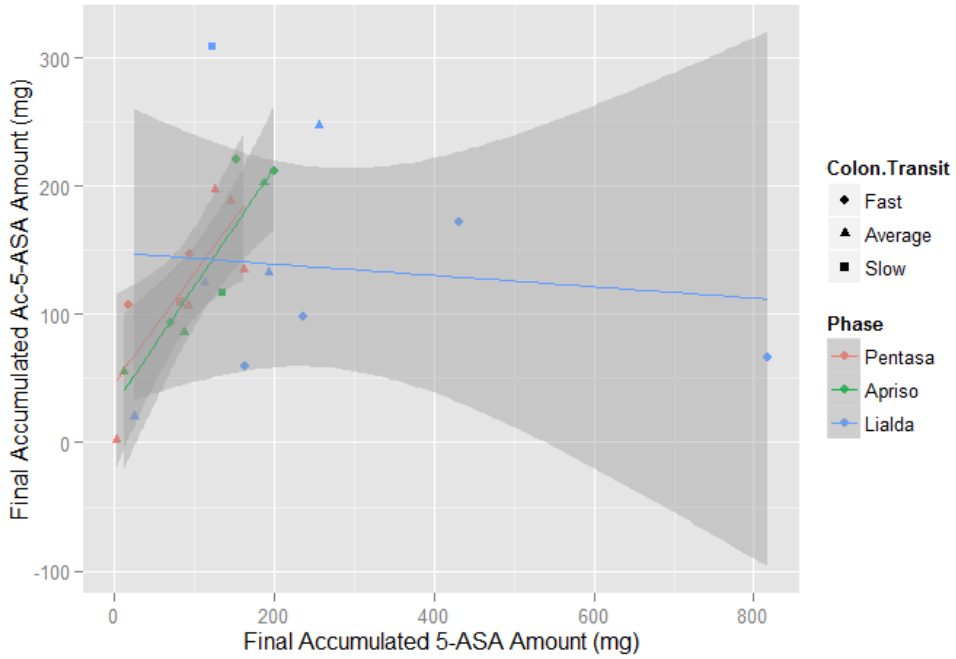

Figure 30. Correlation of accumulated 5-ASA vs Ac-5-ASA in feces in subjects after oral administration of 1000mg Pentasa, 1125mg Apriso, or 1200mg Lialda.

Discussion

Previous understanding of *in vivo* drug release and dissolution has been limited to general recognition as a variable process that can be highly affected by various factors, such as solubility, dosage forms, fluid volume, pH, GI transit, buffer, and motility. In order to predict the *in vivo* dissolution of a formulation, *in vitro* dissolution experiments are conducted to mimic drug release and dissolution. Since *in vivo* drug dissolution can differ significantly from *in vitro* studies, acquiring GI samples allows for a novel quantification of previously undefined variability to better understand *in vivo* drug release and dissolution.

This is the first study to sample and compare *in vivo* GI mesalamine concentrations of three different formulations. There are currently five approved and one discontinued (Asacol) mesalamine oral drug products. Two of those are extended-release capsules (Pentasa, and Apriso), and three of those are delayed-release tablets (Asacol HD, Delzicol, and Lialda).

Knowing the limitation of the study that only upper GI fluid can be sampled and based on the plasma profiles of different mesalamine formulations, three MR products were selected for this study, namely Pentasa, Apriso, and Lialda. A comparison of PK parameters between this study and standard studies with no tube insertion were found to be comparable (data not shown), suggesting that GI tube insertion does not affect drug absorption. Additionally, samples acquired were sufficient to distinguish *in vivo* behavior differences between the three MR products despite being limited to the upper GI region (stomach to distal jejunum).

In general, the release behavior found in the GI generally reflected expectations based on formulation design. The differences in formulation technologies used to manufacture Pentasa, Apriso, and Lialda were anticipated to have distinctly drug release profiles that would exhibit different plasma drug concentration profiles. Pentasa was expected to start drug release throughout GI tract to show early systemic appearance. Apriso with its pH resistant coated granules was expected to start releasing in the intestine with more than pH 6 environment resulting in a burst of systemic appearance. Lialda with its multimatrix design and pH 7 coating was not expected to release until further then followed by sustained release in later small intestine and colon. In this regard, the plasma profile generally reflected the expectations based on formulation design.

Pentasa's release was the earliest with several individuals exhibited a significant release of mesalamine in the stomach. The degree of release varied between individuals but release generally continued down the GI tract. This variability in release would be due to variation in GI transit or dissolution. Apriso's release was significantly delayed compared to than Pentasa. Since Apriso has a pH sensitive coating, there were some individuals where mesalamine was found in the duodenum after 5 hours. For another Apriso dosed individual, mesalamine was found at high

concentrations (2500 μM) in the distal jejunum at 3 hours. This suggests that a pH dependent coating drug product's release behavior is highly variable as a result of transit behavior. Lastly, Lialda with its multimatrix design and more stringent pH 7 coating had an extremely limited release of mesalamine in the sampled regions of the small intestine.

Traditional characterization of residence time would approximate the stomach and small intestine average residence time to be about 30 minutes and 3 hours respectively. However, both Pentasa and Apriso had multiple individuals with significant amounts of release occurring in the small intestine after 4 to 7 hours when the drug would have been expected to be past the regions. Further, the unexpected observation of high 5-ASA concentration present in the stomach even after 7 hours indicates the GI tract transit of drug and drug products is complex and need further investigation

The Composite Appearance Rate (CAR) was deconvoluted from plasma to quantify the drug product's release, dissolution, transit, metabolism, and absorption in the GI tract. Each crossover arm trial deconvolution utilized the single arm solution dosing fitted to a two compartment model as an individualized basis. For mesalamine, two compartment models have been used to describe the plasma profile (94). Since each deconvolution calculation utilizes solution dosing as a baseline, CAR becomes particularly useful in distinguishing *in vivo* behavior of modified release formulations. The CAR of the three mesalamine MR formulations generally mirrored local release and dissolution from 1 to 7 hours in small intestine. Mesalamine is known to be rapidly absorbed in the upper part of the gut but slow in the colon (95). A previous study suggested that intestinal transit rates may impact pharmacokinetics and efficacy of different oral mesalamine preparations (70). Therefore, the direct measurement of local GI drug levels and CAR analysis from plasma concentration-time profile may be used to compare bioequivalence

via plasma for locally-acting mesalamine products when drug dissolution profile in the GI lumen is required for efficacy in the small intestine.

Subjects dosed with Pentasa had consistently high levels of CAR from 1 to 10 hours after administration which was consistent with the concentrations of mesalamine in the small intestine. Pentasa released 5-ASA from stomach to small intestine as directly measured in GI samples, which was consistent with high levels of composite appearance rate (CAR) deconvoluted from plasma drug concentration. Although significant variability was observed in both GI drug concentration and plasma drug concentration in subjects administered Pentasa, individuals with significant concentrations throughout the GI tract exhibited high drug concentration in plasma at early time points, while individuals with low drug concentration in the GI tract with delayed manner showed low and delayed plasma drug concentration. This variability would be due to either different drug release or dissolution in vivo or due to variation in GI pH, transit and motility.

In contrast, the CAR of Apriso was at low levels for the first 3 hours. Apriso's CAR suggested that it released 5-ASA in a burst like effect once environment pH is >6 at jejunum after 4 hours. Apriso showed very little drug release in the stomach. There was a slight increment in drug release in the duodenum past four hours, which was benefited from Apriso's pH resistant microgranules so an extended residence period would explain this behavior. In subjects who had drug release in jejunum from 3 to 7 hours also had a high plasma concentration. The high levels of CAR from 3 to 6 hours correlated with drug release in GI tract and plasma concentration, which suggested burst release of 5-ASA in small intestine regions with pH > 6 (either in jejunum or ileum). Overall, the drug concentration in both the duodenum and jejunum for subjects dosed with Apriso were lower than that of subjects with Pentasa, but

plasma drug concentration in subjects with Apriso was higher from 4 to 8 hours than that of subjects with Pentasa. It was likely that the drug product transited past our last intestinal sampling point (i.e. distal jejunum to ileum) during this time. The CAR of Lialda suggested it had the most delayed release with most release occurring after twelve hours. Lialda had the lowest drug release in the small intestine as measured by GI concentration with low μM peak in comparison to more than 5000 μM seen with Pentasa. The CAR also showed minimal levels from 0-5 hrs and correlated with low plasma concentration. There was one individual with a high gastric pH causing an early release of mesalamine from Lialda. As such, this individual had the earliest and highest appearance of systemic mesalamine after administration of Lialda.

Mesalamine oral drug products have demonstrated clinical efficacy in treating UC (82, 83, 88, 89, 96, 97), which is the only FDA approved indication. However, it has been unclear whether different formulations of mesalamine will provide different clinical efficacy in treating disease in the small intestine. The study results here suggests that different mesalamine formulations will have different drug concentration in the small intestine and thus likely have different efficacy in treating disease in small intestine (98).

While both *in vivo* GI concentrations and CAR suggested that the three MR formulations have distinct *in vivo* dissolution profiles in small intestine, similar levels of both mesalamine and its metabolite were found in the feces across the three formulations despite different dosages. Since local presence of mesalamine is required for efficacy, this suggests that the three MR formulations may have similar effect in colon region. There was however, two subjects with a high accumulated amount of mesalamine in the feces by the 24 hour collect point. This data suggests that transit is likely rapid and that the tablet may not have fully dissolved before being expelled. Very interestingly, regardless the accumulated drug in the feces, all three formulations

generated similar amount of metabolite Ac-5-ASA in the feces. Since metabolism can only occur when 5-ASA is in solubilized form, the similarity in metabolite quantity may suggest similar release and dissolution between the three MR formulations in the colon region. Therefore, the presence of mesalamine and metabolite in feces may also serve as a surrogate marker of efficacy in treating UC. The accumulation of drug and its metabolites in the feces may be used to compare the *in vivo* bioequivalence for locally acting drug products when drug dissolution is necessary for efficacy in the colon.

Acknowledgements

This research was supported by FDA grants HHSF223201000082C and HHSF223201300460A.

Chapter 5 Modeling Extend Gastrointestinal Residence Time Based on Mucoadherence of Modified Release Mesalamine (PENTASA) in the Human Gastrointestinal Tract

High *in vivo* mesalamine concentrations in the stomach after 5 hours was discovered after quantification of human *in vivo* gastrointestinal (GI) samples of post-dose Pentasa (modified release formulation of mesalamine) (53). This observation runs contrary to the typical expectation that stomach empties rapidly in fasted state due to the zero-caloric nature of water, which was confirmed by in a clinical study observed a significant degree of gastric emptying within one hour of water dosing (28). As the *in vivo* dissolution process of modified release oral drug products is not well characterized with existing mechanistic models, developing that a model based explanation that reconciles the two juxtaposed clinical observations can provide valuable insight on gastrointestinal environment and future *in vivo* dissolution considerations.

Mucus was identified as a potential contributor to gastrointestinal drug transport in a recent mechanistic fluid model of the GI (99). In general, the mucus layer in the human GI tract is an efficient physical and chemical barrier that acts as a shield against invading microbes (100). When foreign particles are introduced, these particles typically adhere to the mucus layer (101). While adhesion to mucus (mucoadhesion) is not fully understood, the mechanism has been proposed to a summation of attraction forces such as hydrogen bonding and van der Waals that promote entanglement between polymer and mucin. Many natural polymers and pharmaceutical ingredients such as carbomers, chitosan, starch, polymethacrylic acid, hydroxypropylcellulose,

hydroxypropyl methylcellulose, and sodium carboxy methyl cellulose exhibit these adhesive properties (102).

Hydroxypropyl methylcellulose is one of the excipients used in the formulation of Pentasa that was specifically identified as having mucoadhesive properties. The 500mg capsule formulation of Pentasa is comprised of acetylated monoglyceride, castor oil, colloidal silicon dioxide, ethylcellulose, hydroxypropyl methylcellulose, starch, stearic acid, sugar, talc, and white wax (103). The capsule is intended as a carrier mechanism rather than a modified release function as the labeling for Pentasa notes that Pentasa can be administered in either capsule form or the capsule broken apart and sprinkled into yogurt or applesauce to be consumed immediately (104).

Based on the formulation design and the use of hydroxypropyl methylcellulose, it is likely that Pentasa granules may be adhering to the mucosal layer in the GI, thereby increasing the residence time by slowing transit. Furthermore, the mean granule size of Pentasa is 1mm which further suggests ease of adherence with GI mucus that can vary in thickness from 50 to 400μm based on physical relationship (105).This effect can explain the clinical observation of high stomach concentration of mesalamine at 5 hours. To evaluate the theory of whether mucosal adhesion play a large role in the high concentration of mesalamine in the GI tract, a simulation study using the Dynamic Fluid Compartment Absorption and Transport model was conducted to determine whether extended residence can explain the large concentration of mesalamine in the stomach after 5 hours.

Materials and Methods

Computational Simulation

A modification of the Dynamic Fluid Compartment Absorption and Transport model is detailed in the following expansions to capture the essential components of drug disintegration, dissolution, and absorption along with mucus interactions. The model consists of 162 nonlinear ordinary differential equations (ODE). The stomach is represented by five ODEs (solid dose, drug particles, dissolved drug, mucus, and fluid) with the small intestine represented by 150 ODEs representing a 30-compartment model. Duodenum was recognized as compartment 1, jejunum being compartments 2-13 and the ileum being the remaining 14-30 compartments.

An illustration of the proposed compartment model and avenues of transport is drawn in Figure 31. Matlab 2017a was used for both the simulation of model ODEs and the prediction of rate coefficient parameters. A fixed step ODE solver from the Simulink Package (ODE4) was used in 1s intervals. Visualized data graphics were rendered using Matlab's plot packages. Pharmacokinetic fitting was conducted using Pheonix 64 Build 6.3.0.395 WinNonlin version 6.3 by Pharsight.

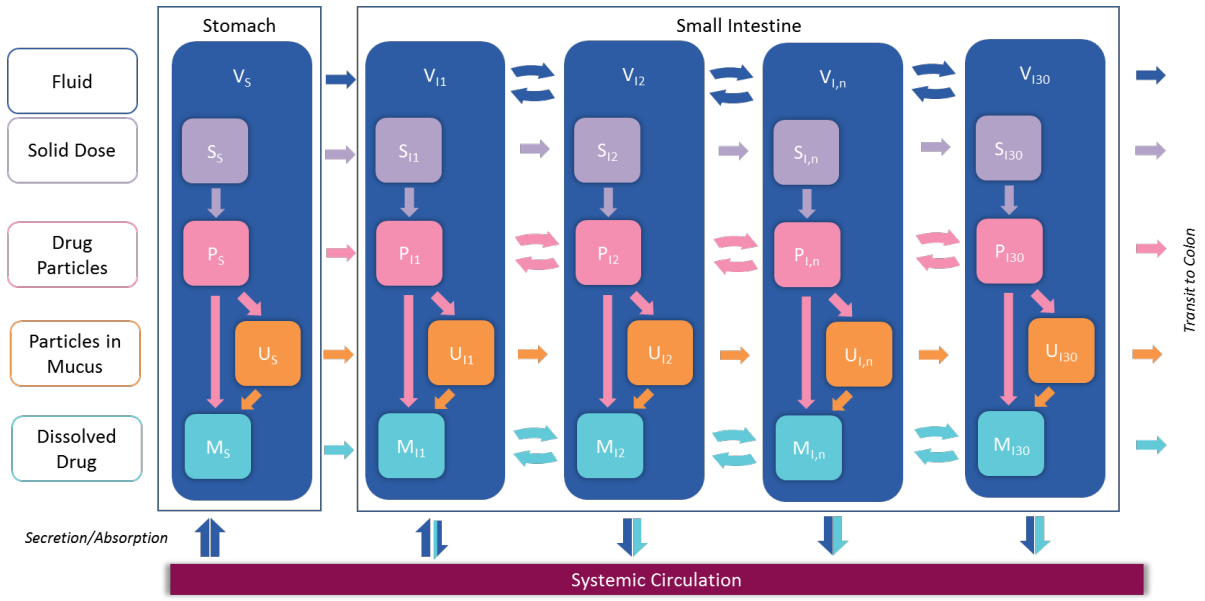

Figure 31. Modified DFCAT model with mucus layer compartments

Equations for Particle Transport with Mucoadherence Consideration

The Pentasa granules were assumed to be released from the capsule delivery mechanism within 10 minutes. This was confirmed to be a likely outcome based on observations from *in vitro* dissolution tests (data not shown). As such, granules were assumed to be the primary undissolved form of mesalamine. In this case, the net transport of drug particles were assumed to be characterized by either the release from capsule, dissolution, mucus adherence, and GI transit (Equation 17). The equations from the Expanded Dynamic Fluid Compartment Absorption and Transport (EDFCAT) model were carried over with the addition of a mucosal adherence term. Mucosal adherence was assumed to be an irreversible process based on a first order mechanism. Transit of the mucosal adherence particles was assumed to occur at a slower pace.

$$\frac{dU}{dt} = + \underbrace{k_{bM}P_n}_{\text{Mucoadherence}} - \underbrace{k_{tM}U_n}_{\text{Transit Forward}} + \underbrace{k_{tM}U_{n-1}}_{\text{Transit From Previous}} \quad (17)$$

Where k_{bM} is the permanent binding coefficient of drug particle to the static mucus layer, P_n is the amount of drug as particles, k_{tM} is the transit rate coefficient for mucoadhered drug particles, and U_n is the amount of drug that is adhered to the mucosal layer.

Modeling Dissolution

The dissolution of drug particles into solubilized form was represented by a single first order coefficient k_{diss} (Equation 18). The use of a single first order to represent dissolution has been previously explored in Margolskee *et al (61)*. Due to modification of the dissolution process, the traditional approach to determining relative dissolution rate based on thermodynamic solubility was not used.

$$\frac{dP_n}{dt} = -k_{diss}(t) * P_n \tag{18}$$

Where k_{diss} is the first order dissolution rate coefficient and P_n is the amount of drug (particle form) in compartment n. The temporal nature of $k_{diss}(t)$ was expected to correct for the true dissolution rate when performing mechanistic deconvolution.

Evaluation Through Mechanistic Deconvolution

Pharmacokinetic parameters were obtained through fitting of a 100mg solubilized mesalamine dosing in 240mL of water. Variations in the mucus adherence coefficient were tested. Mechanistic deconvolution to evaluate the system of interest by deconvoluting the average plasma profile observed for Pentasa. Model verification was based on comparison of plasma profile between simulation and experimental. Model validation was based on comparison of *in vivo* GI concentration profile between simulation and experimental. The *in vivo* GI concentration simulation results were considered the evaluation of mucosal adherence contribution to the model.

Results

Pharmacokinetic parameters were determined based on a 2 compartment extravascular model using Winnonlin. The determined pharmacokinetic parameters are as follows: k_{10} is 0.017min^{-1}, k_{12} is 0.009min^{-1}, k_{21} 0.02min^{-1}, and Vd/F=0.017L. The PK parameters were used to determine the absorption rate coefficient in the DFCAT approach. A range of absorption terms were tested and the term with the lowest residual difference between simulation and experimental plasma profile was selected. The absorption rate coefficient of mesalamine was determined to be 0.87 min^{-1}. A graph of the fitted compartment model simulated using the DFCAT model is shown in Figure 32.

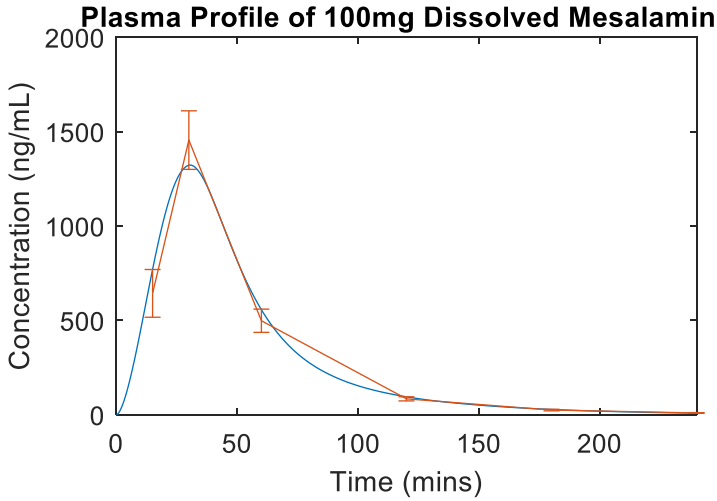

Figure 32. Fitted pharmacokinetic model from 100mg solution dosing.

Deconvolution Verification by Plasma Concentration Profile

The deconvolution algorithm was set to ±0.5 ng/mL tolerance check at every six minutes. Based on this criterion, the algorithm could successfully determine a dissolution rate coefficient to simulate a plasma concentration profile similar to the experimental profile (Figure 33).

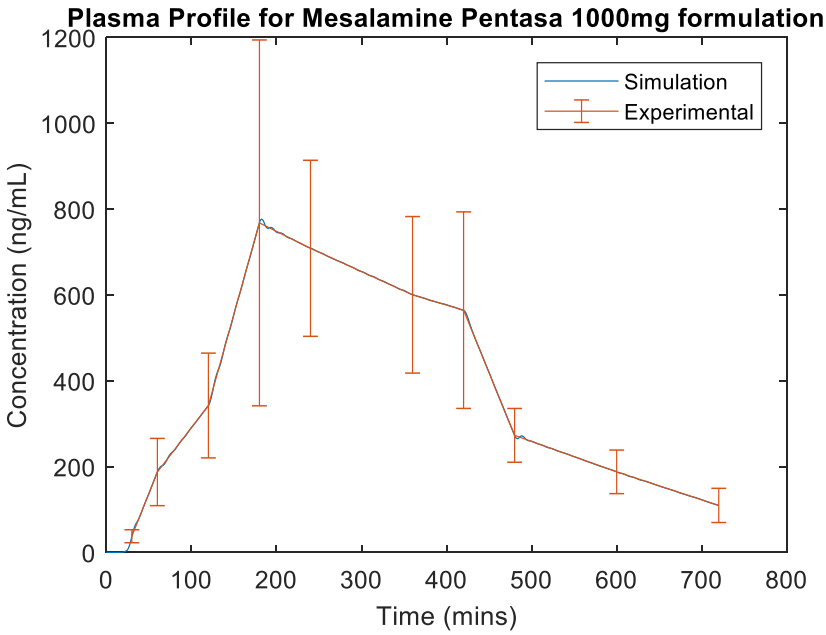

Figure 33. Simulated plasma profile used by mechanistic deconvolution

The deconvolution algorithm could follow the obscure behavior of the plasma profile. There was minor over-estimation of the plasma profile at the Tmax of 180 minutes which can be reduced by reducing the time step from 6 minutes. However, this was not expected to play a major impact on the model results.

Deconvolution Validation by *in vivo* Gastrointestinal Concentration Profile

The simulated *in vivo* GI concentrations based on a determined k_{BM} value of 0.045 min^{-1} and a k_{tM} value of 0.002 min^{-1} resulted in profiles that closely align with the general trend observed experimentally. A simulated Cmax of 2.9e5 ng/mL is similar to the observed 3.5e5 ng/mL in the stomach. Similar observations where the simulated concentrations were in the same order of magnitude as the experimentally observed GI concentrations were observed in the duodenum and early jejunum. For the jejunal region, the simulation over predicted the early presence of mesalamine and underpredicted the later presence of mesalamine.

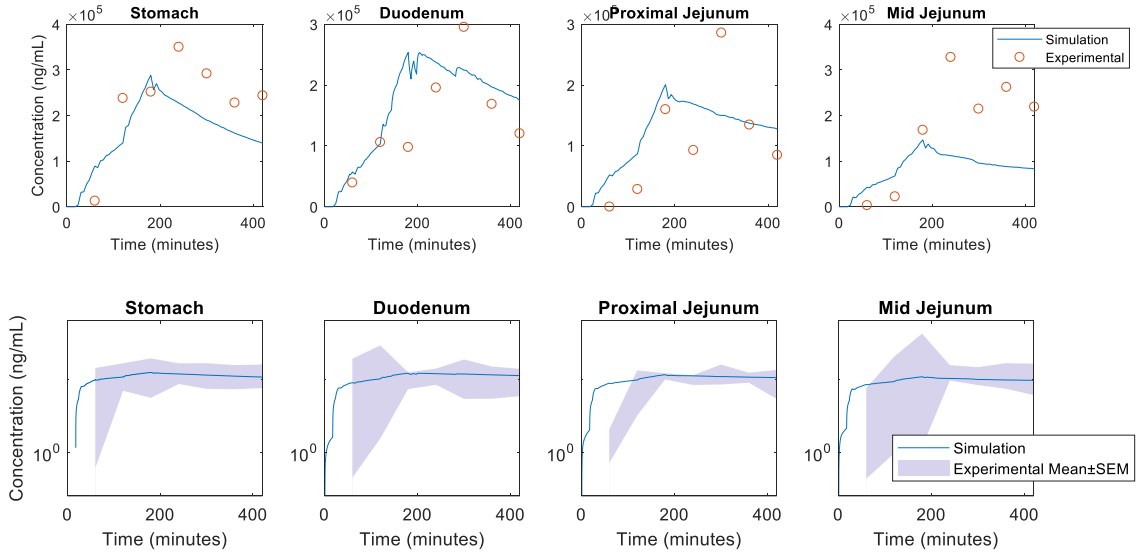

Figure 34. Comparison between predicted concentrations from deconvolution and experimental results. (top) Simulated vs average observed concentration profile. (bottom) Simulated vs experimental 90% geometric confidence interval.

Simulated *in vivo* Dissolution Profile

The rate and extent of regional GI dissolution was calculated based on the assigned compartments and shown in Figure 35. This simulation of mucosal adherence estimates roughly 10% of the modified release formulation releasing in the stomach whereas the traditional expectation would be very limited. In contrast, the duodenal region was predicted to have limited release (~5%) due to the limited area and residence time of the drug in that region. A larger portion of the dissolution process was predicted ot occur in the jejunum and ileum region which aligns better with traditional expectations from both formulation and clinical observation where Pentasa is used to treat Chrohn's disease.

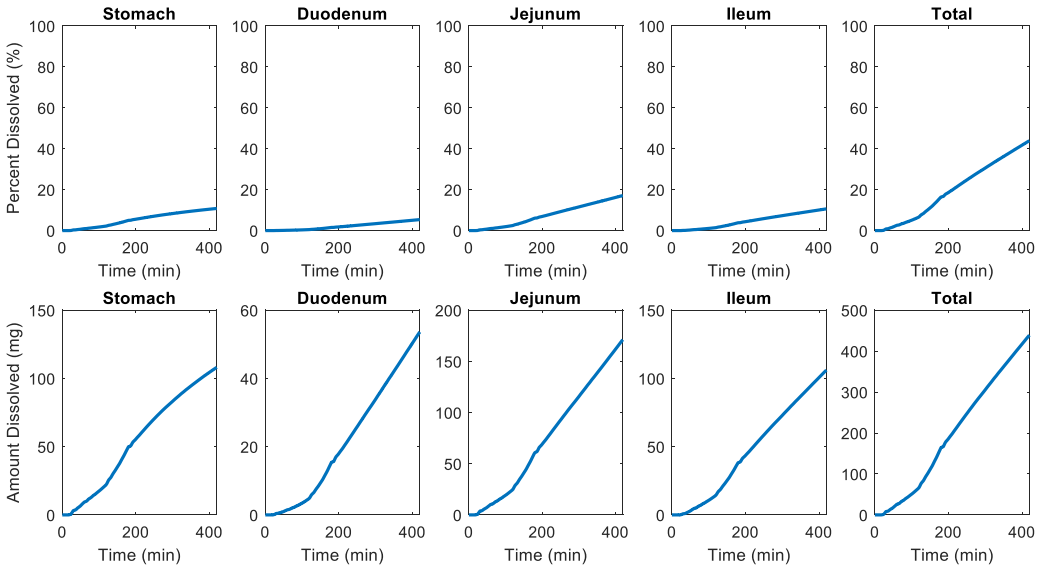

Figure 35. Simulated in vivo dissolution profile from deconvolution results

Discussion

Modified release formulations have remained a challenge in drug development due to the complexity of the formulations (106). Because MR formulations are design to release drug under specific conditions which can vary significantly in the body, it is difficult to stablish a relationship between *in vitro* and *in vivo* dissolution performance. While *in silico* models are often used to interpret *in vitro* data to provide a model based prediction of *in vivo* performance, obtaining accurate prediction of *in vivo* performance is often challenging. This can be attributed to the limited validation of the *in vivo* prediction for current computational models.

The DFCAT model found that including a consideration for the mucus layer can explain the *in vivo* concentrations of fasted state phenol red (non-permeable) dosing (99). In this assessment, a mucus layer was found to contribute significantly to the local GI volume available for dissolution and absorption. When modeling the *in vivo* dissolution, it was found that gastric emptying contributed significantly to the transit of ibuprofen which reflects its properties as a

BCS Class IIa drug. This contrasts with mesalamine (BCS Class IV) where delayed gastric emptying would not be clearly reflected in the plasma profile. Additionally, the formulation of Pentasa was found to contain polymers that possess mucosal adherence properties. When simulated using the mechanistic deconvolution approach, the local GI concentration of mesalamine supports the idea that mucoadherence can extend the GI residence time of drug particles and thus explain the high concentrations in the upper GI.

The simulation suggests that less than 50% of the total formulation based on the dose administered (1000 mg) was expected to be dissolved in the GI tract. The linical study reported an average between 100-200 mg of mesalamine recovered from feces which would suggest a local exposure of roughly 300-400 mg in the colon. This may be sufficient to invoke a pharmacodynamic response which would explain why Pentasa had demonstrated efficacious effect despite significant concentrations being observed in the upper GI tract over an extended period.

The original purpose for conducting the mesalamine clinical study was to evaluate the *in vivo* dissolution based on concentrations as a reference for future regulatory guidance on the bioequivalence of locally acting GI drug products (107). Regulatory guidance on mesalamine has been of debate between *in vitro* dissolution, comparative pharmacokinetics, and clinical endpoints (108). The bio-adherence model of Pentasa dissolution suggests that not only is the plasma concentration profile a critical reference point but the formulation type and excipients used. The capsule containing granules is essential as a convenient delivery mechanism and the hydroxypropyl methylcellulose used in the formulation is essential to replicate any potential mucoadherence behavior.

While the model results and corresponding experimental observations appear to support the general hypothesis that mucoadherence is the explanation for the extended residence time of Pentasa in the GI tract, it is important to note that variations or delays in gastric emptying that was accounted in the ibuprofen simulation were not included when modeling mucosal adherence. As such, the extension of residence time for an oral drug product could likely be a combination of both gastric emptying variation and mucoadherence. The possibility of these additional interactions should be considered in future research and experiment design.

Chapter 6 Summary

The purpose of this research was to develop an *in silico* method to quantify *in vivo* drug dissolution. Recent clinical studies had obtained post-dose gastrointestinal (GI) concentrations of different drug products in effort to quantify drug dissolution. However, concentration alone is indicative of neither rate nor extent of dissolution. Current *in silico* models were unable to reconcile the difference between the simulated and the clinically observed local GI concentration profile. As such, this research determined it was necessary to develop a new *in silico* approach to both quantify *in vivo* drug dissolution and relate to the experimentally observed local GI concentration.

Local GI fluid volume plays a critical role in both the absorption of fluid and drug as well as driving the dissolution of drug product based on the concentration gradient. Based on this perspective, the characterization of GI fluid volume values used in current mechanistic oral absorption models was identified as insufficient to evaluate the local GI concentration. As such, the first step in developing a new *in silico* model was to establish a mechanistic GI fluid transport model. This model adapted a serial compartment based approach akin to existing mechanistic oral absorption models with a special consideration to local GI fluid volumes. The model created dynamic considerations for the local fluid volumes that included absorption, secretion, and transit.

The overall model performance was verified based on clinically observed fluid quantity over time data. MRI images collected the quantified total content of free flowing liquid in the GI via 3 dimensions. To ensure the model adapted the most physiologically representative fluid volumes for use, it was noted that the study observed large regions with little to no fluid observed. Upon confirming the MRI methodology, it was noted that a vicious fluid such as the mucus layer that lines the GI wall would not be detected by the MRI. As it would not be feasible to remeasure the mucus layer volume, an approximation was made for the total volume of mucus based on physiological estimations to provide a quantified volume for each compartment that may contribute to both dissolution and absorption.

The resulting mechanistic model simulated the intake of water into the stomach and the corresponding transport over time. The simulation volume over time results were found to be similar to the experimental results. To validate this model, an additional simulation was conducted with the dosing of phenol red, a non-absorbable marker. This additional data was the result of another separate clinical study which dosed volunteers with 240mL of phenol red (100 μg/mL). The simulation results were found to again to be similar with experimentally observed concentration profiles especially in the earlier GI tract. This confirmed the reasonableness behind the assumption of a mucus layer contributing to local GI fluid volume.

To model *in vivo* dissolution, the mechanistic fluid model was expanded to include considerations for drug transit, disintegration, and dissolution analogous to current mechanistic model. A deconvolution method was adopted to reverse calculate the requisite *in vivo* drug dissolution to obtain the plasma profile. Data to evaluate *in vivo* dissolution came from an intubation based clinical study where healthy human fasted volunteers were dosed with 800mg immediate release tablet formulation of ibuprofen. This clinical study obtained the *in vivo*

ibuprofen concentration from stomach, duodenum, proximal jejunum, and middle jejunum. In this model, systemic circulation was defined by the traditional two-compartmental pharmacokinetic (PK) model where the PK parameters could be determined by fitting to plasma concentration profile from an 800 mg dosing of ibuprofen by infusion. The established PK parameters were then used to determine the absorption rate constant from a 420 mg solution dosing of ibuprofen using the established mechanistic fluid model.

Additional model considerations accounted for ibuprofen's BCS Class IIa nature. The clinical study observed plasma profile behavior reminiscent of a rapid increase in dissolution and therefore absorption. Given that ibuprofen has a high solubility level after reaching the duodenal pH levels, a significant increase in plasma profile was associated with a stochastic gastric emptying event. With these considerations in place, the resulting model estimated a dissolution profile for each clinically observed plasma profile with the resulting plasma profile was within ±1 μg/mL of the observed plasma profile. To validate this model, the distribution of simulated GI ibuprofen concentration over time was compared with the distribution of experimentally observed concentration over time. The resulting observed profiles were similar in trend and approximated the general range of concentration values within an order of magnitude.

This implementation of the mechanistic deconvolution approach was also applied to model the *in vivo* dissolution of a controlled release mesalamine formulation (Pentasa). A similar approach was taken where pharmacokinetic parameters were determined, the mechanistic deconvolution algorithm was utilized to predict *in vivo* dissolution rate, and the simulation results evaluated based on *in vivo* GI concentrations. Unlike ibuprofen however, mesalamine is a BCS class IV compound and not expected to be solely limited by solubility. As mesalamine was also clinically observed to exhibit high concentrations in the stomach after 7 hours,

mucoadherence of the formulation was identified as possible explanation for the extended residence time.

Specifically, hydroxypropyl methylcellulose was identified as an excipient with mucoadherence properties. When consideration for mucosal adherence was included in the mechanistic oral absorption model by establishing additional compartments where particles would "attach" to the mucosal layer and then transit forward slowly, the model simulated *in vivo* GI concentrations that were very similar amongst the GI tracts sampled. In addition, the increased residence time that resulted from the consideration of mucosal adherence ensured a continued release in the upper GI which resulted in the model mimicking the high *in vivo* GI concentrations after seven hours.

In conclusion, the simulation results suggest that quantification of GI fluid and consideration of GI mucus volumes are critical to correctly predicting the dissolution and absorption of oral drug products. Furthermore, considerations of gastric emptying and/or mucoadherence of formulations may be essential to correctly predicting the rate and extent of *in vivo* dissolution as well as the subsequent plasma profile. To continue improving model based prediction of *in vivo* dissolution, additional clinical studies the quantify GI fluid volume in different states (fasted/fed), quantify the presence of the mucus layer, and visual based observation of gastric residence or mucoadherence via ingestible camera pills can be used to further validate the developed model.

Bibliography

1. Jiang W, Kim S, Zhang X, Lionberger RA, Davit BM, Conner DP, Yu LX. The role of predictive biopharmaceutical modeling and simulation in drug development and regulatory evaluation. International journal of pharmaceutics. 2011;418(2):151-160.

2. Huang W, Lee SL, Yu LX. Mechanistic approaches to predicting oral drug absorption. The AAPS journal. 2009;11(2):217-224.

3. Kostewicz ES, Aarons L, Bergstrand M, Bolger MB, Galetin A, Hatley O, Jamei M, Lloyd R, Pepin X, Rostami-Hodjegan A, Sjögren E, Tannergren C, Turner DB, Wagner C, Weitschies W, Dressman J. PBPK models for the prediction of in vivo performance of oral dosage forms. European Journal of Pharmaceutical Sciences. 2014;57:300-321.

4. Zhang X, Duan J, Kesisoglou F, Novakovic J, Amidon GL, Jamei M, Lukacova V, Eissing T, Tsakalozou E, Zhao L, Lionberger R. Mechanistic Oral Absorption Modeling and Simulation for Formulation Development and Bioequivalence Evaluation: Report of an FDA Public Workshop. CPT: Pharmacometrics & Systems Pharmacology. 2017;6(8):492-495.

5. Mudie DM, Amidon GL, Amidon GE. Physiological Parameters for Oral Delivery and In vitro Testing. Molecular pharmaceutics. 2010;7(5):1388-1405.

6. Sutton SC. Role of physiological intestinal water in oral absorption. The AAPS journal. 2009;11(2):277-285.

7. Yu LX, Amidon GL. A compartmental absorption and transit model for estimating oral drug absorption. International Journal of Pharmaceutics. 1999;186(2):119-125.

8. Sjogren E, Thorn H, Tannergren C. In Silico Modeling of Gastrointestinal Drug Absorption: Predictive Performance of Three Physiologically Based Absorption Models. Molecular pharmaceutics. 2016;13(6):1763-1778.

9. Agoram B, Woltosz WS, Bolger MB. Predicting the impact of physiological and biochemical processes on oral drug bioavailability. Advanced drug delivery reviews. 2001;50 Suppl 1:S41-67.

10. Jamei M, Turner D, Yang J, Neuhoff S, Polak S, Rostami-Hodjegan A, Tucker G. Population-Based Mechanistic Prediction of Oral Drug Absorption. The AAPS journal. 2009;11(2):225-237.

11. Sjogren E, Westergren J, Grant I, Hanisch G, Lindfors L, Lennernas H, Abrahamsson B, Tannergren C. In silico predictions of gastrointestinal drug absorption in pharmaceutical product development: application of the mechanistic absorption model GI-Sim. European journal of pharmaceutical sciences : official journal of the European Federation for Pharmaceutical Sciences. 2013;49(4):679-698.

12. de Zwart LL. Anatomical and Physiological Differences Between Various Species Used in Studies on the Pharmacokinetics and Toxicology of Xenobiotics: A Review of Literature: National Institute of Public Health and the Environment; 1999.

13. Parrott N, Lukacova V, Fraczkiewicz G, Bolger MB. Predicting Pharmacokinetics of Drugs Using Physiologically Based Modeling—Application to Food Effects. The AAPS journal. 2009;11(1):45-53.

14. Hendriksen BA, Felix MV, Bolger MB. The composite solubility versus pH profile and its role in intestinal absorption prediction. AAPS pharmSci. 2003;5(1):E4.

15. Zhang X, Lionberger RA, Davit BM, Yu LX. Utility of Physiologically Based Absorption Modeling in Implementing Quality by Design in Drug Development. The AAPS journal. 2011;13(1):59-71.

16. Jamei M. An Introduction to:In Vitro-In Vivo Extrapolation (IVIVE). 2017 July 20. Available from: https://www.slideshare.net/mjamei/an-introduction-toin-vitroin-vivoextrapolation-ivive.

17. Yu LX, Amidon GL. Saturable small intestinal drug absorption in humans: modeling and interpretation of cefatrizine data. European journal of pharmaceutics and biopharmaceutics : official journal of Arbeitsgemeinschaft fur Pharmazeutische Verfahrenstechnik eV. 1998;45(2):199-203.

18. Davis SS, Hardy JG, Fara JW. Transit of pharmaceutical dosage forms through the small intestine. Gut. 1986;27(8):886-892.

19. Fallingborg J, Christensen LA, Ingeman-Nielsen M, Jacobsen BA, Abildgaard K, Rasmussen HH. pH-profile and regional transit times of the normal gut measured by a radiotelemetry device. Alimentary pharmacology & therapeutics. 1989;3(6):605-613.

20. Dressman JB, Berardi RR, Dermentzoglou LC, Russell TL, Schmaltz SP, Barnett JL, Jarvenpaa KM. Upper gastrointestinal (GI) pH in young, healthy men and women. Pharmaceutical research. 1990;7(7):756-761.

21. Wang H-y, Chen X, Jiang J, Shi J, Hu P. Evaluating a physiologically based pharmacokinetic model for predicting the pharmacokinetics of midazolam in Chinese after oral administration. Acta Pharmacologica Sinica. 2016;37(2):276-284.

22. Heikkinen AT, Baneyx G, Caruso A, Parrott N. Application of PBPK modeling to predict human intestinal metabolism of CYP3A substrates - an evaluation and case study using GastroPlus. European journal of pharmaceutical sciences : official journal of the European Federation for Pharmaceutical Sciences. 2012;47(2):375-386.

23. Zhang H, Xia B, Sheng J, Heimbach T, Lin T-H, He H, Wang Y, Novick S, Comfort A. Application of Physiologically Based Absorption Modeling to Formulation Development of a Low Solubility, Low Permeability Weak Base: Mechanistic Investigation of Food Effect. AAPS PharmSciTech. 2014;15(2):400-406.

24. Noyes AA, Whitney WR. THE RATE OF SOLUTION OF SOLID SUBSTANCES IN THEIR OWN SOLUTIONS. Journal of the American Chemical Society. 1897;19(12):930-934.

25. Haber F. Anhang: Zur Theorie der Reaktionsgeschwindigkeit in heterogenen Systemen. Zeitschrift für Elektrochemie und angewandte physikalische Chemie. 1904;10(9):156-157.

26. Wang J, Flanagan DR. General solution for diffusion-controlled dissolution of spherical particles. 1. Theory. Journal of pharmaceutical sciences. 1999;88(7):731-738.

27. Schiller C, Frohlich CP, Giessmann T, Siegmund W, Monnikes H, Hosten N, Weitschies W. Intestinal fluid volumes and transit of dosage forms as assessed by magnetic resonance imaging. Alimentary pharmacology & therapeutics. 2005;22(10):971-979.

28. Mudie DM, Murray K, Hoad CL, Pritchard SE, Garnett MC, Amidon GL, Gowland PA, Spiller RC, Amidon GE, Marciani L. Quantification of gastrointestinal liquid volumes and distribution following a 240 mL dose of water in the fasted state. Molecular pharmaceutics. 2014;11(9):3039-3047.

29. Takashima T, Shingaki T, Katayama Y, Hayashinaka E, Wada Y, Kataoka M, Ozaki D, Doi H, Suzuki M, Ishida S, Hatanaka K, Sugiyama Y, Akai S, Oku N, Yamashita S, Watanabe Y. Dynamic analysis of fluid distribution in the gastrointestinal tract in rats: positron emission tomography imaging after oral administration of nonabsorbable marker, [(18)F]Deoxyfluoropoly(ethylene glycol). Molecular pharmaceutics. 2013;10(6):2261-2269.

30. Hoad CL, Marciani L, Foley S, Totman JJ, Wright J, Bush D, Cox EF, Campbell E, Spiller RC, Gowland PA. Non-invasive quantification of small bowel water content by MRI: a validation study. Phys Med Biol. 2007;52(23):6909-6922.

31. Shingaki T, Takashima T, Wada Y, Tanaka M, Kataoka M, Ishii A, Shigihara Y, Sugiyama Y, Yamashita S, Watanabe Y. Imaging of gastrointestinal absorption and

biodistribution of an orally administered probe using positron emission tomography in humans. Clinical pharmacology and therapeutics. 2012;91(4):653-659.

32. Greger R, Windhorst U. Comprehensive Human Physiology: From Cellular Mechanisms to Integration: Springer Berlin Heidelberg; 2013.

33. Roy H. Short Textbook of Surgery: Jaypee Brothers,Medical Publishers Pvt. Limited; 2010.

34. Johansson MEV, Gustafsson JK, Holmén-Larsson J, Jabbar KS, Xia L, Xu H, Ghishan FK, Carvalho FA, Gewirtz AT, Sjövall H, Hansson GC. Bacteria penetrate the normally impenetrable inner colon mucus layer in both murine colitis models and patients with ulcerative colitis. Gut. 2013.

35. Pelaseyed T, Bergström JH, Gustafsson JK, Ermund A, Birchenough GMH, Schütte A, van der Post S, Svensson F, Rodríguez-Piñeiro AM, Nyström EEL, Wising C, Johansson MEV, Hansson GC. The mucus and mucins of the goblet cells and enterocytes provide the first defense line of the gastrointestinal tract and interact with the immune system. Immunological reviews. 2014;260(1):8-20

.

36. Derrien M, van Passel MWJ, van de Bovenkamp JHB, Schipper RG, de Vos WM, Dekker J. Mucin-bacterial interactions in the human oral cavity and digestive tract. Gut Microbes. 2010;1(4):254-268.

37. Ferrua MJ, Singh RP. Modeling the Fluid Dynamics in a Human Stomach to Gain Insight of Food Digestion. Journal of Food Science. 2010;75(7):R151-R162.

38. Yu LX, Crison JR, Amidon GL. Compartmental transit and dispersion model analysis of small intestinal transit flow in humans. International Journal of Pharmaceutics. 1996;140(1):111-118.

39. Péronnet F, Mignault D, du Souich P, Vergne S, Le Bellego L, Jimenez L, Rabasa-Lhoret R. Pharmacokinetic analysis of absorption, distribution and disappearance of ingested water labeled with D(2)O in humans. European Journal of Applied Physiology. 2012;112(6):2213-2222.

40. Hellström PM, Grybäck P, Jacobsson H. The physiology of gastric emptying. Best Practice & Research Clinical Anaesthesiology. 2006;20(3):397-407.

41. Ogungbenro K, Pertinez H, Aarons L. Empirical and Semi-Mechanistic Modelling of Double-Peaked Pharmacokinetic Profile Phenomenon Due to Gastric Emptying. The AAPS Journal. 2015;17(1):227-236.

42. Davenport HW. Physiology of the digestive tract: an introductory text. Chicago: Year Book Medical Publishers; 1982.

43. Hounnou G, Destrieux C, Desmé J, Bertrand P, Velut S. Anatomical study of the length of the human intestine. Surgical and Radiologic Anatomy. 2002;24(5):290-294.

44. Cronin CG, Delappe E, Lohan DG, Roche C, Murphy JM. Normal small bowel wall characteristics on MR enterography. European journal of radiology. 2010;75(2):207-211.

45. Yu LX, Lipka E, Crison JR, Amidon GL. Transport approaches to the biopharmaceutical design of oral drug delivery systems: prediction of intestinal absorption. Advanced drug delivery reviews. 1996;19(3):359-376.

46. Lennernäs H, Aarons L, Augustijns P, Beato S, Bolger M, Box K, Brewster M, Butler J, Dressman J, Holm R, Julia Frank K, Kendall R, Langguth P, Sydor J, Lindahl A, McAllister M, Muenster U, Müllertz A, Ojala K, Pepin X, Reppas C, Rostami-Hodjegan A, Verwei M, Weitschies W, Wilson C, Karlsson C, Abrahamsson B. Oral biopharmaceutics tools – Time for a new initiative – An introduction to the IMI project OrBiTo. European Journal of Pharmaceutical Sciences. 2014;57:292-299.

47. Kostewicz ES, Abrahamsson B, Brewster M, Brouwers J, Butler J, Carlert S, Dickinson PA, Dressman J, Holm R, Klein S, Mann J, McAllister M, Minekus M, Muenster U, Müllertz A, Verwei M, Vertzoni M, Weitschies W, Augustijns P. In vitro models for the prediction of in vivo performance of oral dosage forms. European Journal of Pharmaceutical Sciences. 2014;57:342-366.

48. Loo JC, Riegelman S. New method for calculating the intrinsic absorption rate of drugs. Journal of pharmaceutical sciences. 1968;57(6):918-928.

49. Wagner JG, Nelson E. KINETIC ANALYSIS OF BLOOD LEVELS AND URINARY EXCRETION IN THE ABSORPTIVE PHASE AFTER SINGLE DOSES OF DRUG. Journal of pharmaceutical sciences. 1964;53:1392-1403.

50. Kesisoglou F, Xia B, Agrawal NGB. Comparison of Deconvolution-Based and Absorption Modeling IVIVC for Extended Release Formulations of a BCS III Drug Development Candidate. The AAPS Journal. 2015;17(6):1492-1500.

51. Lukacova V, Woltosz WS, Bolger MB. Prediction of Modified Release Pharmacokinetics and Pharmacodynamics from In Vitro, Immediate Release, and Intravenous Data. The AAPS Journal. 2009;11(2):323-334.

52. Kakhi M, Marroum P, Chittenden J. Analysis of level A in vitro-in vivo correlations for an extended-release formulation with limited bioavailability. Biopharmaceutics & drug disposition. 2013;34(5):262-277.

53. Yu A, Baker JR, Fioritto AF, Wang Y, Luo R, Li S, Wen B, Bly M, Tsume Y, Koenigsknecht MJ, Zhang X, Lionberger R, Amidon GL, Hasler WL, Sun D. Measurement of in vivo Gastrointestinal Release and Dissolution of Three Locally Acting Mesalamine Formulations in Regions of the Human Gastrointestinal Tract. Molecular pharmaceutics. 2017;14(2):345-358.

54. Koenigsknecht M, Baker JR, Wen B, Frances A, Zhang H, Yu A, Zhao T, Tsume Y, Pai M, Bleske B, Zhang X, Lionberger R, Lee A, Amidon G, Hasler WL, Sun D. In Vivo Dissolution and Systemic Absorption of Immediate Release Ibuprofen in Human Gastrointestinal Tract Under Fed and Fasted Conditions. Molecular Pharmaceutics. 2017.

55. Hens B, Tsume Y, Bermejo M, Paixao P, Koenigsknecht MJ, Baker JR, Hasler WL, Lionberger R, Fan J, Dickens J, Shedden K, Wen B, Wysocki J, Loebenberg R, Lee A, Frances A, Amidon G, Yu A, Benninghoff G, Salehi N, Talattof A, Sun D, Amidon GL. Low Buffer Capacity and Alternating Motility along the Human Gastrointestinal Tract: Implications for in Vivo Dissolution and Absorption of Ionizable Drugs. Molecular pharmaceutics. 2017.

56. Sun D, Baker JR, Wen B, Frances A, Zhang H, Yu A, Zhao T, Tsume Y, Pai M, Bleske B, Zhang X, Lionberger R, Lee A, Amidon G, Hasler WL, Koenigsknecht M. In Vivo Dissolution and Systemic Absorption of Immediate Release Ibuprofen in Human Gastrointestinal Tract Under Fed and Fasted Conditions. Molecular pharmaceutics. 2017.

57. Pavliv L, Voss B, Rock A. Pharmacokinetics, safety, and tolerability of a rapid infusion of i.v. ibuprofen in healthy adults. American journal of health-system pharmacy : AJHP : official journal of the American Society of Health-System Pharmacists. 2011;68(1):47-51.

58. Lockwood GF, Albert KS, Gillespie WR, Bole GG, Harkcom TM, Szpunar GJ, Wagner JG. Pharmacokinetics of ibuprofen in man. I. Free and total area/dose relationships. Clinical pharmacology and therapeutics. 1983;34(1):97-103.

59. Wagner JG, Albert KS, Szpunar GJ, Lockwood GF. Pharmacokinetics of ibuprofen in man IV: absorption and disposition. Journal of pharmacokinetics and biopharmaceutics. 1984;12(4):381-399.

60. Vantrappen GR, Peeters TL, Janssens J. The secretory component of the interdigestive migrating motor complex in man. Scand J Gastroenterol. 1979;14(6):663-667.

61. Margolskee A, Darwich AS, Galetin A, Rostami-Hodjegan A, Aarons L. Deconvolution and IVIVC: Exploring the Role of Rate-Limiting Conditions. The AAPS journal. 2016;18(2):321-332.

62. Heikkila T, Karjalainen M, Ojala K, Partola K, Lammert F, Augustijns P, Urtti A, Yliperttula M, Peltonen L, Hirvonen J. Equilibrium drug solubility measurements in 96-well plates reveal similar drug solubilities in phosphate buffer pH 6.8 and human intestinal fluid. Int J Pharm. 2011;405(1-2):132-136.

63. Hens B, Brouwers J, Anneveld B, Corsetti M, Symillides M, Vertzoni M, Reppas C, Turner DB, Augustijns P. Gastrointestinal transfer: in vivo evaluation and implementation in in vitro and in silico predictive tools. European journal of

pharmaceutical sciences : official journal of the European Federation for Pharmaceutical Sciences. 2014;63:233-242.

64. Rivera-Leyva JC, García-Flores M, Valladares-Méndez A, Orozco-Castellanos LM, Martínez-Alfaro M. Comparative Studies on the Dissolution Profiles of Oral Ibuprofen Suspension and Commercial Tablets using Biopharmaceutical Classification System Criteria. Indian Journal of Pharmaceutical Sciences. 2012;74(4):312-318.

65. CCFA. The Facts about Inflammatory Bowel Diseases. 2015 December 3. Available from: http://www.ccfa.org/assets/pdfs/updatedibdfactbook.pdf.

66. Sutherland L, Macdonald JK. Oral 5-aminosalicylic acid for maintenance of remission in ulcerative colitis. The Cochrane database of systematic reviews. 2006(2):Cd000544.

67. Podolsky DK. Inflammatory bowel disease. The New England journal of medicine. 2002;347(6):417-429.

68. Schroder H, Campbell DE. Absorption, metabolism, and excretion of salicylazosulfapyridine in man. Clinical pharmacology and therapeutics. 1972;13(4):539-551.

69. Peppercorn MA, Goldman P. Distribution studies of salicylazosulfapyridine and its metabolites. Gastroenterology. 1973;64(2):240-245.

70. Ye B, van Langenberg DR. Mesalazine preparations for the treatment of ulcerative colitis: Are all created equal? World journal of gastrointestinal pharmacology and therapeutics. 2015;6(4):137-144.

71. Rasmussen SN, Bondesen S, Hvidberg EF, Hansen SH, Binder V, Halskov S, Flachs H. 5-aminosalicylic acid in a slow-release preparation: bioavailability, plasma level, and excretion in humans. Gastroenterology. 1982;83(5):1062-1070.

72. Fernandez-Becker NQ, Moss AC. Improving delivery of aminosalicylates in ulcerative colitis: effect on patient outcomes. Drugs. 2008;68(8):1089-1103.

73. Yang LP, McCormack PL. MMX(R) Mesalazine: a review of its use in the management of mild to moderate ulcerative colitis. Drugs. 2011;71(2):221-235.

74. Sandborn WJ, Hanauer SB. Systematic review: the pharmacokinetic profiles of oral mesalazine formulations and mesalazine pro-drugs used in the management of ulcerative colitis. Alimentary pharmacology & therapeutics. 2003;17(1):29-42.

75. Nanda K, Moss AC. Update on the management of ulcerative colitis: treatment and maintenance approaches focused on MMX(®) mesalamine. [Corrigendum]. Clinical Pharmacology : Advances and Applications. 2013;5:21-21.

76. Yu DK, Morrill B, Eichmeier LS, Giesing DH, Weir SJ, Lanman RC, Lanman MB. Pharmacokinetics of 5-aminosalicylic acid from controlled-release capsules in man. European Journal of Clinical Pharmacology;48(3):273-277.

77. Pharmaceuticals S. Full Prescribing Information: Apriso. 2015 March 9. Available from: https://www.accessdata.fda.gov/drugsatfda_docs/label/2008/022301lbl.pdf.

78. Shire. Full Prescribing Information: Lialda. FDA. 2015 March 9. Available from: http://www.accessdata.fda.gov/drugsatfda_docs/label/2009/022000s002lbl.pdf.

79. Feagan BG, Macdonald JK. Oral 5-aminosalicylic acid for maintenance of remission in ulcerative colitis. The Cochrane database of systematic reviews. 2012;10:Cd000544.

80. Feagan BG, Macdonald JK. Oral 5-aminosalicylic acid for induction of remission in ulcerative colitis. The Cochrane database of systematic reviews. 2012;10:Cd000543.

81. Sninsky CA, Cort DH, Shanahan F, Powers BJ, Sessions JT, Pruitt RE, Jacobs WH, Lo SK, Targan SR, Cerda JJ, Gremillion DE, Snape WJ, Sabel J, Jinich H, Swinehart JM, DeMicco MP. Oral mesalamine (asacol) for mildly to moderately active ulcerative colitis: A multicenter study. Annals of Internal Medicine. 1991;115(5):350-355.

82. Kamm MA, Sandborn WJ, Gassull M, Schreiber S, Jackowski L, Butler T, Lyne A, Stephenson D, Palmen M, Joseph RE. Once-Daily, High-Concentration MMX Mesalamine in Active Ulcerative Colitis. Gastroenterology. 2007;132(1):66-75.

83. Hanauer S, Schwartz J, Robinson M, Roufail W, Arora S, Cello J, Safdi M, Carlisle WR, Ou-Tim L, Cochran JL, Ingle S, Bristow Iii WJ, Grendell J, Satow J, Jurcik I, White L, Sales D, Gochnour S, Hanan I. Mesalamine capsules for treatment of active ulcerative colitis: Results of a controlled trial. American Journal of Gastroenterology. 1993;88(8):1188-1197.

84. Nanda K, Moss AC. Update on the management of ulcerative colitis: treatment and maintenance approaches focused on MMX(®) mesalamine. Clinical Pharmacology : Advances and Applications. 2012;4:41-50.

85. Ito H, Iida M, Matsumoto T, Suzuki Y, Sasaki H, Yoshida T, Takano Y, Hibi T. Direct comparison of two different mesalamine formulations for the induction of remission in patients with ulcerative colitis: A double-blind, randomized study. Inflammatory Bowel Diseases. 2010;16(9):1567-1574.

86. Paoluzi OA, Iacopini F, Pica R, Crispino P, Marcheggiano A, Consolazio A, Rivera M, Paoluzi P. Comparison of two different daily dosages (2.4 vs. 1.2 g) of oral mesalazine in maintenance of remission in ulcerative colitis patients: 1-year follow-up study. Alimentary pharmacology & therapeutics. 2005;21(9):1111-1119.

87. D'Haens G, Hommes D, Engels L, Baert F, Van Der Waaij L, Connor P, Ramage J, Dewit O, Palmen M, Stephenson D, Joseph R. Once daily MMX mesalazine for the treatment of mild-to-moderate ulcerative colitis: a phase II, dose-ranging study. Alimentary pharmacology & therapeutics. 2006;24(7):1087-1097.

88. Lichtenstein GR, Kamm MA, Boddu P, Gubergrits N, Lyne A, Butler T, Lees K, Joseph RE, Sandborn WJ. Effect of Once- or Twice-Daily MMX Mesalamine (SPD476) for the Induction of Remission of Mild to Moderately Active Ulcerative Colitis. Clinical Gastroenterology and Hepatology. 2007;5(1):95-102.

89. Prantera C, Kohn A, Campieri M, Caprilli R, Cottone M, Pallone F, Savarino V, Sturniolo GC, Vecchi M, Ardia A, Bellinvia S. Clinical trial: ulcerative colitis maintenance treatment with 5-ASA: a 1-year, randomized multicentre study comparing MMX with Asacol. Alimentary pharmacology & therapeutics. 2009;30(9):908-918.

90. Ford AC, Achkar JP, Khan KJ, Kane SV, Talley NJ, Marshall JK, Moayyedi P. Efficacy of 5-aminosalicylates in ulcerative colitis: systematic review and meta-analysis. The American journal of gastroenterology. 2011;106(4):601-616.

91. Wilding I. Bioequivalence testing for locally acting gastrointestinal products: what role for gamma scintigraphy? Journal of clinical pharmacology. 2002;42(11):1200-1210.

92. Adams WP, Ahrens RC, Chen ML, Christopher D, Chowdhury BA, Conner DP, Dalby R, Fitzgerald K, Hendeles L, Hickey AJ, Hochhaus G, Laube BL, Lucas P, Lee SL, Lyapustina S, Li B, O'Connor D, Parikh N, Parkins DA, Peri P, Pitcairn GR, Riebe M, Roy P, Shah T, Singh GJ, Sharp SS, Suman JD, Weda M, Woodcock J, Yu L. Demonstrating Bioequivalence of Locally Acting Orally Inhaled Drug Products (OIPs): Workshop Summary Report. Journal of aerosol medicine and pulmonary drug delivery. 2010;23(1):1-29.

93. Lionberger RA. FDA Critical Path Initiatives: Opportunities for Generic Drug Development. The AAPS Journal. 2008;10(1):103-109.

94. Cuffari C, Pierce D, Korczowski B, Fyderek K, Van Heusen H, Hossack S, Wan H, Edwards AYZ, Martin P. Randomized clinical trial: pharmacokinetics and safety of multimatrix mesalamine for treatment of pediatric ulcerative colitis. Drug Design, Development and Therapy. 2016;10:593-607.

95. Christensen LA, Fallingborg J, Abildgaard K, Jacobsen BA, Sanchez G, Hansen SH, Bondesen S, Hvidberg EF, Rasmussen SN. Topical and systemic availability of 5-aminosalicylate: comparisons of three controlled release preparations in man. Alimentary pharmacology & therapeutics. 1990;4(5):523-533.

96. Takeshima F, Matsumura M, Makiyama K, Ohba K, Yamakawa M, Nishiyama H, Yamao T, Akazawa Y, Yamaguchi N, Ohnita K, Ichikawa T, Isomoto H, Nakao K. Efficacy of Long-Term 4.0 g/Day Mesalazine (Pentasa) for Maintenance Therapy in

Ulcerative Colitis. Medical Science Monitor : International Medical Journal of Experimental and Clinical Research. 2014;20:1314-1318.

97. Miner P, Hanauer S, Robinson M, Schwartz J, Arora S. Safety and efficacy of controlled-release mesalamine for maintenance of remission in ulcerative colitis. Pentasa UC Maintenance Study Group. Digestive diseases and sciences. 1995;40(2):296-304.

98. Lim WC, Hanauer S. Aminosalicylates for induction of remission or response in Crohn's disease. The Cochrane database of systematic reviews. 2010(12):Cd008870.

99. Yu A, Jackson T, Tsume Y, Koenigsknecht M, Wysocki J, Marciani L, Amidon GL, Frances A, Baker JR, Hasler W, Wen B, Pai A, Sun D. Mechanistic Fluid Transport Model to Estimate Gastrointestinal Fluid Volume and Its Dynamic Change Over Time. The AAPS journal. 2017.

100. Sperandio B, Fischer N, Sansonetti PJ. Mucosal physical and chemical innate barriers: Lessons from microbial evasion strategies. Seminars in immunology. 2015;27(2):111-118.

101. ACS. Breaking the "mucus barrier" with a new drug delivery system. 2017 April 4. Available from: https://www.acs.org/content/acs/en/pressroom/newsreleases/2008/august/breaking-the-mucus-barrier-with-a-new-drug-delivery-system.html.

102. Wen H, Park K. Oral Controlled Release Formulation Design and Drug Delivery: Theory to Practice: Wiley; 2011.

103. FDA. PENTASA (mesalamine) Controlled-Release Capsules 250 mg and 500 mg Prescribing Information as of July 2013. 2017 October 5. Available from: https://www.accessdata.fda.gov/drugsatfda_docs/label/2013/020049s026lbl.pdf.

104. US S. Pentasa (mesalamine) Controlled-Release Capsules 250 mg and 500 mg Prescribing Information as of 10/2015 Rx only. 2017 April 7. Available from: http://pi.shirecontent.com/PI/PDFs/Pentasa_USA_ENG.pdf.

105. Domschke W, Konturek SJ. The Stomach: Physiology, Pathophysiology and Treatment: Springer Berlin Heidelberg; 2012.

106. Patel J, Patel A. Chapter 10 - Artificial Neural Networking in Controlled Drug Delivery A2 - Puri, Munish. In: Pathak Y, Sutariya VK, Tipparaju S, Moreno W, editors. Artificial Neural Network for Drug Design, Delivery and Disposition. Boston: Academic Press; 2016. p. 195-218.

107. Wen HZ, Xinyuan. The Science of Therapeutic Equivalence. 2017 October 27. Available from: https://pharm.ucsf.edu/sites/pharm.ucsf.edu/files/cersi/media-browser/OGD_Slides.pdf.

108. Gupta SK. Regulatory filing strategy for generic mesalazine modified release formulations. Indian Journal of Pharmacology. 2011;43(2):221-222.